Experimental Investigation of Thermo-Hydraulic Characteristics of Two-Phase Flow of FC72 in Microchannel Heat Sinks

by

Naveenan Thiagarajan

A thesis submitted to the Graduate Faculty of
Auburn University
in partial fulfillment of the
requirements for the Degree of
Master of Science

Auburn, Alabama
December 18, 2009

Keywords: microchannels, two-phase, silicon, FC72, flow boiling, re-entrant cavities, flow instabilities

Approved by

Sushil H.Bhavnani, Chair, Professor of Mechanical Engineering
Jeyhoon Khodadadi, Professor of Mechanical Engineering
Bogdan Willamowski, Professor of Electrical Engineering

Abstract

Advances in electronics such as chip level integration and die stacking have led to a bottleneck in further development since dissipation of the resulting high heat fluxes continues to be a challenge. Due to the tremendous potential, microelectronics also finds applications in a wide range of industries such as automobiles and aircrafts, along with high power computing which places additional emphasis on thermal management of electronics. Ongoing research in the field of flow boiling to meet the rising demands has resulted in the evolution of potential cooling technologies such as microchannel heat sinks.

Although microchannel heat sinks offer numerous advantages, a number of roadblocks impede its transformation to a commercial heat dissipation device. These include flow instabilities and lack of theoretical models which poses a great difficulty in the prediction of hydraulic and thermal characteristics.

In an effort to understand and characterize the flow boiling in these micro-structures, experiments were conducted using 19 parallel, surface enhanced microchannels with a hydraulic diameter of 253-microns. The working fluid used is a perfluorocarbon (C_6F_{14}), also known as FC72. The surface of microchannels was enhanced by the fabrication of re-entrant cavities which served as vapor trapping sites. Heaters were integrated with the test section to simulate the heat from a chip. The study

was performed at mass fluxes ranging from 500-2000 kg/m^2-s and inlet subcooling up to 20°C.

The performance of the microchannel heat sink was measured in terms of heat transfer coefficient under a wide range of operating conditions characterized by the system variables - heat flux, mass flux and inlet subcooling. The effect of these variables on the Onset of Nucleate Boiling (ONB) and nucleation hysteresis was also studied. Analysis was also carried to compare the obtained heat transfer coefficient with those predicted by empirical models available in the literature and a nucleate boiling correlation has also been proposed, which correlates most of the experimental data within ±15%.

The high heat transfer coefficient observed in flow boiling in microchannels is often accompanied by high pressure drop due to the phase-change taking place in the channels. The pressure drop has to be contained within acceptable levels, as this directly translates into pumping power required to operate the system. The study conducted encompasses the experimental analysis of the aforementioned parametric effects on the pressure drop. The data were also compared with the predictions of conventional homogeneous and separated flow pressure drop correlations.

Flow instabilities were observed under certain subcooled boiling conditions although these were mitigated in saturated conditions by the presence of 20-micron sized cavities incorporated into the base of each microchannel. The influence of system variables on the flow instabilities was studied and the flow instabilities were classified as high and low frequency oscillations based on pressure transducer signals and high speed videos. Investigations were also done to demarcate the stable and unstable flows and hence identify the stable regimes of operation.

However, to completely eliminate the instabilities, it is important to identify the underlying mechanisms. Two possible causative mechanisms are channel-to-channel interaction and the effect of compressible volumes at channel exit and inlet. In order to isolate these causes, a study of a single silicon microchannel was conducted using flow boiling experiments in a single microchannel test section of height 347 microns and width ranging from 100-400 microns. The base of the microchannel was augmented with either two or six re-entrant cavities. The results include the parametric effects of inlet subcooling, mass flux, heat flux and microchannel size on the pressure drop and comparisons with multichannel configurations. Data acquired from pressure transducers and high speed visualization showed that the pressure drop oscillations in the subcooled boiling regime observed earlier in a multichannel configuration, were not observed in the subcooled regime of single channel of width 100 microns, indicating that instabilities reduce with reduced interactions between the channels. However, very slight oscillations were observed under saturated conditions although it did not affect the pressure drop.

Acknowledgments

The author would like to extend his sincere thanks to his advisory committee comprising Professor Sushil H.Bhavnani, Professor Jeyhoon Khodadadi and Professor Bogdan Willamowski for their contributions and time. Special thanks are extended to Dr.Bhavnani for being a constant source of inspiration and motivation.

Much gratitude is extended to Daniel T. Pate and Rory J. Jones for their pioneering work and guidance provided in carrying out this study. The author is also thankful to 3M Corporation for providing the working fluid used in the study. Also thanks to AMSTC for providing the fabrication facilities and materials which made the study possible. Special thanks to Mr. Charles Ellis for the guidance provided in fabricating the test sections.

The author would like to express his sincere gratitude and thanks to all his friends for their love and support.

Above all, the author would like to thank his parents and sister for their endless love, support and encouragement.

Table of Contents

List of Tables

List of Figures

List of Symbols

A_{Ch}	plan form area of microchannel (m^2)
Bo	Bond number
c	function of aspect ratio used in
C	function of aspect ratio used in
C_1	constant used in Equation 4.15
C_2	exponent of heat flux in Equation 4.15
C_c	contraction ratio
C_p	specific heat (kJ/kgK)
CHF	Critical Heat Flux
Co	Convection number
d_d	bubble departure diameter (m)
D_h	hydraulic diameter (m)
f	Fanning friction factor
f_{app}	apparent friction factor for developing single phase flow
G	mass flux (kg/m^2s)
g	acceleration due to gravity (m/s^2)
H	height of microchannel (m)
h	heat transfer co-efficient (W/m^2k)
h_{fg}	latent heat of vaporization (kJ/kg)

I	heater input current (A)
k_d	momentum correction factor
k_∞	function of aspect ratio used in
K	thermal conductivity (W/mk)
l_c	capillary length (m)
L	length of microchannel (m)
L_{hy}	entrance length (m)
M	molecular weight
$\dot{m}$	mass flow rate (kg/s)
N	number of channels
N_{conf}	confinement number
Nu	Nusselt number
ONB	Onset of Nucleate Boiling
OFI	Onset of Flow Instability
p	pressure (kPa)
P	power supplied (W)
Pr	Prandtl number
$q"$	heat flux (W/m^2)
R_h	heater resistance (Ω)
Re	Reynolds number
T	temperature ($°C$)
U	velocity (m/s)
v	specific volume (m^3/kg)

W width (m)

We Webber number

x_e exit quality

Subscripts

a accelerational

amb ambient

app apparent

$appd$ applied

$array$ microchannel array

avg average

c channel

cr critical

d developing

eff effective

exp experimental

f fin; fluid

fd fully developed

fr frictional

g vapor

h heater

in channel inlet

lo liquid only

$losses$ pressure drop losses at various cross-sections of flow passage

out	channel exit
$pool$	pool boiling
sat	saturated
sp	single phase
$snuff$	snuffed
tp	two-phase
$wall$	channel bottom surface

Superscripts

$+$	non-dimensional

Greek symbols

β	aspect ratio
Δp	pressure drop (kPa)
ΔT_{sat}	inlet subcooling ($°C$)
ρ	density (kg/m^3)
σ	contraction ratio
μ	viscosity (Ns/m^2)
Θ_{b-tp}	two phase length temperature difference (°C)

CHAPTER 1: INTRODUCTION

Two of the most prolific fields of research in the past decades have been the development of nuclear technology and thermal management of microprocessors - one in the wake of a disaster and the other on the verge of it. The need for the former was put on the fast track after the Three Mile Island accident, one which changed the outlook of a country, and the latter ringing the alarm bells on the rising chip temperatures. However, both have led to ground breaking research in the fields of heat transfer and even more significantly in the field of boiling heat transfer.

Advances in the electronics and computer industry such as chip level integration allow the manufacturers to pack a billion transistors carrying out a billion calculations into an area the size of a penny. Consequently, this leads to a bottle neck in further development since dissipation of such high heat fluxes is a big challenge. To acquire

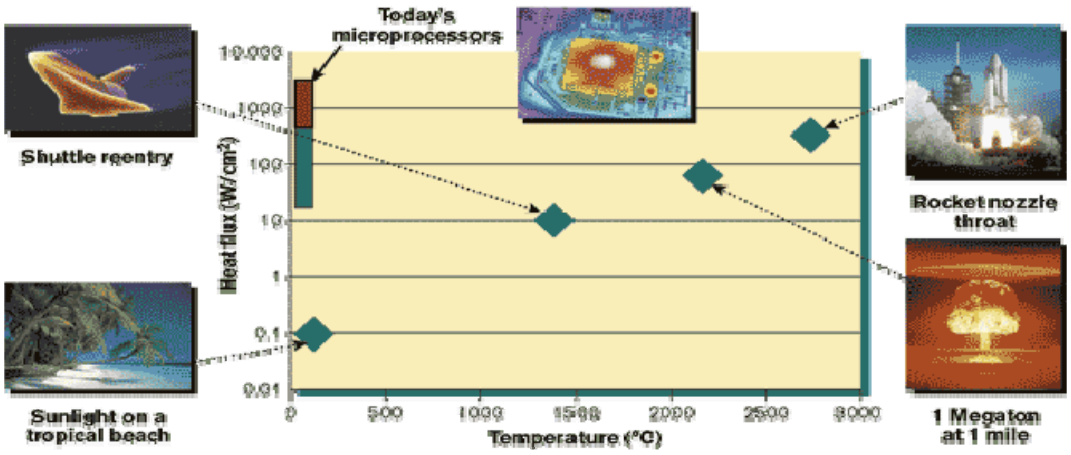

Figure 1.1 Magnitude of challenge posed by rising heat flux (www.semiconductor.net)

sense of magnitude of this challenge, the hot spot heat flux from today's PC microprocessor range anywhere between 10^3-10^4 W/cm^2 which is comparable to the heat flux in a sun spot and greater than those prevalent during a space shuttle's re-entry, nuclear blast or the throat of a rocket nozzle. It is due to this reason along with rising power consumption that manufacturers like Intel and AMD have stalled their chip clock frequencies as seen in Figure 1.2 [1]. While power consumption has been controlled by the introduction of multi-core processors, heat dissipation still remains a challenge.

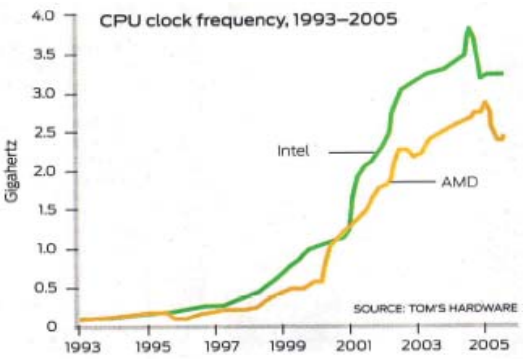

Figure 1.2 Clock frequency trend [1]

Current thermal management technologies such as forced convection air sinks and heat pipes can only handle heat fluxes up to 150 W/cm^2 (Figure 1.3 [2]), falling short of the demands of the current electronics and computer industry. Consequently, researchers have turned their attention towards advanced thermal management techniques such as two-phase flow in microchannels, on-chip refrigeration [3] and miniaturized silicon thermo electric coolers [4].

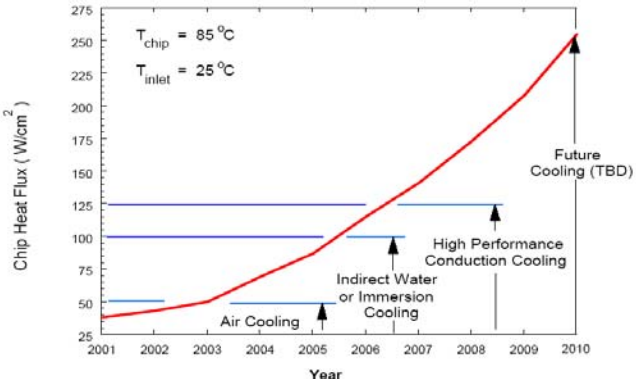

Figure 1.3 Comparison of thermal managenemnt techniques [2]

Among the prospective solutions, single and two phase flow in microchannels have emerged as potential solutions, ever since its introduction in 1981 by Tuckerman

and Pease [5,6] who demonstrated heat dissipation of up to 790 W/cm^2 using a single phase microchannel heat sink.

As part of the ongoing developments, Colgan et al. [7] from IBM Corporation demonstrated a practical implementation of a single phase microchannel heat sink (Figure 1.4) with water flowing through the staggered fin arrangement, capable of dissipating high heat fluxes while maintaining a low pressure drop. However, a single phase microchannel heat sink has its limitations in its heat transfer abilities, and hence a further enhancement to it would be two-phase flow in microchannel heat sink as it provides an order of magnitude increase in heat transferred and it has remained a potential solution due to its advantages such as,

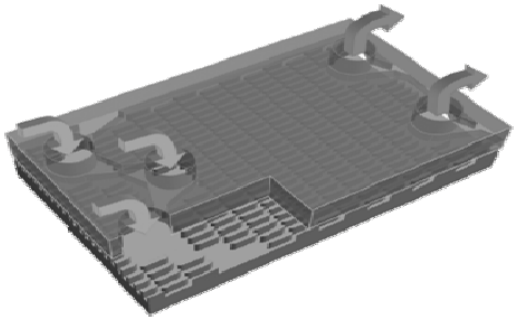

Figure 1.4 Assembled microchannel cooler (Colgan et al. [7])

- high heat transfer coefficient as it scales inversely with hydraulic diameter
- low flow rates required compared to single phase flows in channels to dissipate the same amount of heat.
- chip temperature uniformity

Microchannel thermal performance is a function of working fluids, channel geometry, size, and surface enhancements. Experiments conducted by various researchers over the last decade to investigate the effect of the above mentioned parameters on the thermal performance have led to significant results and understanding of boiling phenomena on a microscale. However, even with the availability of huge data sets, there are number of issues which impede the

practical implementation of microchannels as an effective thermal management technique:

- Discrepancy of data amongst various investigations on the transition to turbulent flow and parametric effects of flow rate, subcooling and pressure on critical heat flux (CHF).
- Flow instabilities like the parallel channel instability and upstream compressible volume instability need thorough understanding and their effects on temperature and pressure drop should be quantified.
- Lack of clear consensus on the agreement/disagreement of thermal characteristics of flow in microchannels trends with those of flow in macrochannels.

The experimental investigation conducted in this study is a step in this direction aiming to address some of these issues. The objectives of the study are to gain insight into

- subcooled flow boiling mechanisms using a high speed camera
- parametric effects of heat flux, mass flux and inlet subcooling on nucleation incipience, heat transfer co-efficient, pressure drop and flow instabilities
- flow oscillations and its effects on pressure drop and estimation of the frequency and amplitude of oscillation
- influence of channel-to-channel interactions on flow instabilities by utilizing a single microchannel
- limits of stable operation of microchannel heat sink
- friction factor and transition to turbulent flow in the microchannels.

CHAPTER 2: LITERATURE REVIEW

As discussed in the previous chapter, the rising heat flux in a microprocessor chip is of great concern which thermal engineers and scientists all over the world are trying to address. To help the reader understand the evolution of this challenge, Table 2.1 which has been reproduced as summarized by Phillips [8] lists the various single chip cooling modules that were developed in 1980s. The table shows that the maximum prevailing chip heat flux then was a mere 40 W/cm^2.

Just a couple of decades later, the challenge now is to dissipate hotspots of the order of 1000 W/cm^2 in a microprocessor. Though solutions exist in the form of micro-refrigerators , thermoelectric coolers (TEC), and microchannel heat sinks, they have been mostly confined to the research laboratories. One such novel effort was the application of thin film TECs [9] by Intel and Nextreme to cool a 1300 W/cm^2 hot spot in a microprocessor chip as shown in Figure 2.1. Although temperature reduction of up to 15°C was realized, dissipation of such high heat flux levels using a TEC often requires power input almost equal to the dissipation level. Hence, a TEC can be a useful solution to localized dissipation of hot spot but not economical otherwise and also if the location of the hot spot varies spatially during microprocessor operation.

One of the potential solutions is two-phase flow of a liquid in microchannels. A microchannel heat sink is a finned structure with the distance between the fins spanning a few hundred microns. The heat dissipated by the chip is conducted to the footprint of the

microchannels which is conducted to the fins to be carried away by the fluid by convection. The earliest study done on microchannels was in 1981 by Tuckermann and Pease [5] who constructed silicon microchannels by precision sawing and ever since microchannel heat sinks has always remained one of the potential solutions to high heat flux dissipation demands.

Table 2.1 Single chip module thermal performance [8]

Technology	Max. Chip Flux (W/cm^2)
Mitsubishi Alumina HTCP	6.26
Mitsubishi SiC	6.25
Hewlett-Packard Finstrate	10.1
Hitachi S-810	13.1
Fujitsu MCC	19.7
Burroughs PGA	24.3
Motorola MCA-2	24.5
Sperry Compact HX	40.0

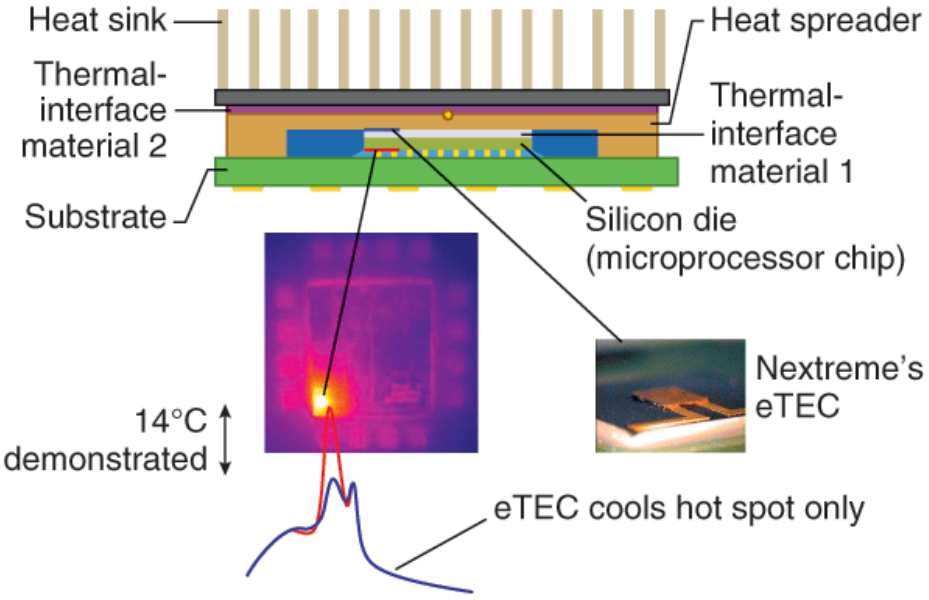

Figure 2.1 Cooling of hotspots using thin film TEC [3]

Microchannel heat sinks have remained in favor, owing to some of the advantages they offers such as:

- High heat transfer coefficients

  According to Newton's law of cooling, the heat flux dissipated by convection is,

$$q'' = h\left(T_s - T_{amb}\right) \tag{2.1}$$

  where, h is the heat transfer coefficient which is inversely proportional to the hydraulic diameter of the channel, since the Nusselt number for internal fully developed flow is a constant.

$$Nu = \frac{hD_h}{k_f} \tag{2.2}$$

- Temperature uniformity of the chip, which is due to the very high convective heat transfer coefficient and the thermal interconnection between the walls of the channel. This feature of microchannel flow is also responsible for dissipation of hot spots as shown by Revellin et al [10] who conducted numerical analysis of dissipation of hot spot heat flux using microchannel flow boiling. It was observed that dissipation of 1000 W/cm^2 at a hot spot is possible without causing dryout of the fluid over it. It was also shown that hotspot heat flux of more than 4000 W/cm^2 can be dissipated without dryout when the hotspot sizes are less than 100μm.

It is due to the aforementioned characteristics that flow boiling in microchannels is an attractive and potential solution to many applications such as uniform or non-uniform

heat flux situations arising in microprocessors that are used in modern day computers or high power electronics such as those used in hybrid and electric cars, and aircrafts.

However, transition to commercialization of the technology requires predictive techniques and models that would accurately estimate the heat transfer, pressure drop and flow instabilities for a given set of operating conditions. While empirical models are available, they have often fallen short when extended to a different experimental set up and operating conditions. One of the road blocks is the knowledge of how small the channels have to be to be considered as microchannels and whether macrochannel theories can predict the flow characteristics in a microchannel.

One of the widely used classifications of channel sizes was given by Kandlikar and Grande [11], according to which a microchannel is one with hydraulic diameter (D_h) ranging from 10μm to 200μm and a channel over 200μm was classified as a minichannel. This classification was based on rarefaction effects of gases at atmospheric pressure. However, the criterion for classification should be based on the flow behavior in the microchannel which is believed to be different from that in macrochannels. A good indicator of flow behavior would be the bubble departure diameter (d_d) and when the bubble attains the size of the channel, the resulting flow patterns and regimes are very different from those in larger channels when there is no confinement. The confinement effects however are largely a function of the fluid and its surface tension, surface characteristics and hence the classification criterion should include the bubble departure diameter. A non-dimensional number which accounts for these factors is the Bond number which is defined as,

$$Bo = \frac{g\left(\rho_f - \rho_g\right) d_d^{\,2}}{\sigma} \tag{2.3}$$

From the above expression, it can be learnt that Bond number is a ratio of buoyancy to surface tension forces the balance between which greatly influences bubble nucleation and departure. Hence, it was proposed by Cheng et al. [12] that the Bond number can be used to classify the channel sizes. For this purpose the Bond number can be thought of as a ratio of capillary length, $l_c = \left[\sigma / \mathrm{g}\left(\rho_{\mathrm{f}} - \rho_g\right)\right]^{0.5}$, to channel hydraulic diameter, D_h. Based on this ratio, a channel is classified as a microchannel if $Bo < 0.05$, a minichannel for $0.05 < Bo < 3.0$, and a macrochannel for $Bo > 3.0$. A small Bond number results in bubble diameters comparable to the size of the channel and hence influences confinement. A large Bond number results in smaller bubble departure diameter and hence does not promote confinement.

Based on this criterion, due to the employment of a highly wetting fluid such as FC72 as coolant, the channel sizes used for the present study can be considered to be microchannels.

2.1 Mechanism of boiling and heat transfer in microchannels

Flow boiling of a liquid in parallel channels has been an active area of research ever since its application in nuclear reactors and even more with its application in thermal management of electronics. One of the significant advantages is the high heat transfer rate associated with flow boiling of liquid compared to a single phase liquid flow. Also, the flow rate required is less in two-phase flow compared to the flow rate required in single phase flow to dissipate the same quantity of heat.

To illustrate the mechanism of boiling and heat transfer, a plot of wall temperature against wall heat flux boiling curve known as the *boiling curve* can be drawn which is shown in Figure 2.2 [13]. As subcooled liquid enters the channel, initially the

heat transfer is mainly by forced convection. As the heat flux increases, the wall temperature increases more than the saturated temperature. Further addition of heat, will cause bubbles to appear on the surface of the channel and this point is called as *Onset of Nucleate boiling* (ONB). This regime of boiling which is characterized by individual bubbles departing from the surface followed by condensation further downstream is known as *partial subcooled nucleate boiling*. When the coolant used is a very highly wetting fluid such as FC72, the re-entrant cavities tend to flood thereby causing a delay in ONB which leads to high wall temperatures known as temperature overshoot. This phenomenon is mainly due to the flooding of the re-entrant cavities which is mainly due to the low contact angle (approximately 1° for FC72). Once the bubble nucleation starts, the wall temperature plunges, as the departing or collapsing bubbles breaks the boundary layer and allows the cooler liquid to come in contact with the surface as shown in the Schlieren images in Figure 2.3 [14]. The high heat transfer is also due to the thin layer of liquid called the '*microlayer*' which vaporizes instantly leading to a sharp drop in wall temperature. In subcooled nucleate boiling, which is mostly the regime concentrated upon in this study, the heat transfer is also aided by thermocapillarity as shown by Brown [15]. Thermocapillarity is the movement of the interfacial liquid film surrounding a bubble, due to a variation in surface tension caused by a temperature gradient in the liquid film. This phenomenon is illustrated in Figure 2.4.

Beyond the ONB, a small increase in wall temperature causes a large increase in wall heat flux, thus illustrating the heat dissipation capabilities of two-phase flow. Further increase in heat flux leads to an increase in bubble departure diameter and in a microchannel this leads to confinement of the bubbles depending on the fluid being used. Further addition of heat, leads to annular flow, where the core of the channel is filled with vapor with a thin layer of liquid separating it from the walls.

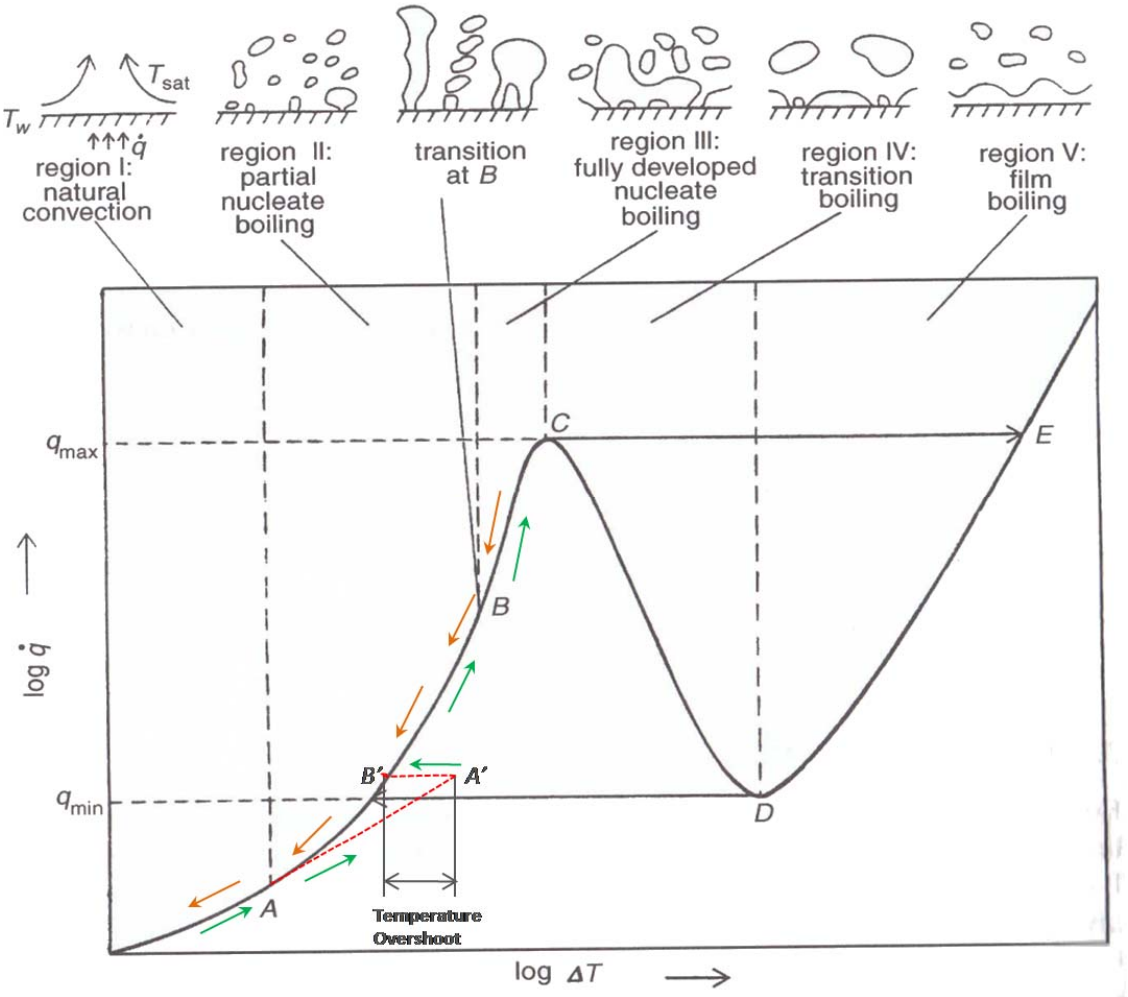

Figure 2.2 Boiling curve for a highly wetting fluid (A-A'-B'-B - C-E) compared to a conventional boiling curve (A–B–C-E) ((Dhir [13])

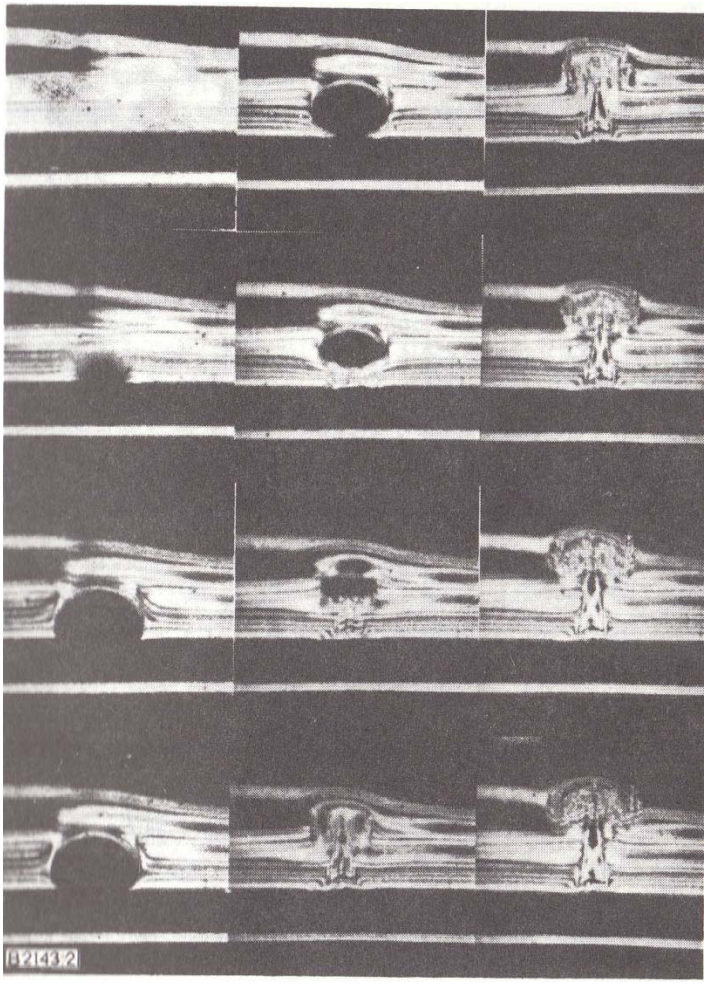

Figure 2.3 Schlieren Images showing the bubble nucleation process in a subcooled pool and the associated boundary layer (Bahr [14])

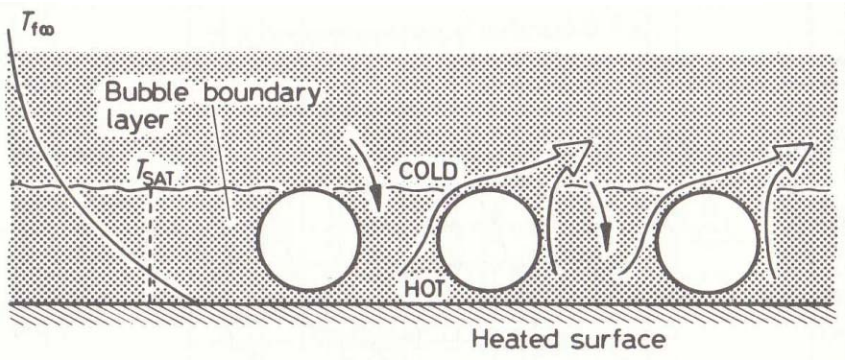

Figure 2.4 Thermocapillarity in subcooled nucleate boiling observed by Brown [15]

Figure 2.5 and Figure 2.6 show the difference between boiling flow regimes in narrow/mini and large channels. In a conventional channel, the slug and annular regimes appear separately whereas in narrow channels, the slug and annular flow appear simultaneously at times as demonstrated by Kandlikar et al. [16] in the case of water. Any further addition of heat will lead to the evaporation of liquid film resulting in *partial dryout*. These flow regimes will be different for FC72 wherein bubbly flow regime will dominant and confinement will be less pronounced compared to water for the same diameter of channel. Two important phenomena along the boiling curve for a highly wetting fluid are ONB and temperature overshoot marked by A' and A'-B' respectively in Figure 2.2.

2.2 Onset of Nucleate Boiling (ONB)

The ONB which marks the transition between single phase and two-phase flow is a very important phenomenon to be analyzed as it forms the upper limit for single phase flow and the lower limit of two-phase flow. The prediction of ONB is paramount in the characterization of any two-phase system. Studies in the past such as one conducted by Bergles and Rohsenow [17] considered a hemispherical bubble and extended the classic Hsu nucleation incipience model, to postulate a correlation for the incipient heat flux. Sato and Matsumura [18] and David and Anderson [19] proposed correlations that were also a function of contact angle and agreed well with the correlation provided by Bergles and Rohsenow over a wide range of pressures and heat flux values. Although these models are accurate for a surface with wide range of cavity sizes [6], they do not perform well in the case of microchannels and highly wetting fluids. However, even a microchannel-flow specific model proposed by Liu et al [20], which was a function of

contact angle, flow velocity, inlet subcooling, microchannel dimensions and fluid exit pressure, and the model developed by Qu and Mudawar [21] over predict the ONB by a

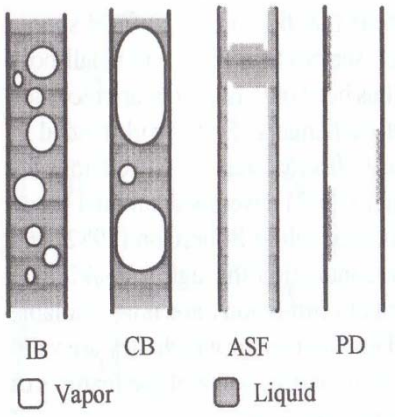

IB – Individual Bubbles
CB – Confined Bubbles
ASF – Annular Slug Flow
PD – Partial Dryout

Figure 2.5 Boiling flow regimes in narrow channels observed by Kandlikar et al [17] for water.

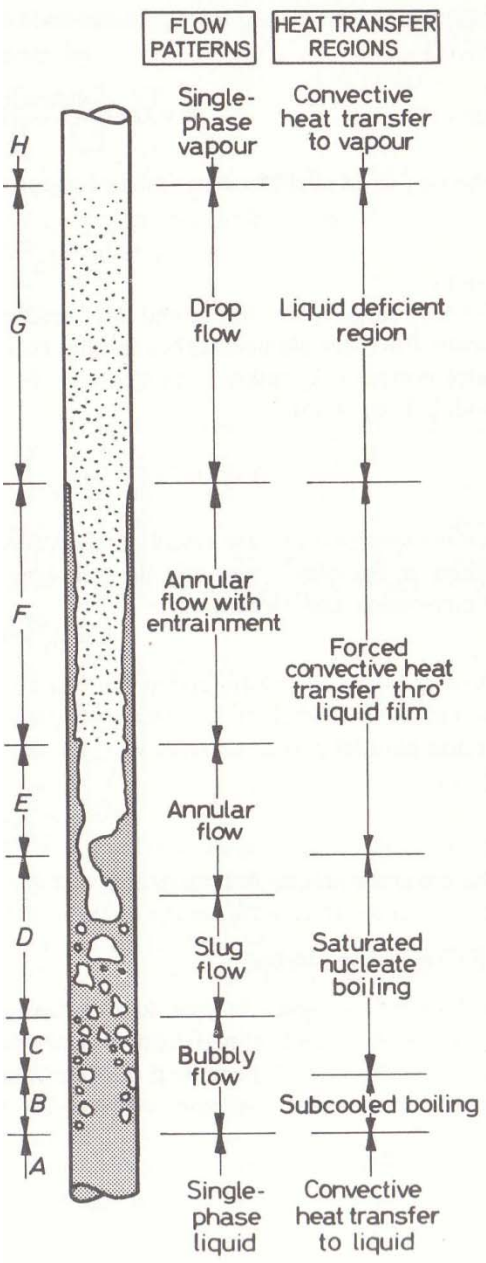

Figure 2.6 Boiling flow regimes in large channels [16]

large margin, which might be attributed to the effectiveness of the re-entrant cavities in triggering ONB. Hence, characterization of ONB is still limited to empirical data and

experimental observations and illustrates the need for further research in this area. Studies in the past have investigated the parametric effects of mass flux, cavity size and spacing on ONB.

Jones et al. [22] conducted two-phase flow boiling experiments in surface enhanced microchannels of width 200μm with FC 72 and analyzed the effect of mass flux on the incipient flux to show that the incipient heat flux increases with increasing mass flux. Similar studies were conducted by Liu et al. [20], on microchannels that were 275μm wide and 636μm deep with water as working fluid. Experimental results for ONB were presented and a model for ONB was developed which was a function of contact angle, flow velocity, inlet subcooling, microchannel dimensions and fluid exit pressure.

2.3 Temperature overshoot or nucleation hysteresis

A phenomenon which accompanies ONB in flow boiling of highly wetting fluids is called the temperature overshoot. Highly wetting fluids flood cavities because of low contact angle resulting in a high wall superheat to initiate ONB. It is an important phenomenon that requires thorough understanding and research since excessive wall temperature cannot be tolerated, especially in electronics cooling applications. Thorough study of temperature overshoot and its mitigation in pool boiling was carried out successfully by altering the surface condition by Nimkar et al. [23]. However, available literature on hysteresis in flow boiling in microchannel is very limited. Pate [24] studied the effect of mass flux on hysteresis and observed that increase in mass flux results in the mitigation of temperature overshoot. Similar trends were also reported by Lie and Lin [25] who performed flow boiling experiments using R-134a in narrow ducts. It was also observed that 7°C increase in liquid subcooling caused an overshoot reduction of 5°C

(Figure 2.7). Contrary to these findings, experiments conducted by Piasecka and Poniewski [26] in vertical microchannels of depth 1mm and width 40 mm, to study the boiling incipience and the associated hysteresis, showed that the effect of mass flux on temperature overshoot had no consistent trend.

The current study aims to further analyze the effect of mass flux and inlet subcooling on temperature overshoot.

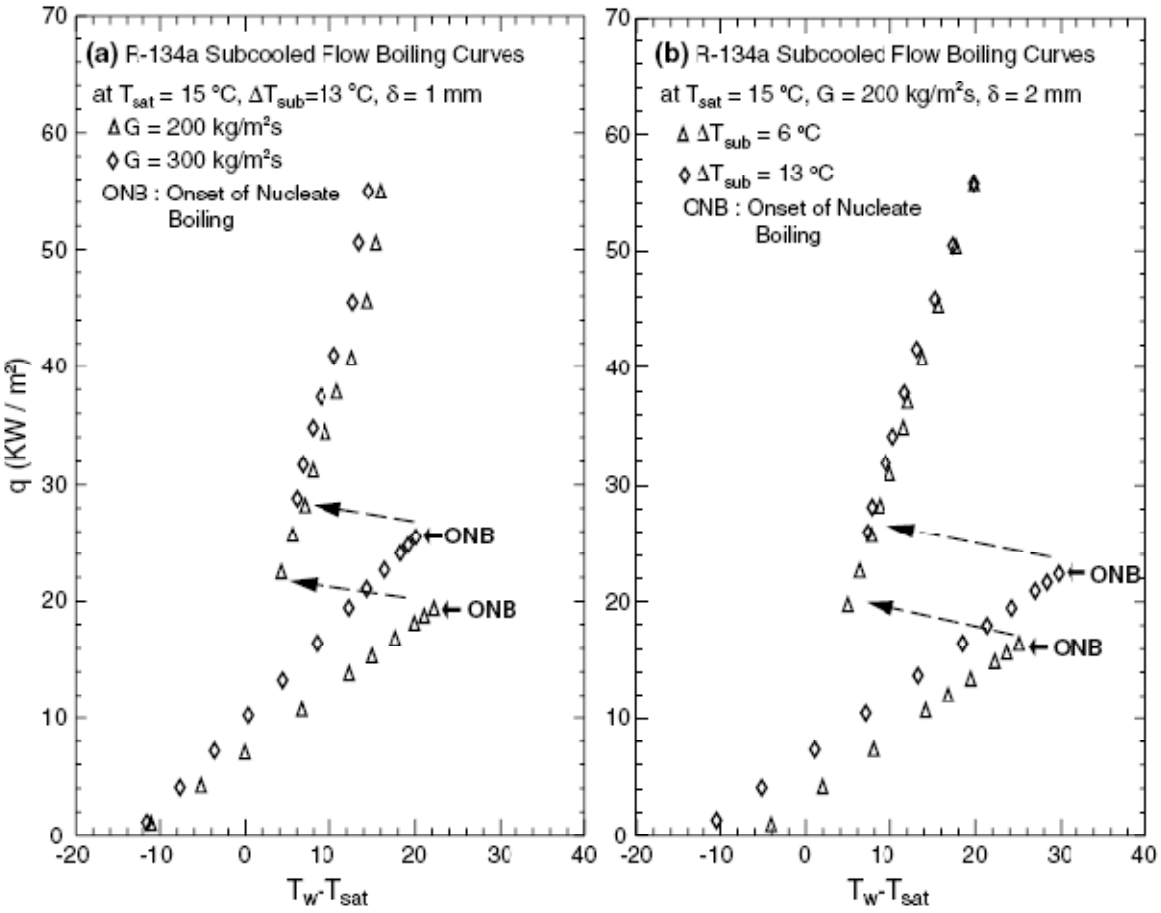

Figure 2.7 Effect of mass flux and subcooling on temperature overshoot (Lie and Lin [26])

3.1 Effect of surface on microchannel flow boiling

As discussed earlier, microscale surface irregularities such as pits and cavities on the surface serve as vapor trapping sites and help initiate heterogeneous nucleation at

relatively low wall superheats. This role of the surface in promoting boiling is paramount in electronics cooling applications since a low wall superheat also leads to a lower junction temperature in the microprocessor being cooled. The bubble nucleation process is related to the geometry of the cavity containing trapped vapor. The mouth diameter of the cavity defines the embryonic bubble size, and hence, the wall superheat at which the cavity will be activated. In a saw cut copper surface, the size of the cavities range from 1 – 100μm, and on a silicon surface fabricated by standard etching processes, the surface roughness is of the order of 100nm. Inception of boiling on such smooth surfaces takes place at the corners of channel walls which act as vapor trapping sites and the heat flux at ONB is higher compared to a rough surface. Hence, surface enhancement by fabricating artificial vapor trapping sites such as cavities augment the heat transfer as demonstrated by Nimkar et al [23]. Further, the stability of a trapped vapor nucleus is also determined by the cavity's shape. Naturally occurring pits or scratches due to the fabrication process possess a conical cross-section. To further enhance the vapor trapping abilities of the surface, cavities of various types such as bulb shaped [27], and pyramidal re-entrant type []were fabricated, tested and compared with plain surfaces by researchers at the Heat Transfer Research Laboratory at Auburn University. Figure 2.8 and Figure 2.9 show images of cavities of various cross-sections constructed.

Two primary parameters that affect the rate of heat transfer during boiling are the bubble diameter at departure and the frequency of departure of the bubbles, since the inception and departure affects the thermal boundary layer. Bubbles departing from closely spaced cavities tend to coalesce and hence spacing of the cavities also plays an important role in heat transfer enhancement.

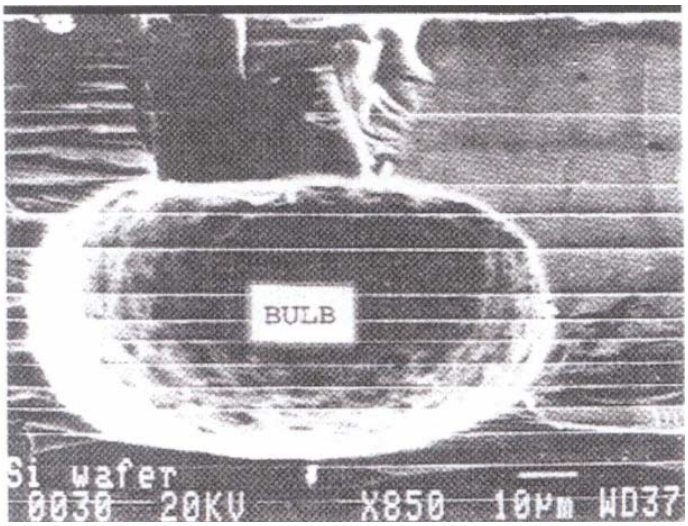

Figure 2.8 Re-entrant cavity with a bulb shaped cross-section fabricated by Baldwin [27]

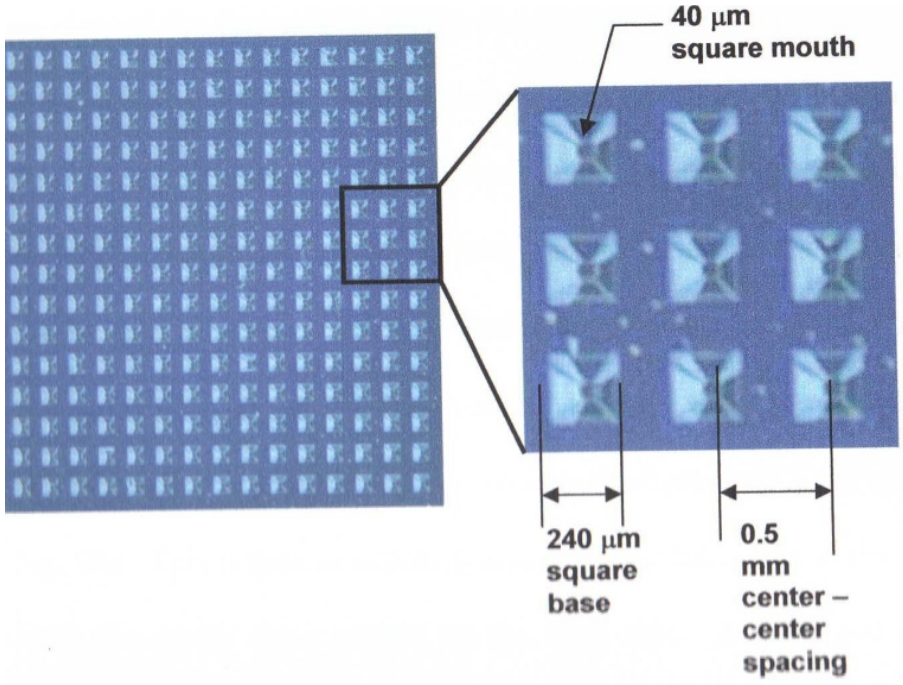

Figure 2.9 Pyramidal re-entrant cavities fabricated by Nimkar [28]

Nimkar [28] conducted pool boiling tests using FC72 on surfaces enhanced by pyramidal re-entrant cavities of varying center-to-center spacing. It was observed that, as spacing between the cavities increased, the bubble coalescence decreased and hence increased the CHF due to dryout under the bubble. Also, the temperature overshoot associated with nucleation incipience decreased as the spacing increased as shown in Figure 2.10. Pate [24] extended the usage of such pyramidal cavities to microchannel flow boiling, and analyzed the effect of density of re-entrant cavities (two cavities per channel and six cavities per channel) on flow boiling heat transfer in the microchannels. Like the results of Nimkar [28], the sparse cavity arrangement (two cavities per channel) yielded higher heat transfer co-efficient than the dense cavity arrangement (six cavities per channel) for a given heat flux, mass flux and inlet subcooling.

The general advantages of the cavities can be summarized:

- Cavities promote nucleation at low heat flux and low wall superheat.
- By controlling the spacing and size of cavities, CHF can be increased.

Similarly, surface enhancement in the form of cylindrical re-entrant cavities both isolated and interconnected in microchannel surfaces shown Figure 2.11 were tested by Kosar et al [29] yielding a 50% reduction of incipient heat flux compared to a plain surface without cavities. Kandlikar et al. [30] fabricated pits of size 100μm by using punches on the surface of microchannels as shown in Figure 2.12 to analyze its effects on nucleation incipience and flow instabilities.

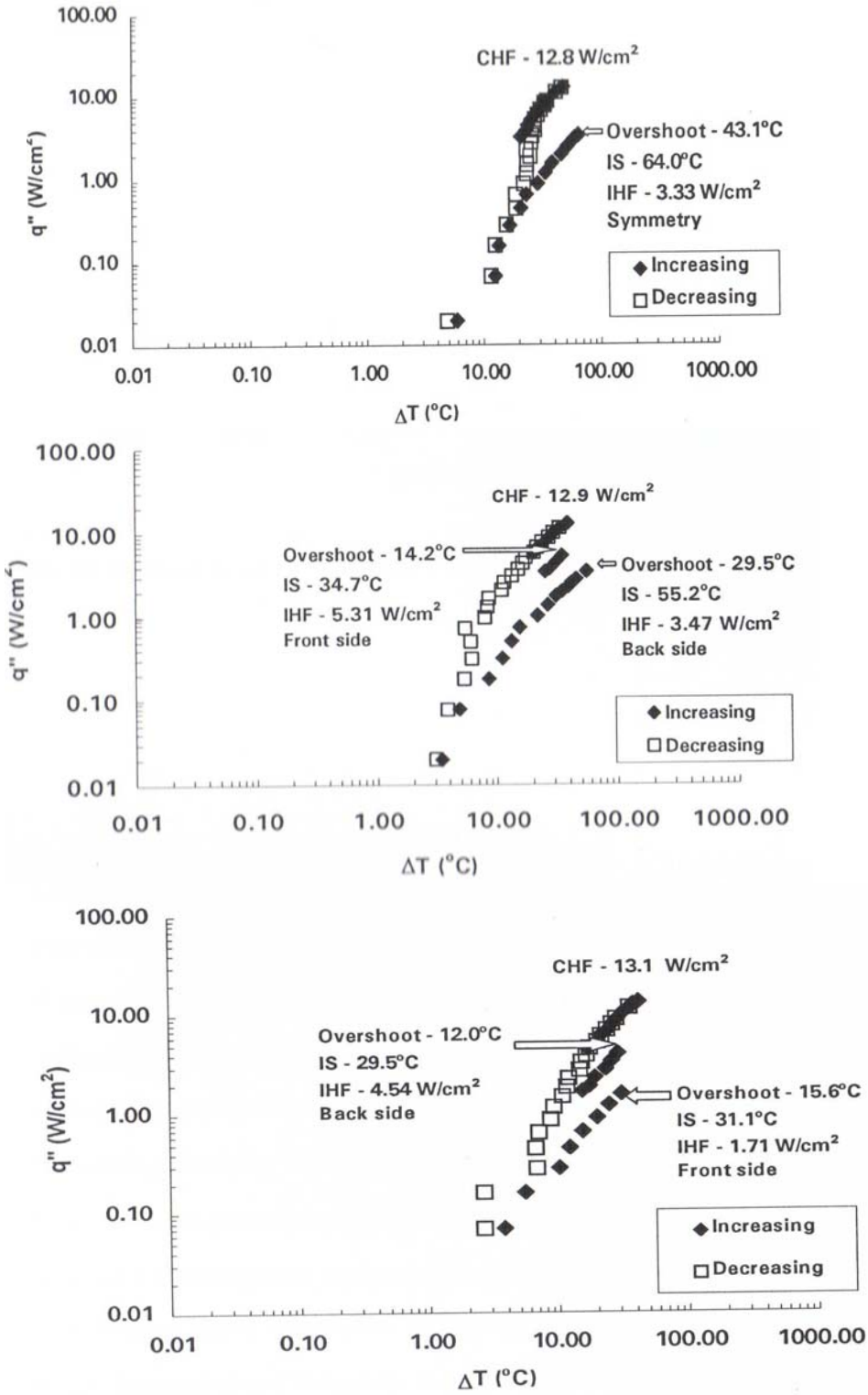

Figure 2.10 Effect of cavity spacing on temperature overshoot (a) Center to center spacing of 0.5 mm (b) 0.75 mm (c) 1 mm (Nimkar[28])

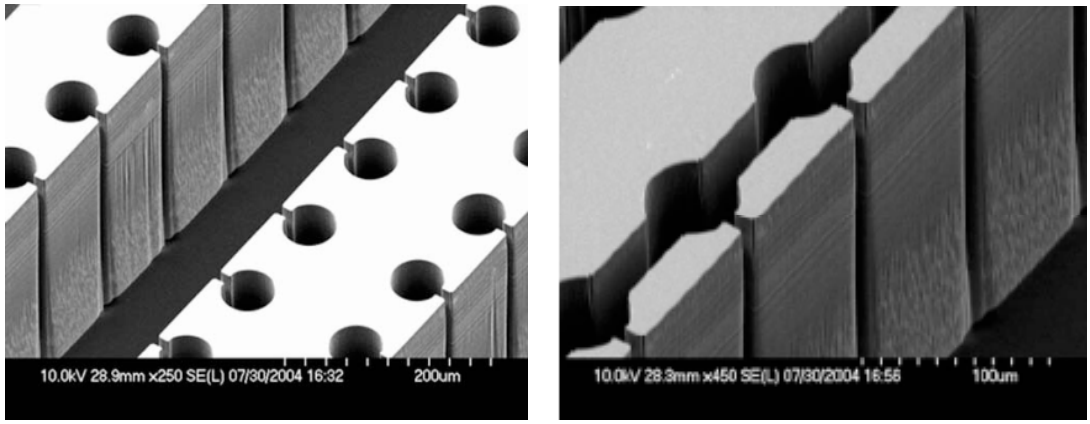

Figure 2.11 Nonconnected and interconnected re-entrant cavity microchannel [29]

Figure 2.12 Nucleation cavities formed in microchannels by punches [30]

2.4 Choice of coolant for electronics cooling applications

A wide range of working fluids have been used in microchannel research. Some of the essential characteristics that a coolant used in electronics thermal management applications must possess include

- High latent heat of vaporization

  This is one of the most important properties that directly indicates the heat carrying capacity of the liquid while boiling. Liquids with low latent heat of vaporization have to flow at a higher flow rate to remove the same quantity of heat and hence placing additional load on the coolant pumping system.

- A boiling point preferably in the range of 20-80°C [31]

  A very high boiling point is disadvantageous in phase change cooling systems as the temperature attained by the device being cooled by the time boiling is achieved is significantly high which might cause a failure of the device. Use of highly boiling point liquids, hence, substantiates the need for sub-atmospheric conditions to lower the boiling point. Conversely, a very low boiling point coolant will cause condensation problems and hence requires a pressurized container.

- High dielectric strength

  High dielectric strength prevents any current flow through the liquid, thereby avoiding any damage to the IC by short circuit.

- Low environmental impact

  Choloroflourocarbons (CFCs) which were thought to be as safe alternatives for ammonia based refrigerants were found to cause depletion of the atmospheric

ozone layer and possesses global warming potential. Hence a coolant used in phase change system should have zero or very low environmental impact to comply with global protocols to safeguard the environment.

With these properties and constraints taken into careful consideration, a wide range of coolants have been used and developed to be used as electronics cooling liquid. Some of the most widely used coolants for electronics thermal management and their properties have been tabulated in Appendix A. Most single phase studies have rightly chosen water for its excellent heat transfer properties but water poses a problem during two-phase boiling for electronics applications. The atmospheric boiling point of water is too high for reliable electronics cooling. This is one of the reasons why the electronics cooling community has turned its attention to Fluorinert coolants and refrigerants for their low boiling point and dielectric characteristics. Also, bubble sizes in dielectric fluids are an order of magnitude smaller and therefore lead to bubbly flow and/or slug flow patterns over the flow passage which is reported by Mukherjee and Mudawar [32]. The advantages offered by bubbly flow in the context of stability will be discussed in Chapter 4.

Liquid cooling of electronics can be classified as direct and indirect. Indirect cooling, as the name implies does not involve any contact between the coolant and the IC or the microprocessor being cooled. Instead, it involves the usage of a thermal interface material (TIM) which in turn comes in contact with the coolant. Cooling using water falls under this category because of its low dielectric strength and corrosive nature. Direct contact cooling on the other hand, obviates the thermal resistance involved with the TIM. Perflourocarbon coolants such as FC72 permit this type of cooling owing to a high

dielectric strength and non-corrosive nature. IBM in 1970s developed the *Liquid Encapsulated Module* (LEM) which used FC72 as a pool of coolant into which the system to be cooled was submerged. Similar flourocarbons which offer the same advantages include FC 77 which has been tested by Harirchian and Garimella [33] and FC 84 tested by Warrier et al [34].

Some of the drawbacks of dielectric coolants are the very poor heat transfer properties as well as an extremely low surface tension. ONB is typically triggered by a scratch or imperfection in the heated surface that trap existing vapor. Bergles and Kandlikar [35] suggest that by having a low surface tension as dielectrics do, the vapor triggering sites have a tendency to be flooded out postponing ONB and causing large temperature overshoots. This phenomenon is portrayed in the flow boiling data presented by Bowers and Mudawar [36] that used R-113 as their working fluid. Other commonly used refrigerant used in microchannel cooling include R-134a which has been used as the working fluid in a number of studies in the literature [x-y].

The choice of fluids also directly affects the observed flow patterns in microchannels and thereby also affects the stability of the flow. Water which possesses a higher contact angle, produces bubbles more spherical and larger [] compared to FC72 and other fluorocarbons and hence promotes slug flow which tends to fill up the cross-section of the channel, which in turn causes flow reversal in the channel, the causes and effects of which will be discussed in the sections following. While flow instabilities remain a challenge in two-phase microchannel flow boiling, even in single phase flow of liquids through narrow or micro channels have posed interesting questions pertaining to the adherence to conventional theories of flow through macro channels.

2.5 Single phase flow of liquid through microchannels

Several investigators have noticed anomalies in flow behavior in microchannels, including the earliest study on the single phase forced convection study conducted by Tuckerman and Pease [6]. The investigations by Wu and Little [37] and Choi et al. [38] on gas flow in microchannels have shown that the friction factors (*f.Re*) for laminar flow deviated from the conventional theories existing for macrochannel flow.

Peng et al. [39] studied the flow of water in rectangular microchannels with hydraulic diameters of 0.133-0.367 mm observing that the friction factors for flow in microchannels deviated from the theoretical predictions as the channel size reduced. It was also observed that the flow transition from laminar to turbulent occurred at *Re* = 200-700 compared to the conventional transition Reynolds number of 2300. Early transition to turbulence at *Re* = 750-1250 was also reported by Xie et al. [40] who conducted single-phase forced convection experiments with FC72 and ethanol in parallel microchannels.

However, investigations by Garimella and Singhal [41] on flow in microchannels of hydraulic diameters 250-1000μm, showed that the conventional macrochannel theories predicted both the friction factors and flow transition to good accuracy. Particle Image Velocimetry (PIV) measurements were done by Lee et al. [42] on an acrylic microchannel of hydraulic diameter 380μm yielding laminar profiles up to *Re* = 2100. Hao et al. [43] showed that the early transition (*Re* < 900) occurred due to roughness elements and transition in smooth channels still occurred at $Re \approx 2100$.

To address these concerns and to gain further understanding of flow through microchannels, the current study includes an analysis of the single phase flow of FC72 through microchannels of various dimensions.

Some of the properties of the fluid, that directly affect the heat transfer in microchannels include the temperature of the coolant at the inlet i.e. the inlet subcooling, and the mass flux of the coolant, the effects of which will be described in the subsequent sections.

2.6 Effect of coolant mass flux

In single phase flow of the working fluid, increase in mass flux will cause the heat transfer to increase, as the Nusselt number (*Nu*) is directly proportional to the Reynolds number (*Re*) raised to the power of one half in the case of laminar flow and four-fifth in the case of turbulent flow [44].

However, in the case of two-phase flow the relationship between heat transfer and mass flux is not always directly proportional, and depends more on the flow regime. In the case of fully developed nucleate boiling increasing the mass flux will produce no effect on the heat transfer as observed by Harirchian and Garimella [33]. This is due the fact that increase in mass flux results in increased convection effects which tends to reduce the wall temperature thereby suppressing the bubble nucleation process. In the case of partial nucleate boiling regime, increase in mass flux will produce an increase in heat transfer, although not significant, which will be shown in the *Results and Discussion* section of the current study. At higher heat flux, in the convection dominated flow regime, heat transfer increases with increase in mass flux.

Mass flux of the fluid also directly affects the single phase and two-phase pressure drop. In both single and two-phase, increasing the mass flux produces an increase in pressure drop as shown by previous studies at HTRL conducted by Jones et al. [22]. However, as discussed earlier, increasing the mass flux suppresses bubble nucleation and hence delays ONB too. This phenomenon at times results in the reverse trend which will be discussed later in the *Results and Discussion* chapter. By affecting the flow pattern, the mass flux also affects the flow instabilities. Operating at high mass flux, allows the flow to remain in bubbly flow and hence prevents slug formation thereby preventing or reducing flow instabilities. To further substantiate this, the results obtained in the current study show that no or very little flow instabilities were observed and hence high mass flux is a favorable operating region for the microchannel heat sinks.

2.7 Effect of inlet subcooling

The effect of the temperature of the fluid at inlet on the heat transfer is one of the important topics that will be analyzed in the current study. When the flow enters at very low inlet subcooling i.e. high temperature, the heat flux required for inception of boiling is very low and because of the higher wall superheat, the heat transfer coefficient will be low at a given quality. As the inlet subcooling increases, the wall temperatures decrease for a given heat flux and results in higher heat transfer co-efficient at a given quality. Like mass flux, the effect of inlet subcooling on the heat transfer also depends on the flow regime.

At fully developed nucleate boiling conditions, inlet subcooling has no effect on the heat transfer. This is because as the inlet subcooling increases, the process of bubble nucleation is suppressed to some degree and hence although heat transfer enhancement

by the bubbles is reduced, it is compensated by the increase in heat transfer due to low liquid temperature or high temperature difference between the wall and fluid.

Due to the suppression of boiling at high inlet subcooling, the pressure drop will also be affected and consequently the flow instabilities. Hence increase in subcooling decreases the two-phase pressure drop, which will be shown in the current study. It will also be shown that the instabilities reduce at low inlet subcooling owing to the reduced subcooled boiling regime which is conducive for bubble collapse which is being hypothesized as one of the causes of flow instabilities. The following section describes the phenomenon of flow instabilities elaborately.

2.8 Flow instabilities

From the previous sections, it can be concluded that the factors influencing microchannel thermal performance such as working fluids, channel geometry, size, and surface enhancements is generally well understood owing to the data sets available from experiments conducted over the last decade. However, there are a number of issues that need to be sorted out before flow boiling in microchannels can become an effective thermal management solution. Some of them as identified by Thome [45] include a better understanding of flow boiling instabilities in microchannels, more critical heat flux data, and the effect of non-uniform heat flux and inlet header geometries on flow pattern. One of the primary objectives of the current study is to gain a thorough insight into flow instabilities and its characterization, and the influencing factors.

Flow instabilities in a parallel channel flow system can generally be classified as static and dynamic. Static instabilities which are excursive in nature, were studied as early as 1940 by Ledinegg [46] in nuclear reactors. Ledinegg instability may occur when

boiling initiated in one of the channels causes redistribution of flow to others causing flow deprivation in the hot channel leading to CHF in the form of *departure from nucleate boiling* (DNB). It has been determined in the past by Maulbetsch and Griffith [47] and many other investigators that such instabilities arise when the gradient of the system pressure drop plotted against flow rate curve, also known as the *demand curve* becomes more negative than the gradient of the external pump curve. This expressed as,

$$\frac{d(\Delta P_{external})}{dQ} > \frac{d(\Delta P_{demand})}{dQ} \tag{2.4}$$

In microchannel flow boiling, an instability that is closely related to the aforementioned kind is a parallel channel instability, which arises due to the development of vapor slugs which fill the entire channel causing the flow to reverse. This was discussed by Kandlikar et al. [30], who conducted flow boiling experiments with water in parallel rectangular microchannels of hydraulic diameter 332 μm. This phenomenon of parallel channel instability is shown in Figure 2.13.

Dynamic instabilities can be classified into three types as given by Stenning [48] – density wave type, pressure drop type and thermal oscillations. These type of instabilities, also termed *compressible volume instability,* are mainly due to the interaction between vapor generation in the channels and a compressible volume present upstream of the microchannels [49].

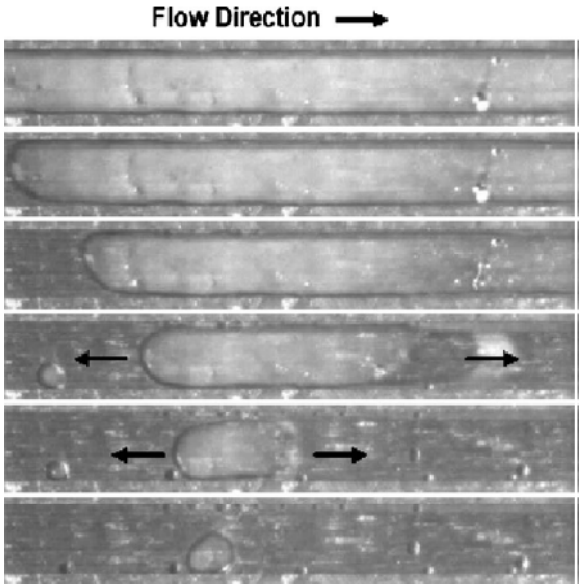

Figure 2.13 Parallel channel instability in microchannels observed by Kandlikar et al. [30]

The problem of flow instabilities in microchannel flows is protracted further by the resulting fluctuations in pressure drop as well as spikes in wall temperature owing to the premature dryout caused, with some studies such as Hetsroni et al. [50] and Hetsroni et al. [51] reporting variations in surface temperature as high as 20°C. Other investigators have reported that these fluctuations have extremely long periods lasting several tens of seconds (Wu and Cheng, [51]). Figure 2.14 shows local temperature fluctuations observed during unstable flow in microchannel devices with and without cavities [52]. Existing theories on reasons for the instabilities are based on the formation of randomly sized vapor slugs in specific microchannels leading to increased pressure drops in those channels, and a consequent reduction of flow rate. The reduction of flow rate in some channels precipitates an increase in flow through the other channels reducing the likelihood of formation of vapor. These patterns oscillate as local temperatures fluctuate. Studies have shown that these instabilities can be caused by the *channel-to-channel*

interaction i.e. conduction interactions between microchannels and also significantly by the design of inlet headers.

However, it has been shown that these instabilities can be significantly reduced or even eradicated in microchannel flow boiling by using pressure drop elements in the form of flow restriction elements such as inlet orifices which was shown experimentally by many investigators.

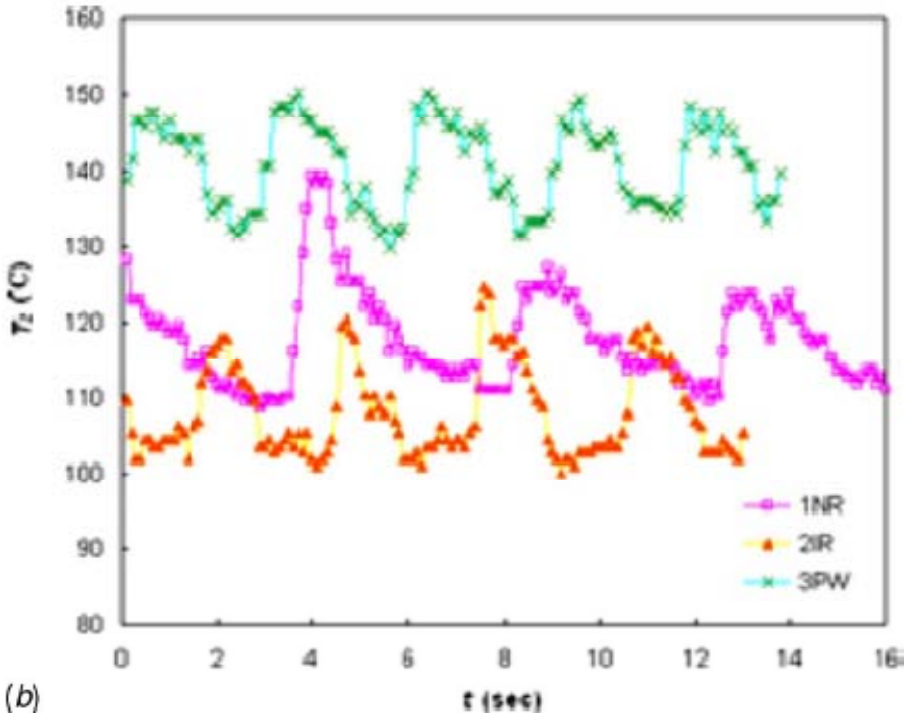

Figure 2.14 Local temperature fluctuation during unstable flow observed by Kosar et al. [29]

Kosar et al. [29] conducted flow boiling experiments in parallel microchannels of width 200µm and height 265µm, to investigate the effects of orifice geometries in suppressing the flow instabilities. The flow restrictors employed, suppressed the instabilities efficiently and pressure fluctuations were less than 1kPa. Similarly flow restrictors were also employed by Kandlikar et al [30] and Lee and Mudawar [53]. However, it was observed that such measures also lead to an increase in pressure drop.

The flow instabilities arising due to the formation of vapor slugs in the channel can be eradicated by controlling the nucleation process using artificial nucleation sites in the form of re-entrant cavities. Experiments conducted by Kandlikar et al. [30] demonstrated that by the employment of a combination of pressure drop elements and artificial nucleating cavities, significant reduction in flow instabilities can be achieved. However, use of artificial cavities alone were found to increase the instabilities which is contrary to the findings of Zhang et al. [54], where cavities acted as stable nucleating sites and helped in alleviating the flow instabilities. It has also been demonstrated by studies conducted at HTRL at Auburn University by Jones et al. [55] that instabilities were completely eliminated when the flow regime at the exit was saturated and also under certain subcooled conditions. The instability due to slug formation was completely eradicated due to the controlled release of bubbles by the re-entrant cavities and the low contact angle of FC72 which results in low bubble departure diameter, thereby resulting in bubbly flow. The current study will corroborate this observation in the later sections.

Since modeling of flow instabilities have proven to be difficult due to the complex nature of two-phase flow, characterization and prediction of *onset of flow instability* (OFI) based on experimental data and empirical relations is of great importance to avoid premature dryout which will cause failure of the system being cooled. Significant amount of research has been done to achieve this in the field of nuclear reactors to prevent burnout and recently in microchannel flows.

Kennedy et al. [56] conducted experiments to predict the onset of flow instability in a circular geometry and the results indicate that the Saha and Zuber correlation over

predicted the heat flux at the onset of fluid instability for Peclet numbers below 25000, but good agreement was found with experimental data for higher Peclet numbers.

Numerical analysis of flow instabilities was carried out by Chavan et al. [57] to predict the onset of flow instabilities and identify the regions of stable and unstable flow.

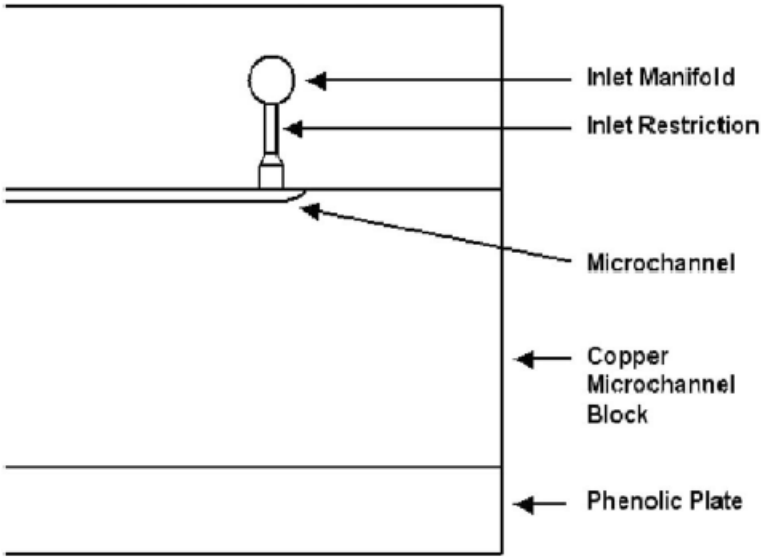

Figure 2.15 Cross section of inlet restrictor used by Kandlikar et al. [30]

To effectively eliminate the flow instabilities and mitigate their effects and to arrive at theoretical predictions a thorough understanding of the flow oscillations is required. To achieve this, it is beneficial to isolate the causative mechanisms such as channel-to-channel interaction and flow maldistribution, which can be accomplished by studying the flow boiling in single microchannel test devices.

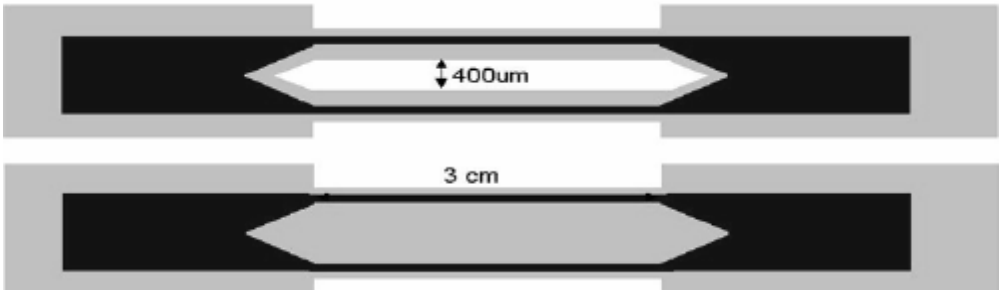

Figure 2.16 Thermally isolated and thermally connected channels fabricated by Flynn et al. [58]

Zhang et al. [54] constructed single and multichannel test sections out of silicon and comparison of pressure drop and wall temperature measurements were made. It was observed that the pressure drop difference between the devices was negligible.

An in-depth analysis of channel-to-channel interaction was conducted by Flynn et al. [58] who constructed two parallel microchannels with the ability to connect the channels thermally and with fluidic connections as shown in Figure 2.16. It was observed that connecting the walls thermally, increased the instability of the system. Similar results have also been obtained in the present study which will be discussed later.

Flow boiling of water in a single polydimethylsiloxane (PDMS) channel was studied by Huh et al. [59]. Flow oscillations with long periods and amplitude were observed and they were attributed to the transition between bubbly/slug and slug/semi-annular regimes.

2.9 Summary of literature review

In the light of the literature reviewed for the study, it can be highlighted that flow boiling in microchannel heat sinks is a very attractive thermal management technique owing to its high heat transfer along with a number of advantages that it offers over other techniques and single phase flow.

It has been proven by Nimkar [28] and Pate [24] that heat transfer in microchannel heat sinks can be further enhanced using surface enhancement techniques like employment of reentrant cavities. It was observed that these cavities also serve other purposes such as early inception of ONB, and mitigation of temperature overshoot as demonstrated by Jones et al. [22] and Nimkar [28] respectively. Pate [24] and Liu et al. [20] also demonstrated that ONB could be triggered early by decreasing mass flux and

decreasing the inlet subcooling. Similarly, it was shown by Lie and Lin [25] that temperature overshoot can be mitigated by increasing the mass flux and decreasing the inlet subcooling. The current study also investigates the influence of system variables on ONB, nucleation hysteresis, heat transfer coefficient and pressure drop.

However, one of the significant challenges in the application of two-phase microchannel heat sinks is flow instabilities. Investigators have noticed different kinds of flow instabilities such as parallel channel instability [30] and upstream compressible volume instability [49] to name a few. However, these instabilities can be mitigated by the use of flow restrictors as demonstrated by Kandlikar et al. [30] and Kosar et al. [49], but they also resulted in a large pressure drop. It was demonstrated by Jones et al. [55], that by the employment of reentrant cavities, the bubble release can be controlled and hence instabilities due to slug formation can be eliminated without a significant rise in pressure drop. However, it was observed that the flow instabilities did exist under subcooled exit conditions which are attributable to vapor condensation in the channel as shown by Liu and Peng [60]. One of the primary goals of the study is the characterization of instabilities and to understand the influence of system variables on it.

To completely eliminate the instabilities, a deep understanding of the phenomenon is required which requires the causative mechanisms such as channel-to-channel interaction to be isolated. Such measures include construction of single microchannel as demonstrated by Flynn et al. [58]. It was shown that instabilities reduced in an isolated single microchannel thus underlining the role of thermal interaction between the channels. On this basis, one of the objectives of the current study is to compare the flow boiling process in a single and multichannel test device , thus leading to

a thorough insight of flow instabilities and its causative mechanisms. To achieve this important goal, high speed video footage and data from pressure transducers will be utilized.

CHAPTER 3: EXPERIMENTAL SETUP

The test-devices used for the flow boiling experiments fall into two categories - multichannel configuration and single channel configuration. Each configuration can further be classified based on the width of the channels and the number of cavities in each channel. The matrix in Table 3.1 shows the physical characteristics of various microchannel test sections used. The sections following will discuss the geometric characteristics of the test devices used and the flow loops associated with the corresponding test device.

Table 3.1 Geometry of test devices used

Test Section	No. of channels	L_c (µm)	W_c (µm)	H_c (µm)	D_h (µm)	W_f (µm)	No. of cavities/ channel
Multi channel (MC 200-2)	19	10000	200	347	253	320	2
Single channel (SC 100-2)	1	10000	100	347	155	NA	2
Single channel (SC 100-6)	1	10000	100	356	156	NA	6
Single channel (SC 400-2)	1	10000	400	317	353	NA	2
Single channel (SC 400-6)	1	10000	400	321	356	NA	6

3.1 Multichannel configuration

The multichannel arrangement consists of nineteen parallel microchannels spread over an area of 1cm x 1cm. The channels were fabricated from a silicon wafer using a process known as *Deep Reactive Ion Etching* (DRIE). Each channel is rectangular in cross-section and has a width of 200µm and a depth of 346µm. The geometric characteristics of the multi-microchannel test sections used is shown in the matrix in Table 3.1 and illustrated in Figure 3.1.

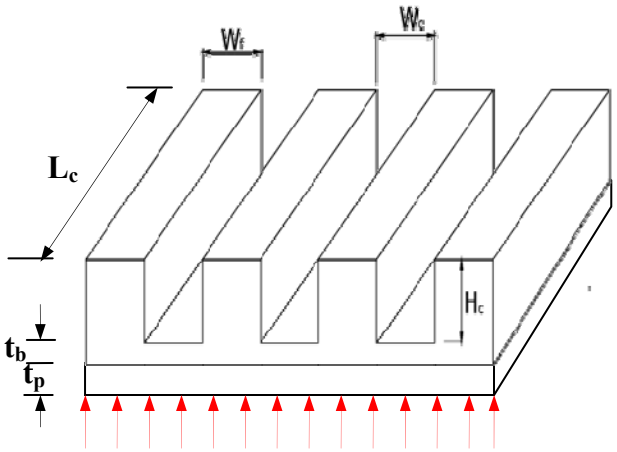

Figure 3.1 Schematic of a multichannel test device

One of the salient features of the heat sink is the reentrant cavities formed at the base of the channel, which are used to trigger nucleation in the channels. The pyramidal shaped cavities were fabricated by anisotropic etching, which has been in discussed by Pate [24]. Each cavity has a square mouth of size 20 µm and a corner angle of 54.6°.The cavities in a channel were distributed equidistant from each other in two different ways – a dense configuration which consisted of six cavities and a sparse configuration with two cavities per channel. An image of the cavity-enhanced microchannels with sensors is shown in Figure 3.3. However, results produced in this study pertain only to the sparse

configuration and those pertaining to dense configuration have been published in [22]. Figure 3.1 represents the schematic of a multichannel test device used for the study.

The heat sink was sandwiched between a top Pyrex® glass wafer comprising the Resistance Temperature Detectors (RTD) and a bottom Pyrex® wafer comprising the heaters, and this Pyrex®-Silicon-Pyrex® structure was bonded together by a process known as anodic bonding. The twelve RTDs in the top Pyrex were used for temperature measurement of fluid along the channel, with four each spaced equally in three selected microchannels (two adjacent channels to study the effect of channel-to-channel interaction and a channel at the end of the heat sink), as shown in Figure 3.3. However, data obtained from these sensors were not used for the analysis and hence out of scope of this study. In the bottom wafer, seven Aluminum serpentine heaters connected in series covered the foot print of the microchannel test section. The voltage measurements tapped at the individual heaters, served to extend the heater's functionality as a temperature sensor, which were used for the channel wall temperature measurements. The heaters were designed intelligently, allowing them to be powered individually and with varying current input, which could simulate hot spots in a chip. However, the study conducted for this thesis does not encompass hot spot experiments.

Isolation trenches, or air gaps, as the name suggests, isolated the microchannel array from its surroundings, to reduce the thermal spreading from the heaters into other surrounding materials, thereby justifying the assumption of one dimensional conduction in the heat sink.

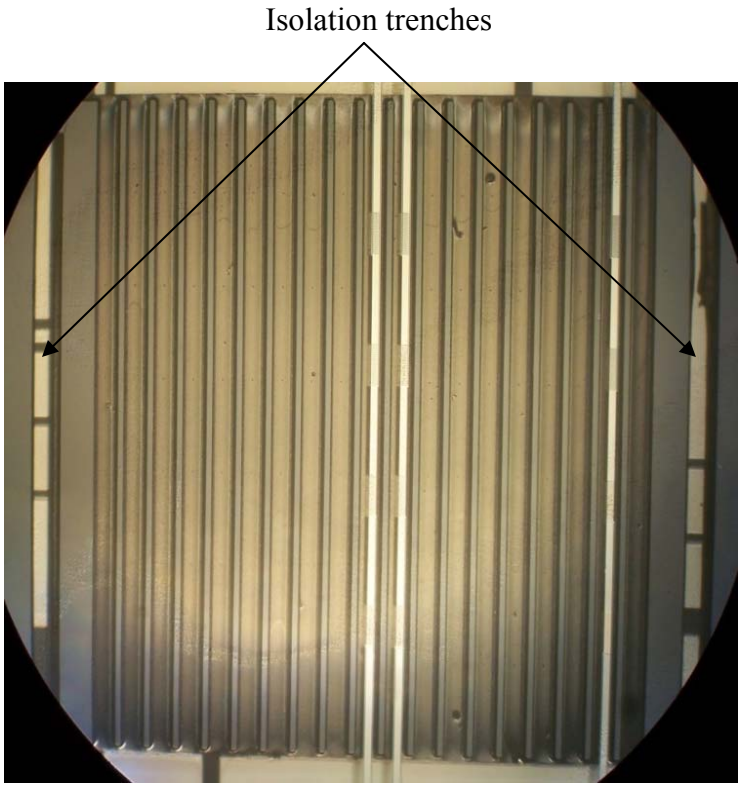

Figure 3.2 Microchannel heat sink – multichannel configuration

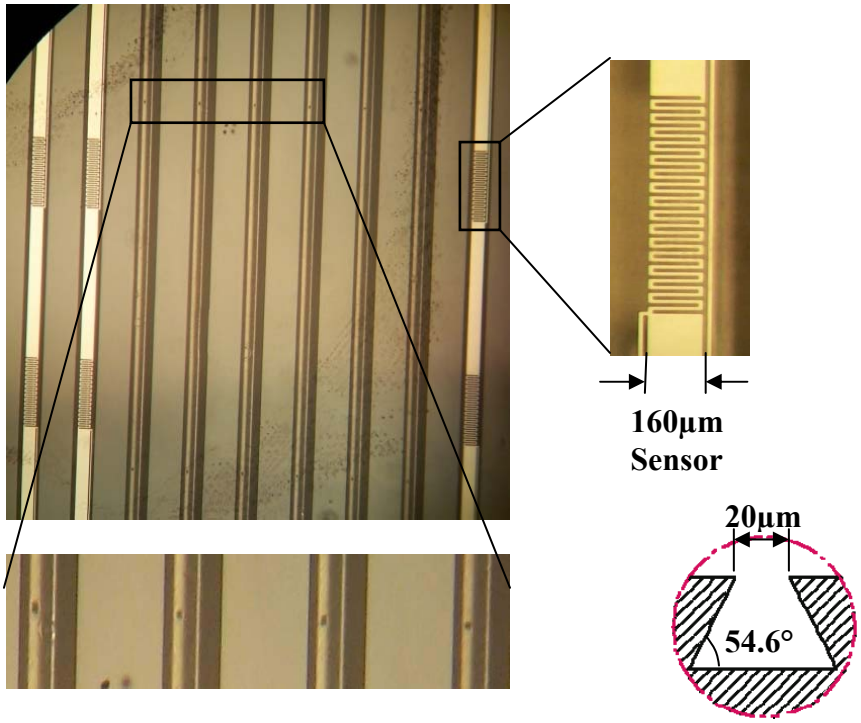

Figure 3.3 Microchannels enhanced with pyramidal re-entrant cavities

3.2 Single channel configuration

This configuration consists of a single silicon microchannel fabricated in the same way as the multichannel configuration. The objective of a single channel setup is to eliminate the channel-to-channel interaction and study the effect of number of channels on flow instabilities, hydraulic and thermal characteristics. This setup also eliminates the scenario of a common plenum for multiple channels which is believed to affect the parallel channel oscillation in a multichannel configuration. An assembled single microchannel test section (SC 400-2) is shown is Figure 3.4 and the schematic of the same is shown in Figure 3.5.

The cross-sectional shape of the single channel test sections remained rectangular and the width of the channels varied between 100 μm and 400 μm**.** Like the multichannel configuration, the pyramidal re-entrant cavities at the base of the channel were sized similarly, and the number of cavities was either two or six, equally spaced along the channel. In this way, four different test sections were utilized each varying in width and the number of cavities. This permitted the analysis of the effects of channel width and number of cavities on the thermal and flow characteristics. The matrix in Table 0.1 shows the characteristics of various single channel test sections utilized.

Unlike the multichannel configuration, only one serpentine Aluminum heater was used for heat input in a single channel set up. The heater located in the top Pyrex plate, like in the multichannel configuration, also served as a temperature sensor, which was made possible by the voltage measurements at six locations along the heater. On the top Pyrex® plate, five RTDs as shown in Figure 3.4 were employed to measure the temperature of the fluid along the channel.

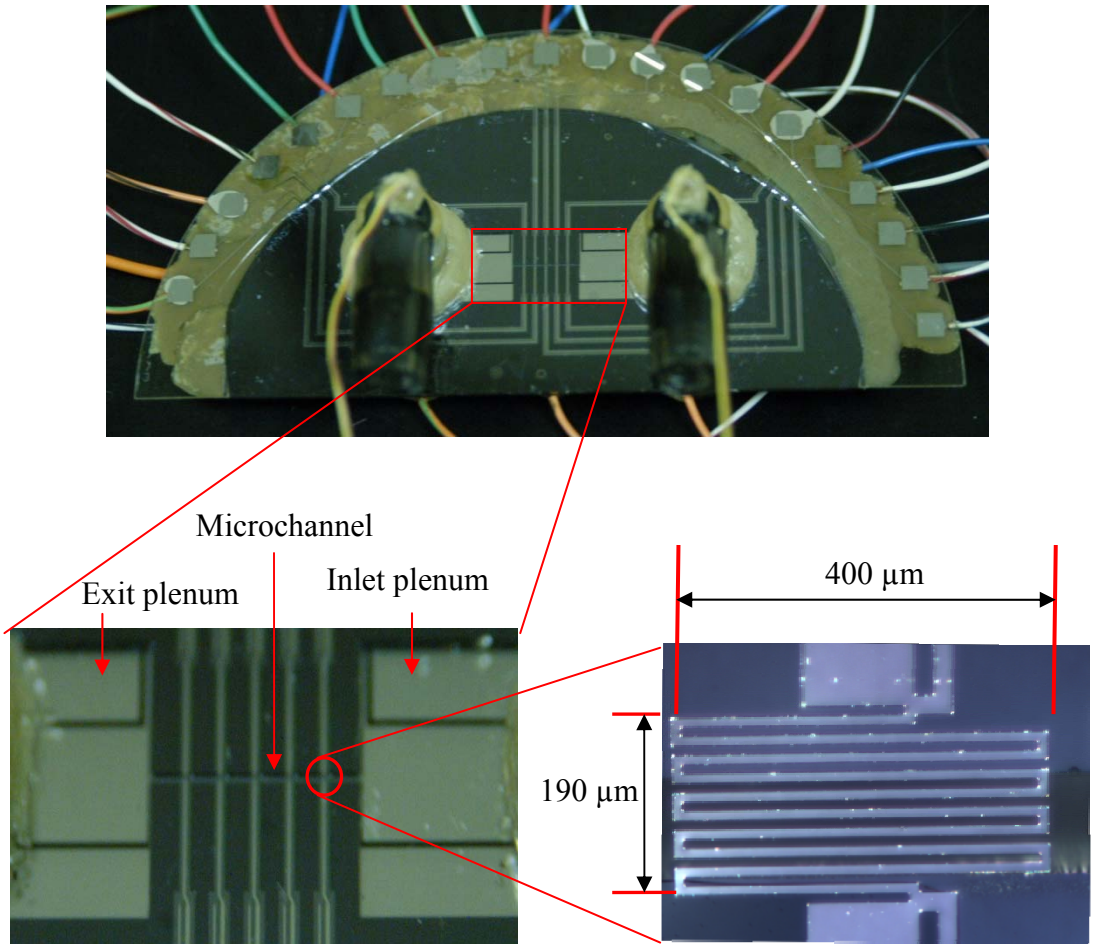

Figure 3.4 (a) Assembled single channel test section (b) Microchannel of width 400 µm (c) RTDs in the top Pyrex glass plate

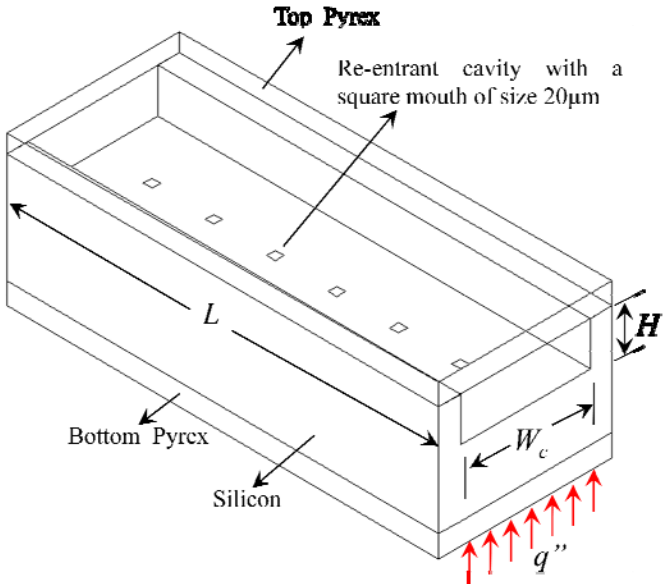

Figure 3.5 Schematic of a single channel test device

3.3 Flow Loop

A schematic diagram of the experimental setup used for the multichannel test device is shown in Figure 3.6. The working fluid used in all the experiments was a chlorofluorocarbon named FC-72 (C_6F_{14}), a widely used electronics cooling fluid from 3M®. The flow loop has the flexibility to permit experimentation over a range of pressures, heat flux, and inlet subcooling. A magnetic drive gear pump (MicroPump® model no.75211-30) was used to drive the fluid to the test section at mass fluxes ranging from 535kg/m^2-s to 2138kg/m^2-s, without producing any pulsations. The fluid was thoroughly degassed before all the experiments by vigorous boiling in the condenser vessel.

Two heat exchangers were used in the system. The first, a shell and tube heat exchanger was used to transfer heat from a hot water bath to the fluid, thus heating the fluid up to the required inlet temperature i.e. to achieve the required inlet subcooling. The other heat exchanger running a mixture of water and heat transfer enhancing fluid (Redline Water Wetter) was used to remove the sensible heat stored in the fluid.

Temperature was measured at the inlet and exit by k-type thermocouples and pressure was measured by gage pressure transducers. The pressure at the microchannel exit was maintained by heating the condenser vessel located downstream. The pressure was measured at locations away from the inlet and exit, and hence the pressure measurements had to include the losses in the inlet and exit plenum due to the sudden contraction and expansion respectively. The heaters were powered by DC current using a HP® power supply (6654A) at voltages ranging from 0~40V. The voltage measurements from the heaters, pressure transducers and the thermocouples were acquired by a NI

DAQ® (SCXI 1000 chassis; SCXI 1120, 1100 terminal blocks) data acquisition system at a sampling frequency of 60 Hz.

Flow was visualized using a Kodak Motion Corder Analyzer (Model 1000) at 600 fps. For this purpose a Dolan Jenner fiber optic lighting system was used.

In a single channel configuration, the flow loop underwent a number of modifications, owing to the lower volume flow rates. The heat exchanger used to preheat the fluid was replaced by an Omega® rope heater (FGR-030) with a maximum power of 125 W, which was wrapped around the copper tubes carrying the fluid. The inlet temperature was maintained at a constant value by an Omega temperature controller (Model no.CN 7533). A schematic of the flow loop used in shown in Figure 3.7.

Owing to the low volume rates, the heat loss in the inlet and exit Vinyl® tubes were high leading to inaccurate inlet and exit temperature measurement. This prompted the relocation of the inlet and exit thermocouples closer to the inlet and exit of the microchannel. Fine wire k-type thermocouples were employed for temperature measurements.

The pump head was also replaced by a low volume flow rate pump head (model no.GA X21 CFSA) to cater to the needs of the single channel setup. The volume flow rate required in a single channel setup was low because of the reduction in number of channels, but the mass flux had to remain the same to make meaningful comparisons with the multichannel data.

3.4 Experimental procedure

The first and foremost step in any experiment was to degas the fluid, a three-step process which involved vigorously boiling of fluid in the condenser vessel. In the first step, the condenser vessel was isolated by shutting off the inlet and exit valves and boiling the fluid for about 15 minutes, regularly punctuated by opening the valve located atop to allow the gas to escape. Now the inlet and exit valves were opened and the pump was powered to run the fluid through the bypass loop, and the procedure was repeated for another 20 minutes. Finally, the bypass loop was shut and the fluid was directed to the main loop which included the microchannels, and the procedure was repeated. Degassing was followed by setting up the microchannel exit at atmospheric pressure by regulating the heat supplied to the condenser vessel using a variable transformer. This step was followed by turning the heat exchangers on to achieve the required inlet subcooling (rope heater in the case of single channel configuration). The third variable in the experiments which is mass flux was set at the required value.

The range of operating conditions for the experiments is tabulated in Table 3.2.

Table 3.2 Range of operating conditions

Controlled variables	Range
Mass Flux (kg/m^2-s)	535 - 2138 (25-100 ml/min : Multichannel); 800 - 1605 (1 – 2 ml/min : Single channel);
Inlet Subcooling (°C)	5 – 20
Pressure at channel exit	Atmospheric
Applied Heat Flux (W/cm^2)	0 – 50 => Multichannel; 0-250 => Single channel;

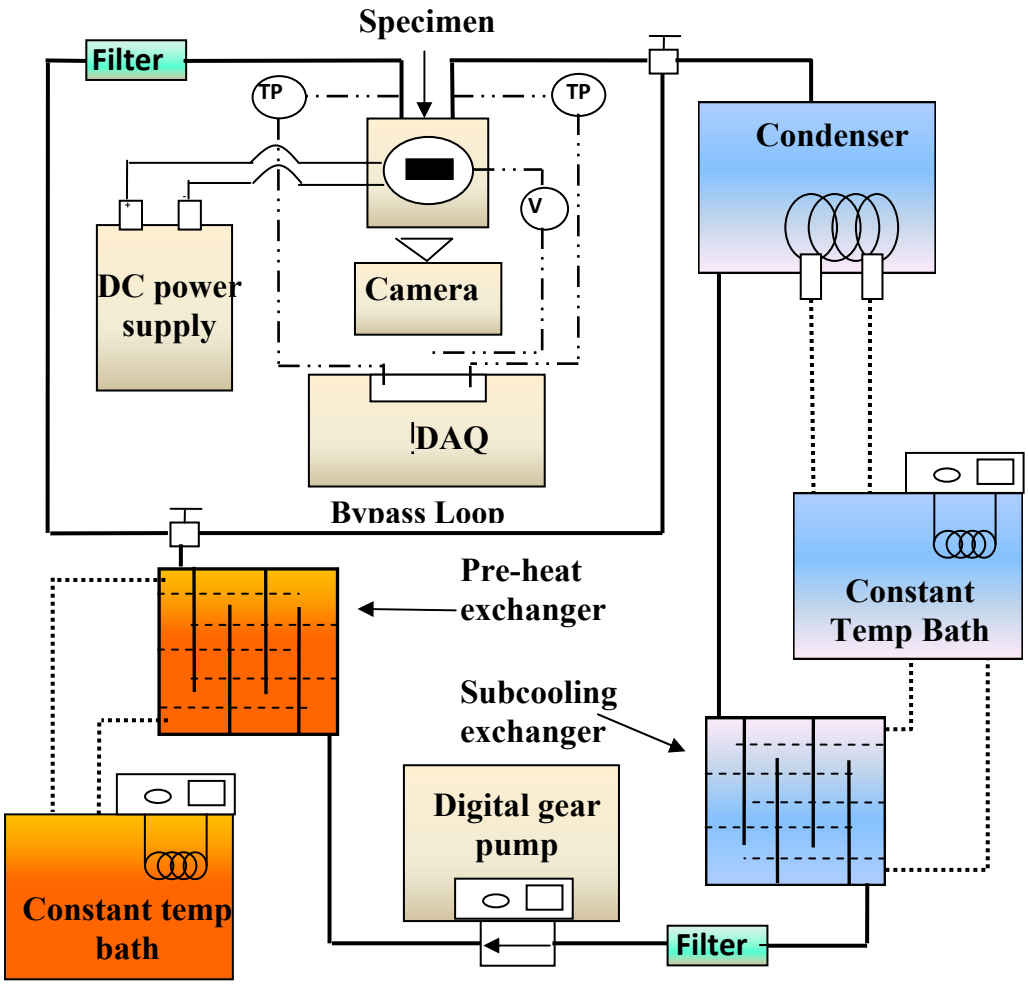

Figure 3.6 Flow loop used for a multichannel test device

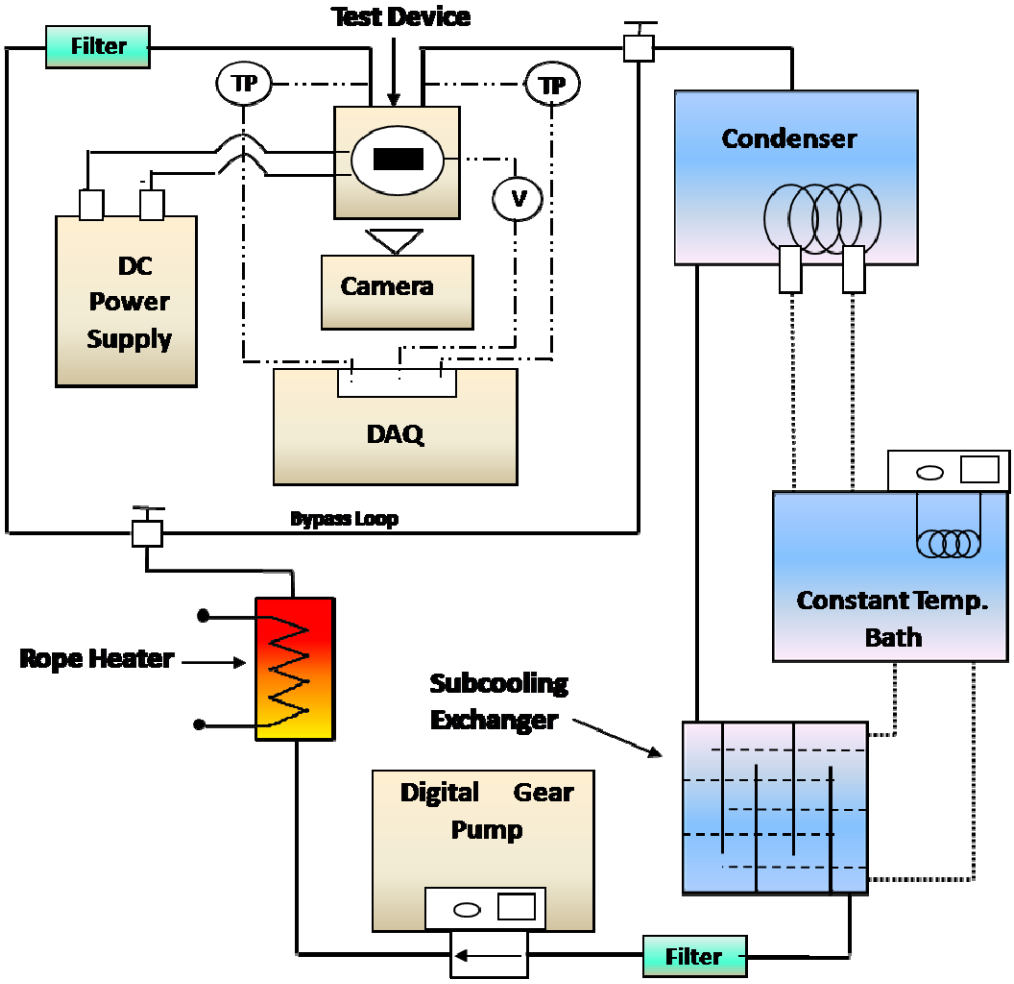

Figure 3.7 Flow loop used for a single channel test device

CHAPTER 4: RESULTS AND DISCUSSION

This chapter describes and quantifies the experimental investigation conducted on the flow of FC72 in surface augmented microchannels. The raw data acquired include voltage signals from temperature sensors, pressure transducers and heaters. Using the pressure drop data, an analysis of friction factor is performed to study the applicability of conventional theory in predicting the friction factor for flow in a microchannel. A detailed study of the effect of system variables such as inlet subcooling, mass flux and heat flux on pressure drop and heat transfer coefficient is performed. Assessment of the applicability of conventional theories is also extended to predict the pressure drop and heat transfer in microchannels with an emphasis on subcooled nucleate boiling. The discussion also includes the characterization of flow instabilities using high speed videos acquired and pressure transducer signals. The influence of system variables on flow instabilities is also explored and flow instability pattern maps are constructed to demarcate the stable and unstable flows.

4.1 Fluid flow characteristics

This section describes the single phase flow characteristics of FC72 in single and multiple parallel microchannels. Although single phase flows in microchannels have been well analyzed and studied, and found to confirm to the macrochannel flow prediction methods, studies on flow friction factors have produced anomalous results as reported in

a number of studies in the literature [6,37,39]. Hence the purpose of this section is to analyze flow development in microchannels and thereby deduce the validity of the fully developed flow conditions which usually is assumed a priori in many studies. Flow friction characteristics in single and multichannel configurations of varying width will be discussed and the ability of macrochannel flow models to predict the microchannel flows has been investigated.

4.1.1 Boundary layer development in the channel

Sufficiently far from the pipe entrance, the boundary layer developing on the pipe wall reaches the pipe centerline and flow becomes entirely viscous. The velocity profile remains constant after the inviscid core disappears. When the profile shape no longer changes with distance the flow is termed *fully developed*. The distance from the entrance to the location at which fully developed flow begins is called entrance length (i.e. length of developing region). For a laminar flow in a rectangular channel, the length of developing region (L_d) is expressed as a function of channel aspect ratio (β) by Shah and London [61] as,

$$L_d = \left(0.06 + 0.07\beta - 0.04\beta^2\right) Re_{ch} D_h \tag{4.1}$$

Figure 4.1 shows the velocity entry length plotted as a function of Reynolds number for several of the test devices used in this study. The tested range of Re differs with the test device so as to maintain a constant mass flux. For a constant width, the entry length increases with Re and this is due to the increasing inertial forces which are destabilizing in nature. For a constant *Re*, the entry length increases with the width of the channel. It is evident that the entrance length in most of the microchannel configurations is more than the channel length and hence, the assumption of fully-developed flow will

not be justified. Even in cases where the entrance length is less than the channel length, a major part of the channel is in the developing flow regime and hence the velocity boundary layer will be considered to be developing in all the cases.

4.1.2 Friction Factor

Adiabatic experiments were conducted for Reynolds numbers ranging from 200–1500 to study the flow characteristics of FC72 through the single microchannel and multichannel test devices, whose geometries have been summarized in Table 0.1. The experimentally determined friction factors were plotted against Reynolds number and comparisons were drawn with the classical theory for flow in macrochannels. In the past, some studies have shown that flow in microchannels does not obey the conventional theories of flow resistance and flow transition described by the Navier-Stokes equations.

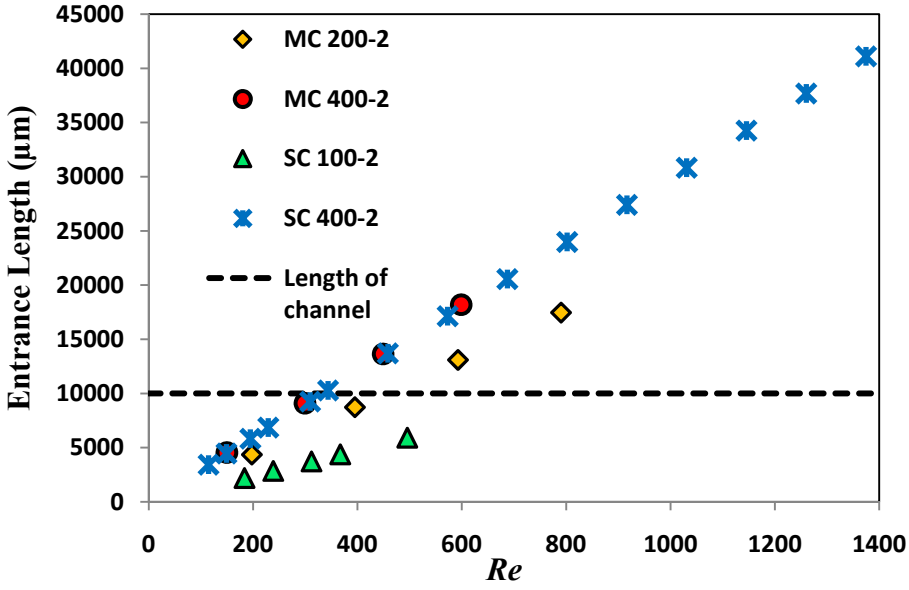

Figure 4.1 Entrance length for the flow of FC72 through various microchannel configurations

The experimental friction factor (f_{exp})for the single phase flow was calculated using the expression,

$$f_{\exp} = \frac{2D_h \Delta p_{microchannel}}{\rho U^2 L} \tag{4.2}$$

Where $\Delta p_{microchannel} = \Delta p_{total} - \Delta p_{losses}$

For flow in macrochannels the friction factor scales inversely with Reynolds number and it is equal to 64 Re^{-1} for a circular tube. For laminar flow (Re<2300) in a channel, the friction factor can be expressed as,

$$f.Re = C \tag{4.3}$$

where f is the Darcy friction factor and C is a function of the channel aspect ratio determined by the correlation given by Shah and London [19] for a fully developed flow in a rectangular channel.

$$C = 96\left(1 - 1.35538\beta + 1.9647\beta^2 - 1.7012\beta^3 + 0.9564\beta^4 - 0.2537\beta^5\right) \tag{4.4}$$

For developing flow, the apparent friction factor, f_{app} given by Shah and London [19] is,

$$f_{app}Re = \frac{13.76}{L_{hy}^{+0.5}} + \frac{\frac{k_\infty}{4L_{hy}^+} + f\,Re - 13.76L_{hy}^{+-0.5}}{1 + cL_{hy}^{+-0.2}} \tag{4.5}$$

where, $k_\infty = 0.6740 + 1.2501\beta + 0.3417\beta^2 - 0.8358\beta^3$

$$c = \left(0.1811 + 4.3488\beta - 1.6027\beta^2\right) \times 10^{-4}\,;\; L_{hy}^+ = \frac{L_{hy}}{Re\,D_h}$$

For the multichannel test device, MC 200-2, the theoretical friction factors were calculated using the developing flow correlation expressed in Equation 4.3. The

experimental friction factor was calculated using Equation 4.2 and plotted against *Re* in Figure 4.2 and as expected the friction factor holds an inverse relation with *Re*. Figure 4.2 also illustrates that classical theory for flow in macrochannels predicts the friction factor to good accuracy in the case of multichannel test device of hydraulic diameter 253µm. However, in the case of a single microchannel test devices, SC 100-2 and SC 400-2 of hydraulic diameter 155µm and 354µm respectively, the results plotted in Figure 4.3show that the theoretical friction factors, under predicted the experimental values in the case of SC 100-2 and over predicted in the case of SC 400-2. These results agree with the findings of Peng et al. [39]where for test devices with an aspect ratio approximately one, $(f_{exp} \ / f_{theoretical}) > 1$ and $(f_{exp} \ / f_{theoretical}) < 1$ for aspect ratios adjacent to 0.5.

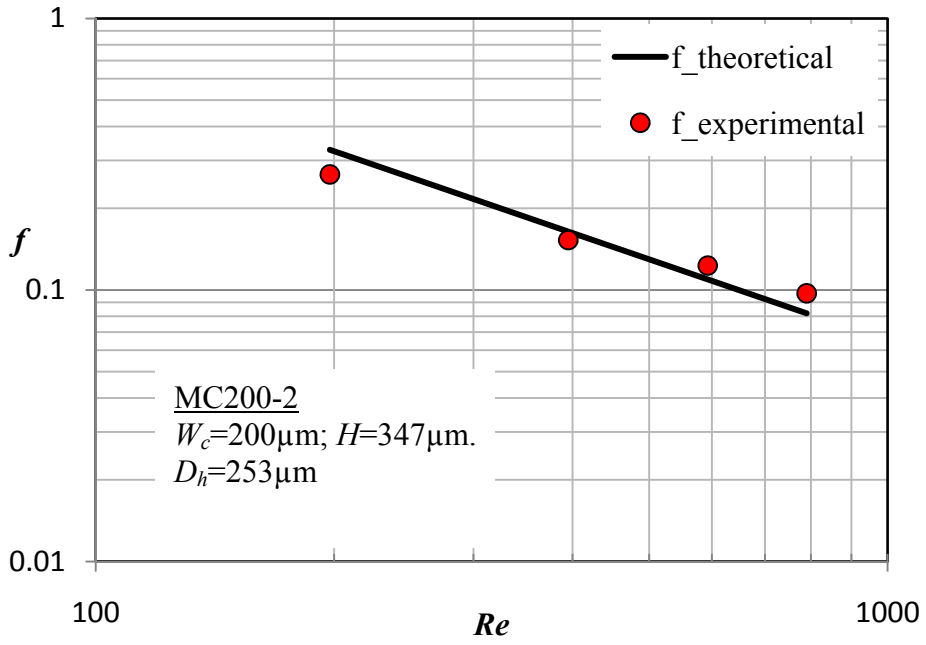

Figure 4.2 Comparison of experimental friction factors with the theoretical friction factor for MC200-2

From Figure 4.2 and Figure 4.3 , it can be inferred that the friction factors decrease with the hydraulic diameter. Similar trends were also reported by Peng et al. [39], for the flow of water through parallel microchannels and Xie et al [40] for the flow

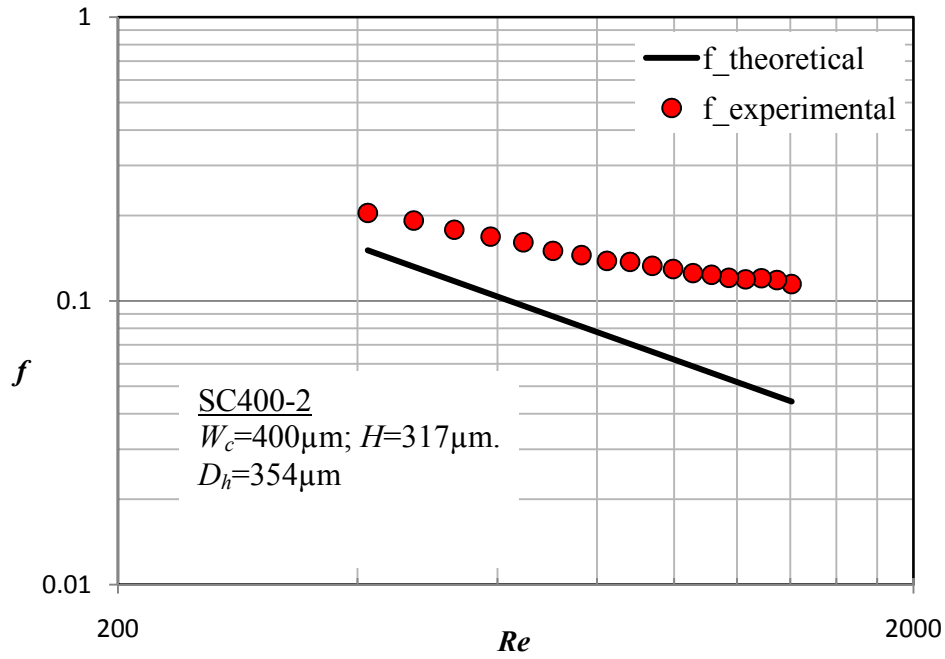

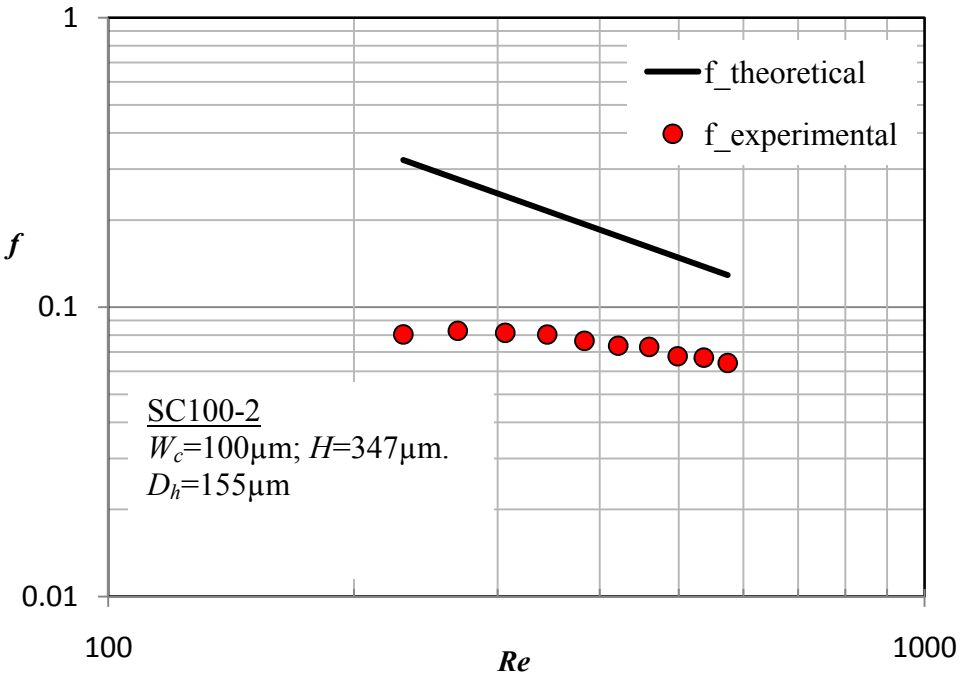

Figure 4.3 Comparison of experimental friction factors with the theoretical friction factor for (a) SC400-2 (b) SC100-2

of ethanol-water solution through parallel microchannels. However, investigations by the latter on the flow of FC72 through 19 parallel microchannels, which is identical to the multichannel module (MC 200-2) used in this study, showed that the friction factor increased with hydraulic diameter at low *Re*.

A correlation for the friction factor was proposed by Xie et al. [40].

$$f = 0.04743Re^{-0.9553}\left(\frac{D_h}{L}\right)^{-1.5349}\left(\frac{H}{W_c}\right)^{-0.09793} \quad ,300 < Re < 750 \qquad (4.6)$$

In Figure 4.4, the product of $f.Re$ is compared with those from the literature. It can be seen that the correlation given in Equation 4.6 for the flow of FC72 in a multichannel geometry under predicts the friction factors significantly. Also, the product of $f.Re$ from experiments increased with Re, while the results of Wu and little [37], and Choi et al. [38] project a constant $f.Re$ for the laminar regime. In contrast, Peng et al. [39] reported that $f.Re$ decreases with Re. In general, little agreement was found between the experimental results and the available literature, but deviations from classical theory have been reported by many studies.

Unlike the reports of early transition to turbulence in [39,40], the friction factors reported in Figure 4.2 for the multichannel test device indicate that the transition to turbulence did not occur at least until the highest tested Reynolds number of 800. A study conducted by Garimella and Singhal [41] for flow of water in microchannels of hydraulic diameter in the range of 250-1000μm, illustrates that the flow behavior is same as in conventional channels in terms of transition and friction factors.

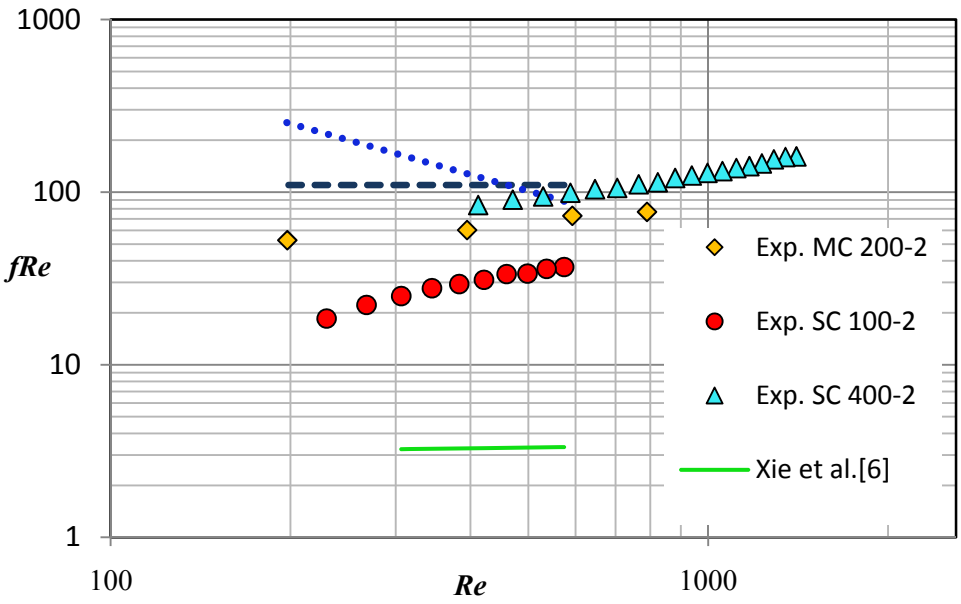

Figure 4.4 Comparison of experimental friction factors with those in the literature

4.2 Thermal characteristics

This section quantifies the phenomena of ONB and temperature hysteresis and analyzes the parametric effects on the same. The study includes brief overview of the heat transfer mechanism due to flow in a microchannel and the estimation of heat transfer coefficients. This section also explores the effect of system variables on the heat transfer co-efficient, which also highlights the dominant mode of heat transfer. Also, applicability of conventional theories for the prediction of heat transfer in a microchannel has been proven by some of the studies in the literature to be inadequate owing to the small size of the channels. Hence, an investigation of the existing heat transfer correlations is performed with emphasis on nucleate boiling. A correlation is also developed to predict the heat transfer coefficient in the flow of FC72 in microchannels.

4.2.1 Heat loss

a) Heat loss in multichannel configuration

Quantification of heat losses in the heat sink are very essential to estimate the amount of heat that is supplied to the base of the microchannels. The various heat losses that need to be accounted for are the conduction heat losses in the substrate and the low conductivity pyrex glass, convective heat loss from the back of the test section to the ambient, and radiative heat losses. Instead of estimating the heat loss in the aforementioned paths, heat loss is quantified by expressing it as all the heat that is not carried by the fluid. Hence, it is a difference between the total power supplied and the sensible heat gain of the fluid.

The power supplied to the heater (P_{in}) is expressed as,

$$\boldsymbol{P_{in} = I^2 R_h} \tag{4.7}$$

The sensible heat gained by the fluid in the single phase regime (q_{sp})can be quantified as,

$$\boldsymbol{q_{sp} = \dot{m} C_p (T_{out} - T_{in})} \tag{4.8}$$

Properties are taken at the average between the inlet and outlet thermocouple readings. The heat loss is calculated by taking the difference between Equation (4.7) and Equation (4.8) and plotting the losses as a function of the difference between heater temperature and ambient temperature (T_h–T_{amb}), as shown in Equation (4.9). The heat loss data thus obtained was extrapolated to the two phase flow regime using a linear curve fit. The value of heater temperature (T_h) is calculated by using the average heater resistance as a function of temperature.

$$\boldsymbol{q_{loss} = a(T_h - T_{amb}) + b} \tag{4.9}$$

b) Heat loss in single channel configuration

Unlike the multichannel configuration, which is a finned structure, the single channel configuration is similar to a duct flow, with the walls of the channel connected to a large conductive silicon layer and hence projecting a sufficiently large surface for the heat to be lost. So, the method of estimating heat loss used for the multichannel test devices failed in the case of single channel test devices as it produced erroneous wall temperature data.

Other efforts were taken to estimate the heat loss such as supplying heat to an empty test section with all the fluid evacuated, and corresponding heater temperatures were recorded. This was repeated for different heat power inputs and a linear relationship was obtained between the heater power (heat loss) and heater temperature [1] or temperature difference between ambient and heater [2]. The calibration curves for heat loss thus obtained are presented in the Appendix. It was observed that even this method proved to be insufficient. This drawback resulted in a disability to obtain wall heat flux data and hence the wall temperatures and heat transfer co-efficient.

4.2.2 Boiling curve

The plot of wall temperature versus wall heat flux, known as the *boiling curve* (red data points in Figure 4.5), is useful to gain a thorough understanding of the boiling process and its effectiveness. For the flow in microchannels, the boiling curve traverses through the following regions that are generally found in forced-convection internal boiling. The data points represented in blue is the temperature at the inlet which is always maintained at a set value. The green data points represent the temperature of the fluid at the channel exit. As the applied heat flux increases, the exit temperature increases until it

reaches the saturation temperature of the fluid. Any further increase in heat flux would result in phase change indicated by a constant exit temperature.

In the boiling curve, during the initial single phase flow regime prevailing at low wall superheats, the heat transfer is dominated by forced convection effects. As the heat flux is increased further, the wall temperature exceeds the fluid saturation temperature, and incipience takes place as the heat flux increases further (18.5 W/cm^2 in this case). It can be noticed that the wall temperature takes an appreciable dip immediately after the *onset of nucleate boiling* (ONB) at a constant heat flux. Further increase in heat flux leads to fully developed nucleate boiling.

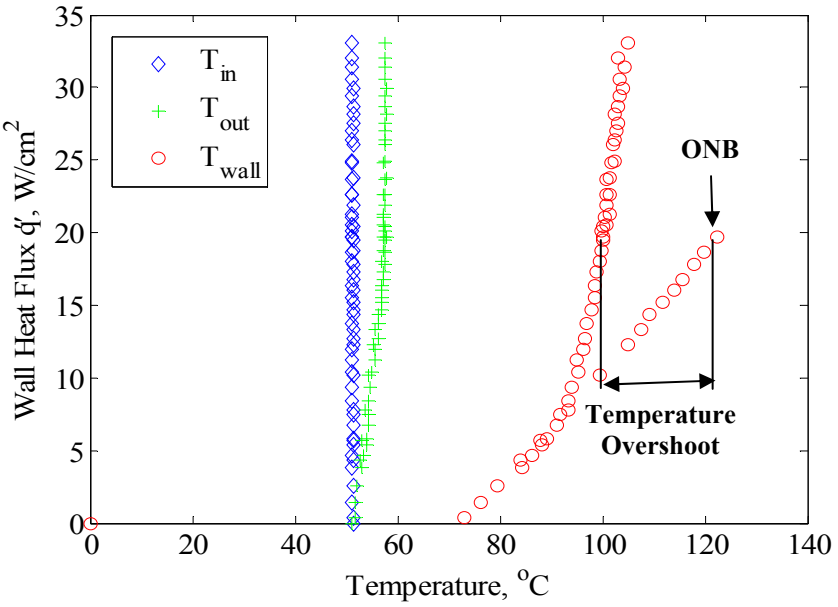

Figure 4.5 Inlet, exit and wall temperature at G = 2138 kg/m^{2}s and ΔT_{sat}=10°C in MC200-2

The delay in ONB termed as '*temperature overshoot*' or '*hysteresis*' is a characteristic of boiling of dielectric fluids owing to their highly wetting nature causing the cavities to snuff out. This phenomenon was also reported by Bowers and Mudawar

[36] and Piasecka and Poniewski [26]. While traversing down the heat flux, the fully developed boiling region was found to merge smoothly with the single phase region.

ONB and nucleation hysteresis will be studied in the following sections and the effects of inlet subcooling and mass flux on the above mentioned phenomena will be analyzed.

4.2.3 Onset of nucleate boiling

From the previous section, it can be seen that the Onset of Nucleate Boiling (ONB) is a significant and an important phenomena along the boiling curve, since it forms the upper limit of single phase flow and the lower limit of two-phase flow. Hence the prediction of ONB is critical in the design of phase change systems. Although, models for predicting the ONB such as the Bergles and Rohsenow [17] correlation are available, studies have shown that the available models do not perform well in the case of flow boiling in microchannels. However, empirical models based on experimental data have been developed by various researchers. This section investigates the effects of mass flux and inlet subcooling on ONB and compares the models available in the literature. Experimentally, the ONB is recorded as the flux at which the first set of bubbles was seen departing the fabricated cavities while the heat flux was increased.

Figure 4.6 shows the effect of inlet subcooling and mass flux on ONB. The incipient heat flux was found to increase with increase in inlet subcooling i.e. decrease in fluid inlet temperature. This can be attributed to the lower wall temperatures at higher subcooling. It can also be observed that the incipient heat flux increases with increasing mass flux which is also due to the lower wall temperature at high mass flux. The reported results show that it would be favorable to operate at lower mass flux and higher fluid inlet temperature so as to prevent the high wall temperatures. The trends portrayed also agree

with those reported by Jones et al. [22] who conducted flow boiling experiments with FC72 in silicon microchannels and Liu et al. [20] who investigated the flow of water through microchannels of width 275 μm wide and 636 μm deep.

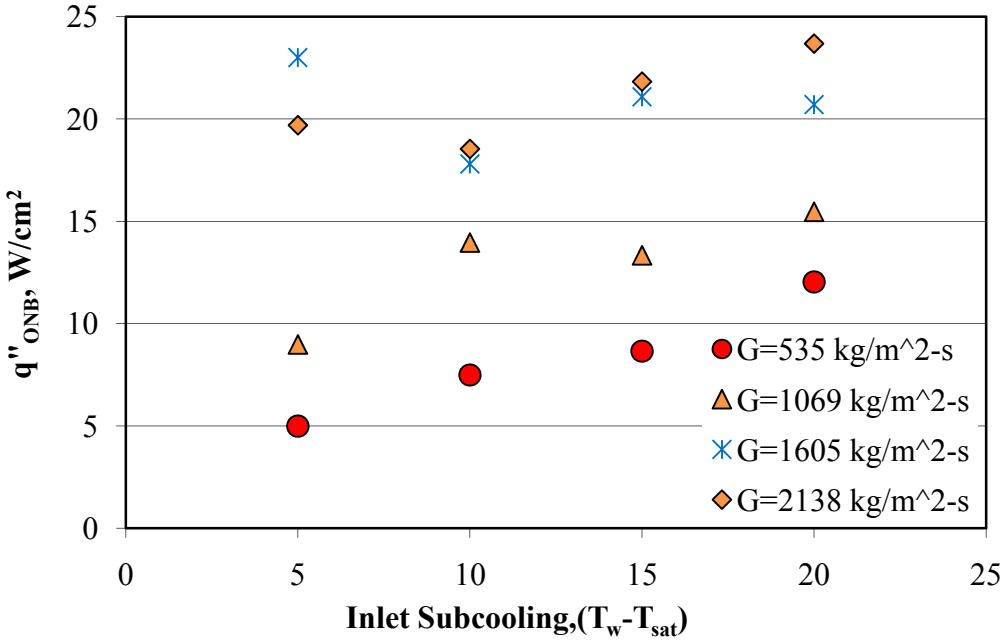

Figure 4.6 Effect of subcooling and mass flux on ONB

The fabricated re-entrant cavities act as vapor trapping sites and trigger ONB earlier than for plain microchannels and promote uniform bubble generation. In flow boiling experiments conducted with water in microchannels, Kuo and Peles [52] reported that heat flux required for ONB condition in augmented surfaces is up to 25% lower than that for plain microchannels. However in the current study, the effectiveness of cavities was countered by the wetting nature of FC72, thus delaying the ONB.

4.2.4 Nucleation hysteresis

As seen in the boiling curve, the hysteresis or temperature overshoot associated with the ONB is a commonly observed phenomenon in dielectric fluids such as the one used in this study. It is due to the highly wetting nature of FC72 which causes the

nucleation cavities to be filled with liquid leading to larger temperature overshoots than those observed in water which has a higher contact angle. The experimental analysis of nucleation hysteresis is presented in Figure 4.7 which shows the effect of subcooling and mass flux on the temperature overshoot. It can be noticed that the temperature overshoot decreases with increasing inlet subcooling, though there are couple of deviations at G=535 kg/m^2-s and inlet subcooling of 20°C, and at G=1069kg/m^2-s and an inlet subcooling of 5°C, where the data points deviate from the trend. However, it can be concluded in general that the temperature overshoot decreases with subcooling. However, the flow rate did not have any effect on the temperature overshoot which was the trend reported by Piasecka and Poniewski [26].

4.2.5 Heat transfer coefficient

One of the biggest advantages that flow boiling in microchannels offers is the high heat transfer coefficient, which scales inversely with the hydraulic diameter of the channel. This is further enhanced by the phase change process which results in orders of magnitude increase in heat transfer coefficient. However, the heat transfer coefficients obtained with the phase change of FC72 are low compared to that of water, which is due to the poor thermal characteristics and the highly wetting nature of FC72. The properties of FC72 are summarized in Appendix A.

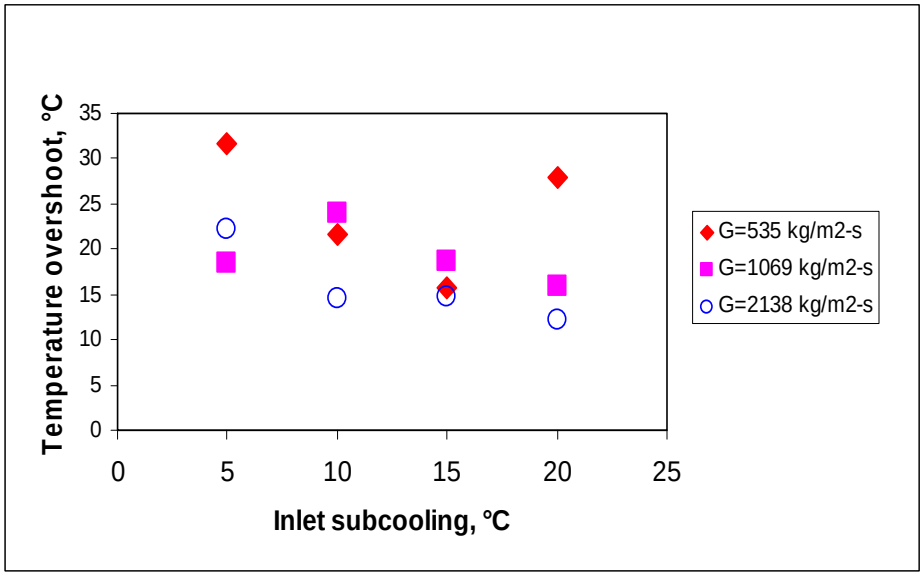

Figure 4.7 Effect of mass flux and inlet subcooling on temperature overshoot

In the case of flow boiling wherein fluid enters the heated area with a subcooled liquid, the microchannel experiences some heated length that is exposed purely to single phase convection or sub-cooled nucleate boiling. The quality at the exit of the microchannel (x_e) is estimated using Equation 4.10. To quantify differences between this region and the saturated portion of the channel along the axial length of the test section, a single phase or subcooled length (L_{sp}) is calculated as defined by Equation 4.11. The heat transferred to the fluid over this subcooled length of the test section (q_{in}) is calculated by Equation 4.12. Using these two values, an iterative method is used in conjunction with the adiabatic tip fin equation to solve for the average heat transfer coefficient (h_{sp}) over the single phase length (L_{sp})

$$x_e = \frac{q_{wall} - \dot{m} C_p (T_{sat} - T_{in})}{\dot{m} h_{fg}} \tag{4.10}$$

$$L_{sp} = \frac{\dot{m} C_p (T_{sat} - T_{in})}{\left[\frac{q_{wall}}{q_{array}}\right] W_{array}} \tag{4.11}$$

$$q_{in} = \frac{q_{wall}}{A_{array}} N (W_f + W_c) L_{sp} \tag{4.12}$$

The saturated portion of the channel is treated in similar fashion. After the heat transfer coefficient (h_{sp}) for the subcooled portion of the channels is calculated, a saturated length is calculated as follows.

$$\boldsymbol{L_{tp} = L_{array} - L_{sp}} \tag{4.13}$$

$$\boldsymbol{\Theta_{b\text{-}tp} = (T_{wall} - T_{sat})} \tag{4.14}$$

The temperature difference used for the saturated case is the difference between T_{wall} and T_{sat} as opposed to the subcooled case which uses the T_{mf} or the average of the inlet and outlet thermocouples. With these two values tabulated, the exact procedure carried out to calculate the heat transfer coefficient (h_{sp}) for the subcooled region is repeated for the saturated length (L_{tp}) to calculate (h_{tp}). A weighted averaging method based on the lengths (L_{sp} and L_{tp}) are used to quantify the average heat transfer coefficient for the entire channel array as seen in Equation (4.15).

$$\boldsymbol{h_{avg} = \frac{L_{sp}h_{sp} + L_{tp}h_{tp}}{L_{array}}} \tag{4.15}$$

4.2.5.1 Heat Transfer Mechanism

The mechanisms involved in the transfer of heat between the heated wall and the subcooled liquid can be explained with the help of average heat transfer coefficient plotted against exit quality in Figure 4.8.

With the application of uniform heat flux at the bottom wall of the microchannel, as the subcooled FC72 enters the microchannel, the heat transfer in the single phase flow regime is driven completely by forced convection and largely a function of flow velocity. As the heat flux increases further, the wall superheat increases and results in the ONB which along with nucleation hysteresis has been discussed in detail in the previous sections. At this point, there is a significant increase in heat transfer, which can be attributed to the sudden decrease in wall superheat which accompanies ONB. Further

increase in heat transfer will cause bubbles to grow and depart and this cycle of bubble growth is known as the ebullition cycle [62]. Further increase in supplied heat will increase the bubble activity and leads to microlayer evaporation [14], thus resulting in higher heat transfer coefficient. This phase of flow boiling is termed as partial nucleate boiling. Most of the experiments reported here fall into this category of flow boiling regime, where convective effects do not play a significant role. Subsequent increase in heat transfer results in bubble coalescence, leading to fully developed nucleate boiling followed by dryout resulting in a decrease in heat transfer rate which is mainly driven by convection effects.

It should be noted that the data reported here were obtained in an effort to study the subcooled flow boiling regime and hence the critical heat flux phenomenon was not studied.

In the following sections, the effects of inlet subcooling and mass flux on the heat transfer coefficient will be discussed.

4.2.5.2 Parametric effects

a) Effect of Inlet Subcooling

In the partial nucleate boiling regime, increasing the subcooling at a constant mass flux reduces the exit quality at a given heat flux. Hence, at a given quality, the heat transfer will be higher for highly subcooled flow because of the lower wall temperature prevailing in those conditions. This phenomenon is further illustrated in Figure 4.8 - Figure 4.11 where the average heat transfer coefficient is plotted against exit quality. A negative exit quality represents subcooled exit and a positive exit quality represents

saturated exit. It can be observed that as exit quality increases, the heat transfer coefficient increases which illustrates that the heat transfer mechanism is partial nucleate boiling. Because at higher qualities, where the flow is not dominated by nucleate boiling, the ebullition cycle increases and the dry region under the bubbles increase which would lead to a trend of constant or decreasing heat transfer co-efficient versus quality as noted by Warrier et al. [34] who conducted flow boiling experiments using FC84 in small rectangular channel of hydraulic diameter 0.75 mm.. Further, it can also be observed that as inlet subcooling increases, the heat transfer coefficient increases at a given exit quality. The highest heat transfer coefficient obtained was 5100 W/m^2K at 20C inlet subcooling and a mass flux of 2138 kg/m^2s. To compare this value with that of water flowing through microchannels, Kosar et al. [29] obtained a heat transfer coefficient of 80000 W/m^2K using flow boiling of water in microchannels of similar geometry, size and surface enhancement in the form of reentrant cavities at a comparatively low mass flux value of 302 kg/m^2s. This order of magnitude difference in heat transfer coefficient is mainly due to the poor heat transfer properties of FC72.

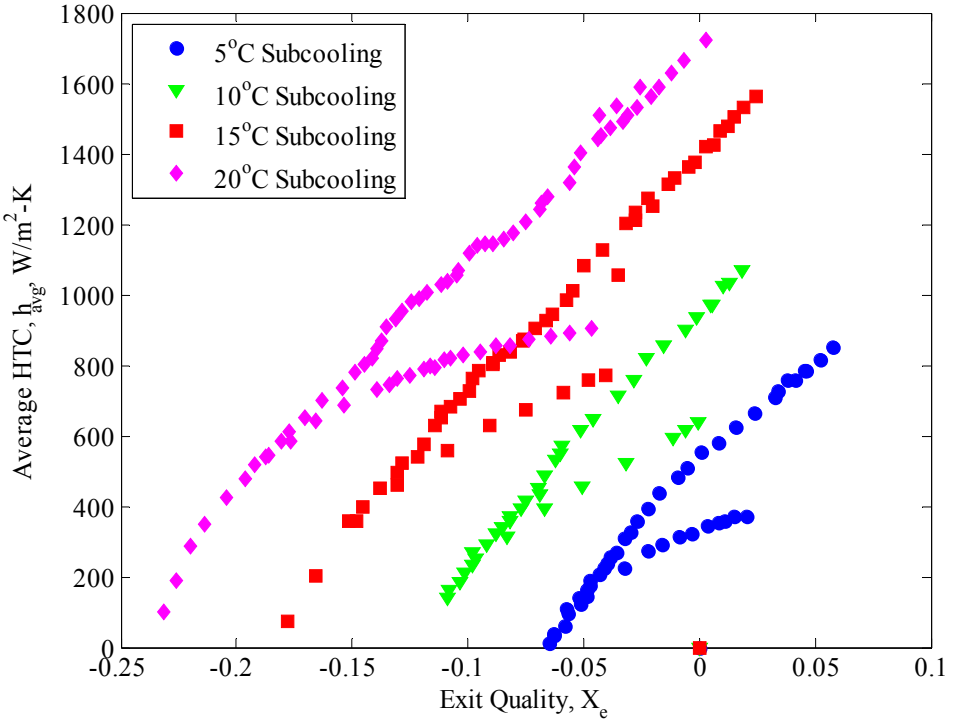

Figure 4.8 Average two-phase heat transfer coefficient at G = 535 kg/m^{2}s

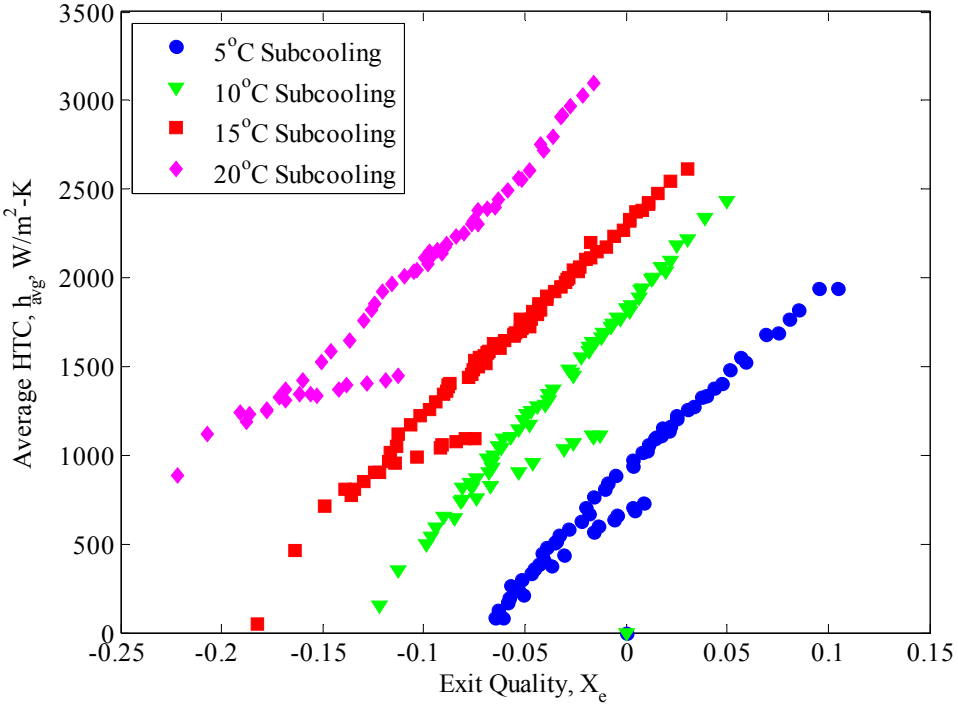

Figure 4.9 Average two-phase heat transfer coefficient at G=1069 kg/m^{2}s

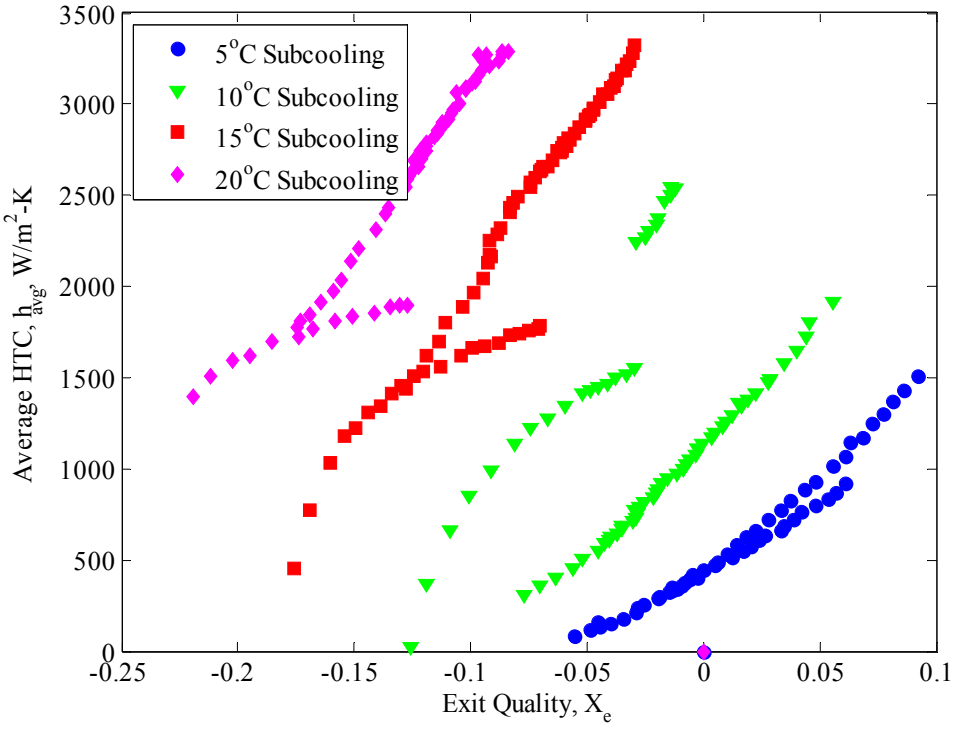

Figure 4.10 Average two-phase heat transfer coefficient at G = 1605 kg/m^{2}s

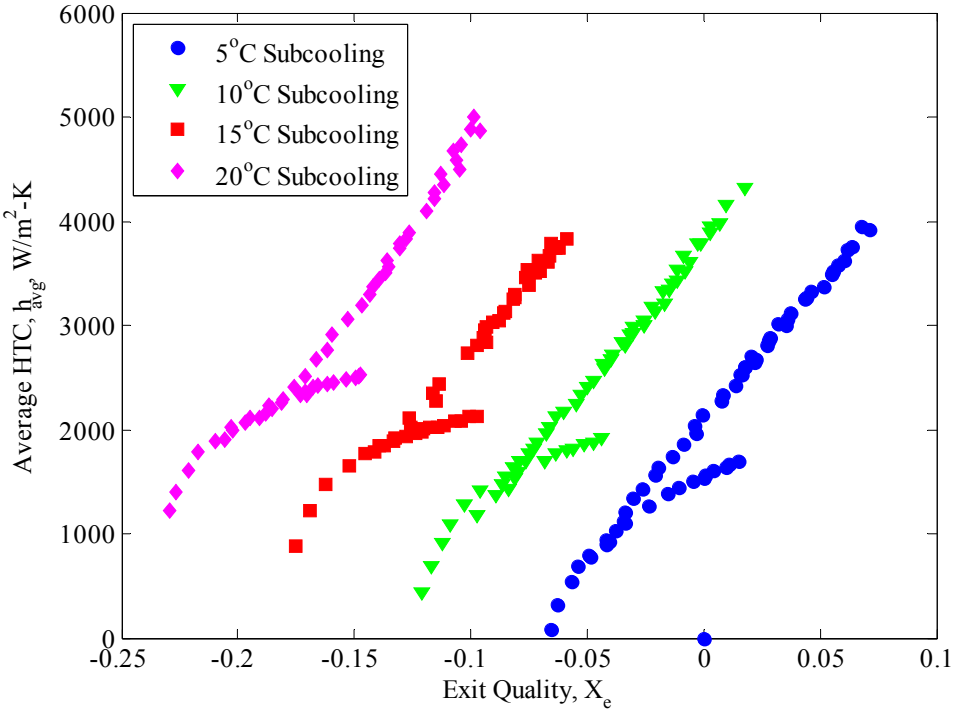

Figure 4.11 Average two-phase heat transfer coefficient at G = 2138 kg/m^{2}s

b) Effect of mass flux:

Mass flux, like inlet subcooling has a similar effect on heat transfer. At a given inlet subcooling, increasing the mass flux would reduce the exit quality. Hence at a given exit quality, higher mass flux would lead to higher wall superheat and hence higher heat transfer coefficient as illustrated by Figure 4.12 - Figure 4.15. Increasing the mass flux, which influences the convective effects is not complimentary to the nucleate boiling, but suppresses it. Hence, increasing the mass flux at a given heat flux does not have any effect on the heat transfer coefficient which will be evident in the plots of heat transfer coefficient against heat flux.

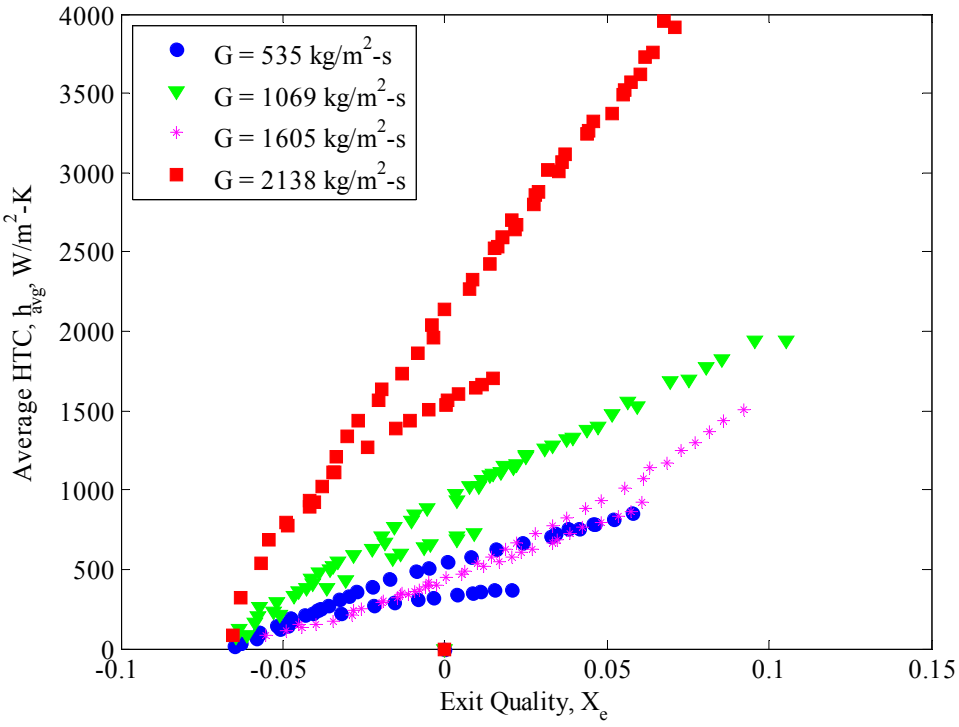

Figure 4.12 Average two-phase heat transfer coefficient at ΔT_{sat} = 5°C

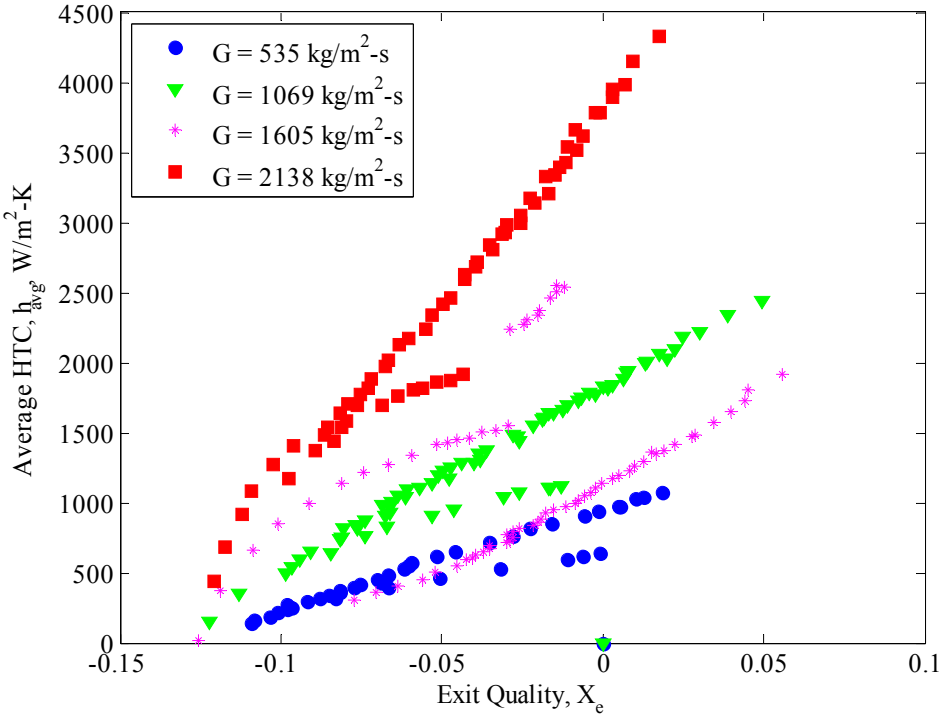

Figure 4.13 Average two-phase heat transfer coefficient at ΔT_{sat} = 10°C

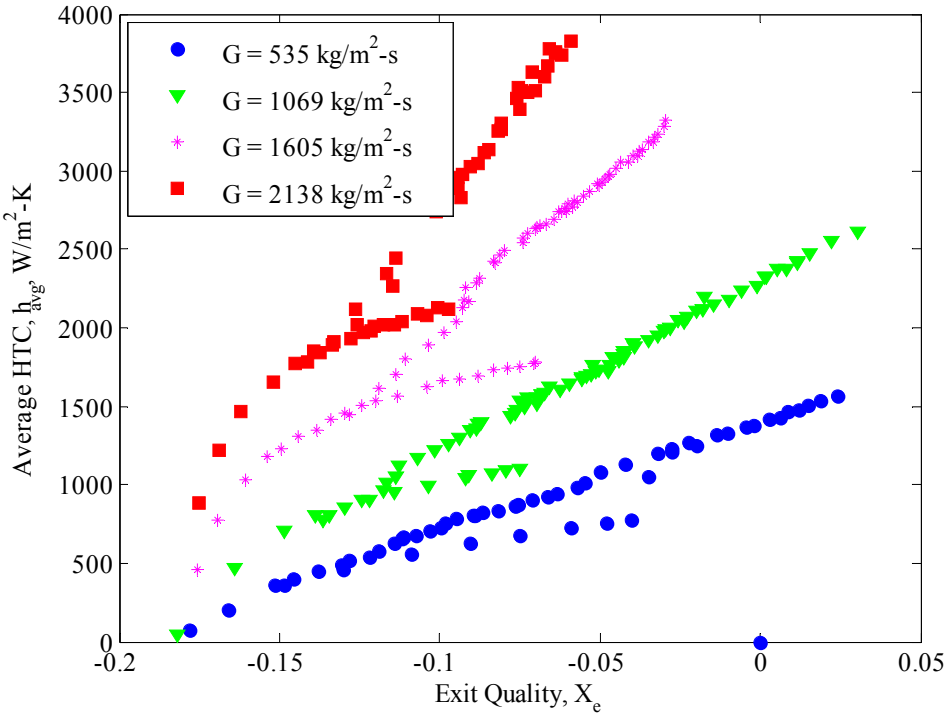

Figure 4.14 Average two-phase heat transfer coefficient at ΔT_{sat} = 15°C

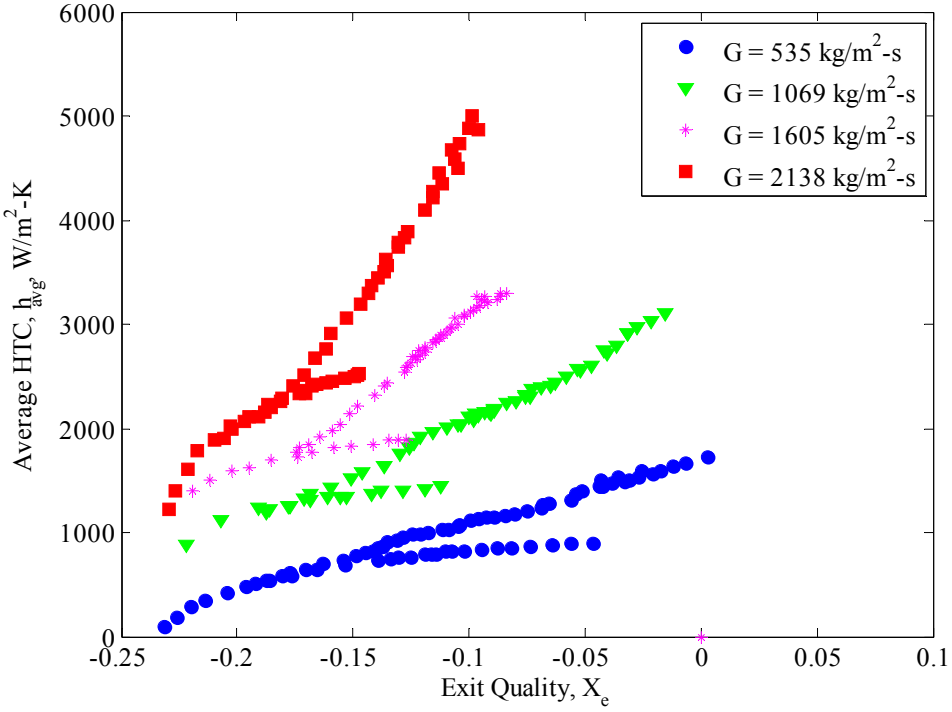

Figure 4.15 Average two-phase heat transfer coefficient at ΔT_{sat} = 20°C

As illustrated earlier, when nucleate boiling is the dominant mode of heat transfer, the effects of inlet subcooling and mass flux are negligible [62]. As can be seen in figures, increase in inlet subcooling has little or no effect on the average two phase heat transfer co-efficient, although it tends to increase the heat transfer in the single phase regime. Similarly it can be learnt from figures that mass flux has only a slight effect on the two-phase heat transfer co-efficient since the nucleate boiling regime is only partial and convective effects do prevail although not appreciable. However, mass flux does affect the single phase heat transfer, thus illustrating the dominance of convective effects. This phenomenon is clearly evident in Figure 4.16 - Figure 4.20.

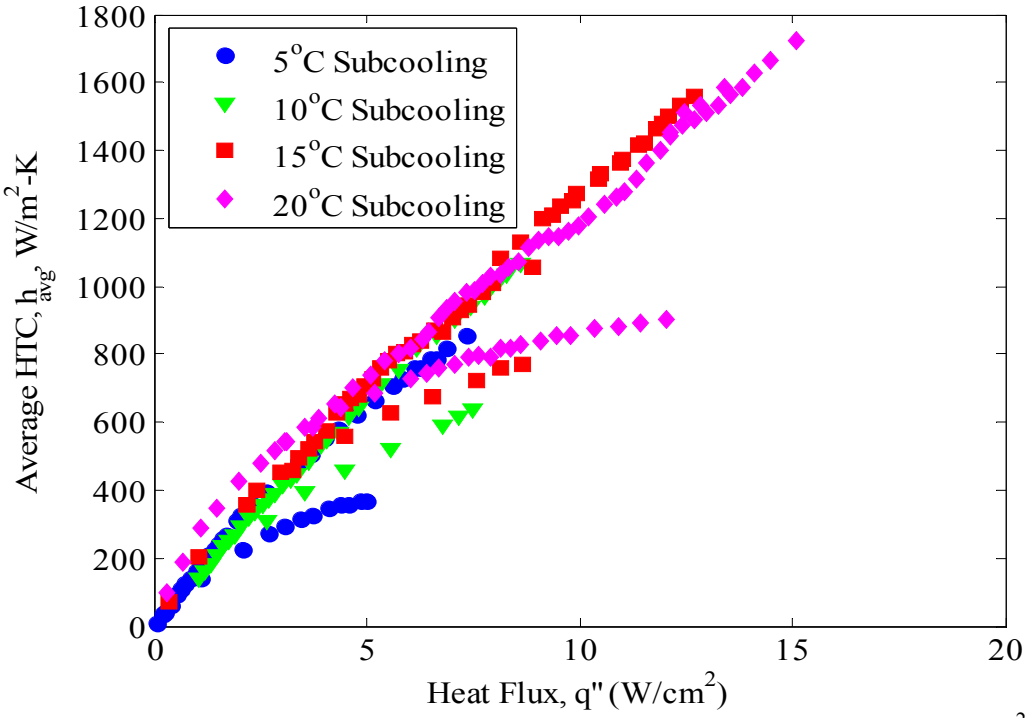

Figure 4.16 Effect of subcooling on avg. heat transfer coefficient at G=535 kg/m^{2}s

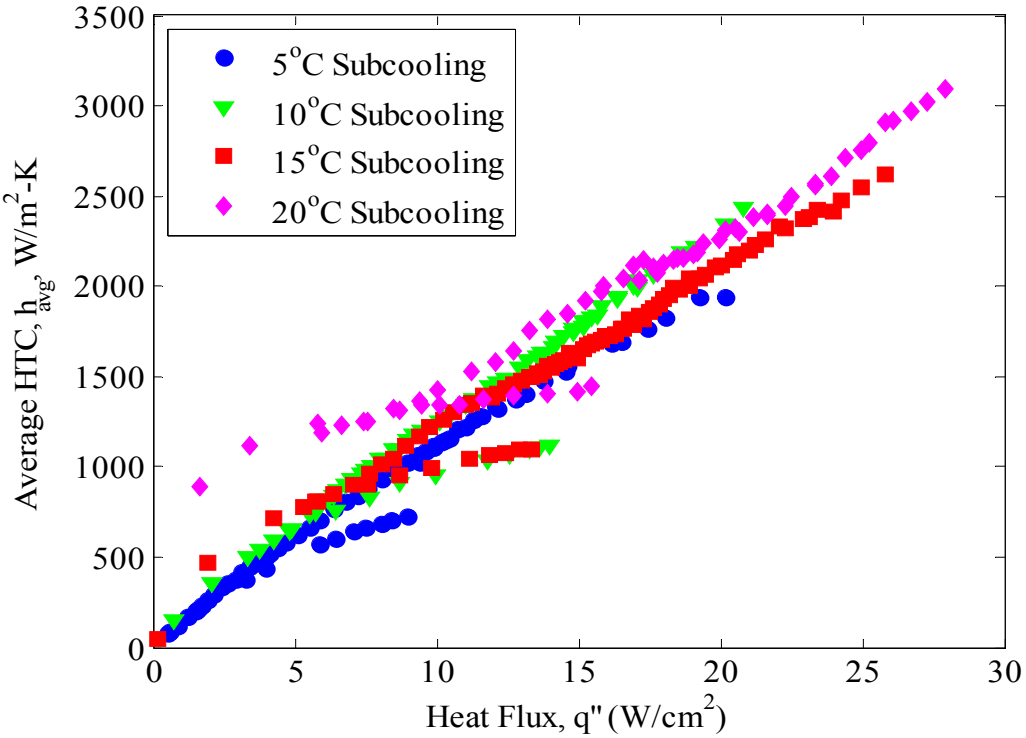

Figure 4.17 Effect of subcooling on avg. heat transfer coefficient at G=1069 kg/m^{2}s

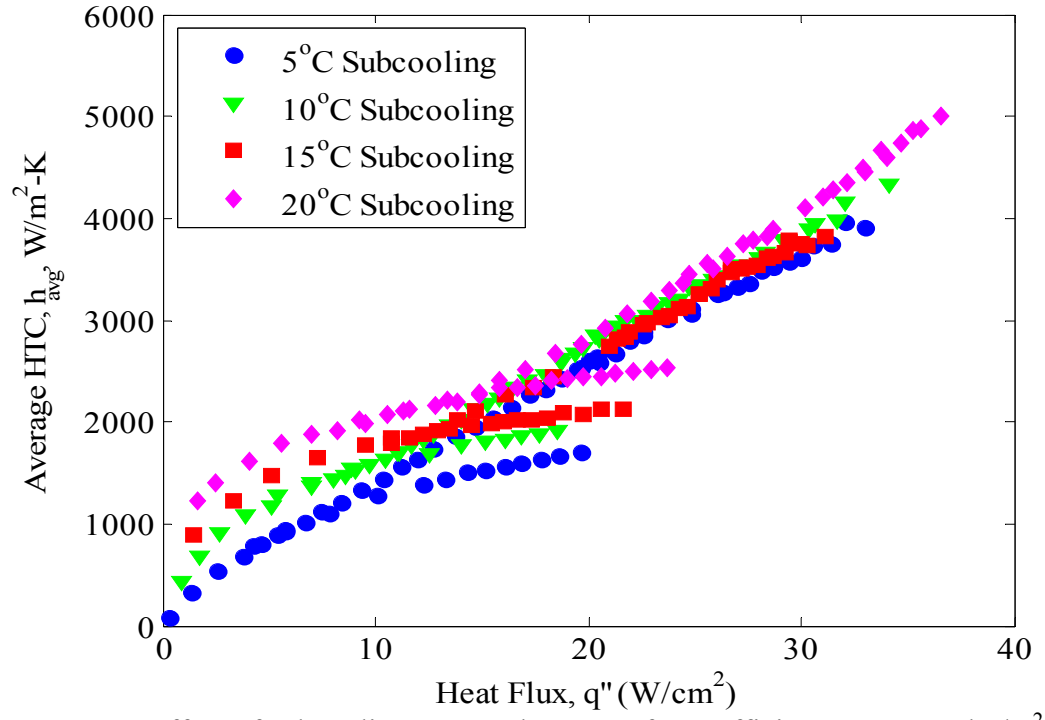

Figure 4.18 Effect of subcooling on avg. heat transfer coefficient at G=2138kg/m^{2}s

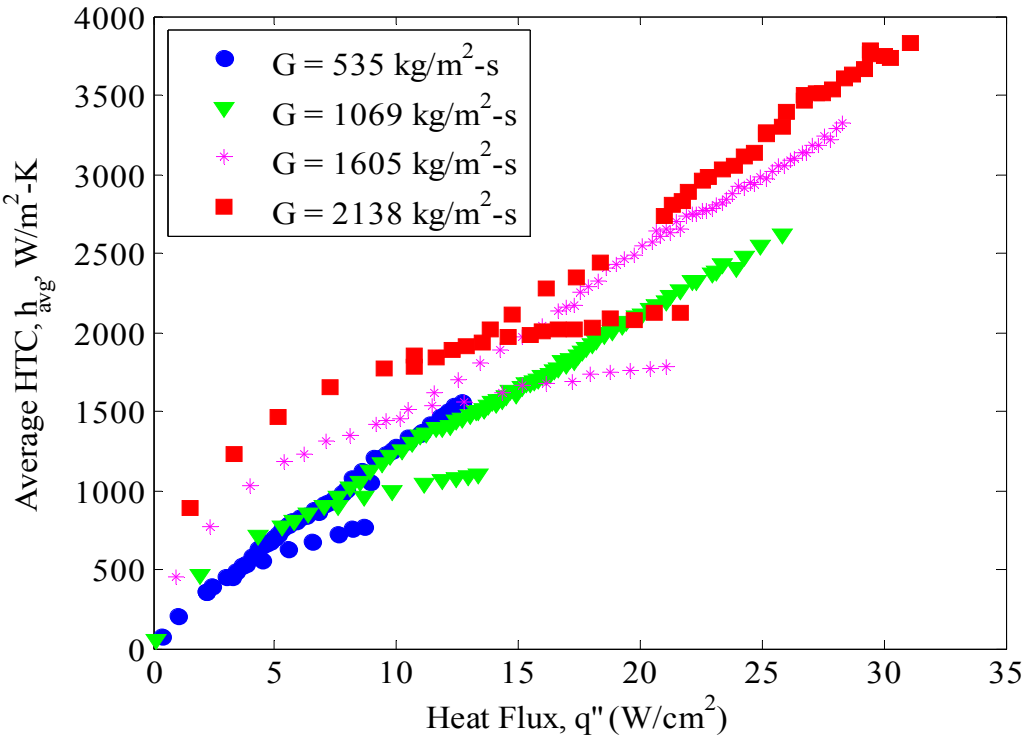

Figure 4.19 Effect of mass flux on avg. heat transfer coefficient at ΔT_{sat} = 15°C

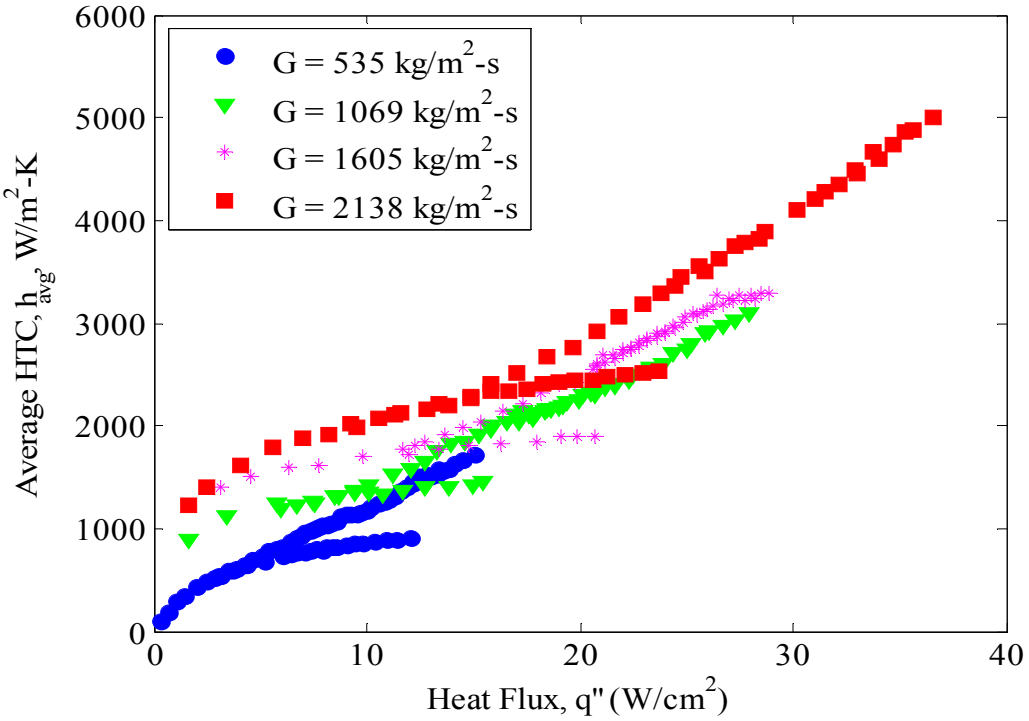

Figure 4.20 Effect of mass flux on avg. heat transfer coefficient at ΔT_{sat} = 20°C

4.2.5.3 Subcooled flow boiling heat transfer - Prediction methods.

Since the majority of the study concentrates on the subcooled flow boiling regime and the flow instabilities in that regime, data pertaining to saturated flow boiling are very limited. Hence, only the prediction methods developed for nucleate and subcooled flow boiling correlations will be analyzed to compare with the experimental results.

Since, nucleate boiling dominant heat transfer is not affected by inlet subcooling and mass flux, correlations which involve a power law relationship between heat transfer co-efficient and heat flux were developed in the past,

$$h = C_1 q''^{C_2} \tag{4.16}$$

where C_1 and C_2 are coefficients of fit. Some pool boiling correlations such as the Stephan-Abdelsalam [62] correlation were also of the same form as Equation 4.17. Using the available data, a similar relationship can be obtained for the subcooled nucleate

boiling of FC72 using method of least squares to fit the heat transfer coefficient data plotted against heat flux. The general relationship obtained can be expressed in the form of Equation 4.17

$$h = 0.15\, q''^{0.82}_{eff} \tag{4.17}$$

where q''_{eff} is the heat flux effective heat flux supplied to each microchannel. The values of C_1 and C_2 are consistent with the studies listed in Table 4.1. The references in table include experiments done in a wide range of channel sizes - macro and microchannels and tubes. It can be observed that the values of the co-efficient agree well with the macrochannel studies, indicating that the nucleate boiling regime of flow boiling in microchannels follows the trends of macrochannels.

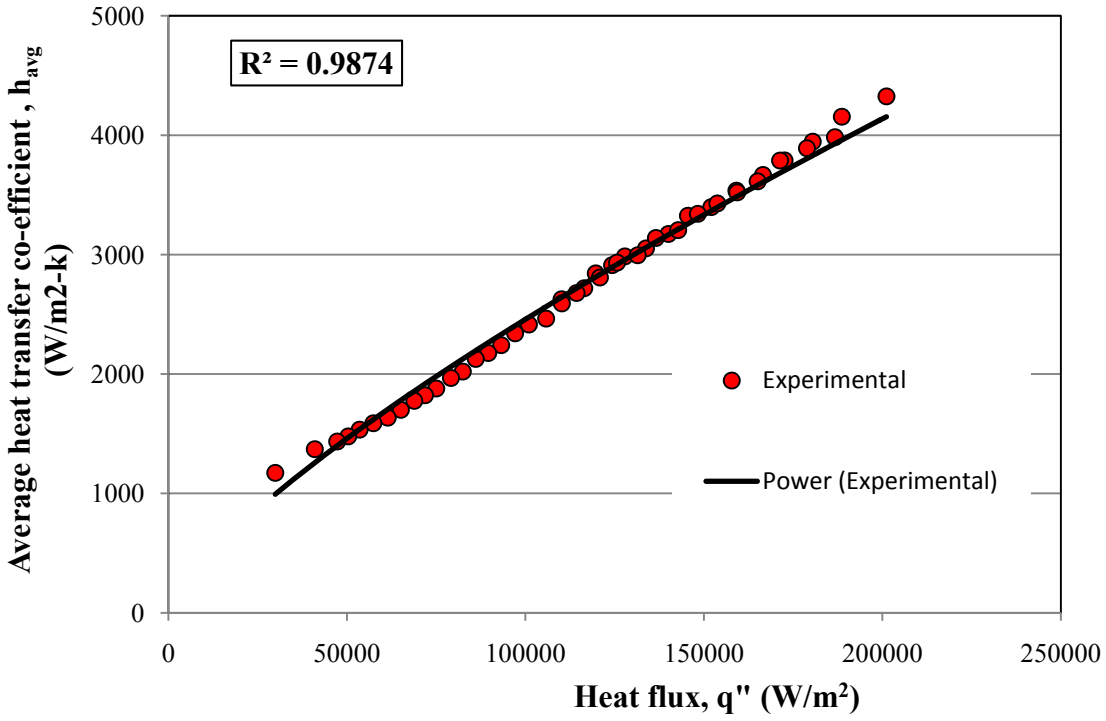

Figure 4.21 Curve fitting of the average heat transfer coefficient

Table 4.1 Nucleate boiling correlations for two-phase heat transfer coefficient as a function of heat flux

Reference	Channel Size/ Fluid	Co-efficients in Equation ()	
		C_1	C_2
Steiner and Taborek [63]	Conventional/ Water	-	0.67 – 0.8
Bao et al. [64]	Cu tube 1.95 mm/ R11, HCFC123	2.23, 2.84	0.735, 0.712
Kosar et al. [29]	Water	1.28	0.64
Current study	Microchannels D_h=255 µm/ FC72	0.15	0.82

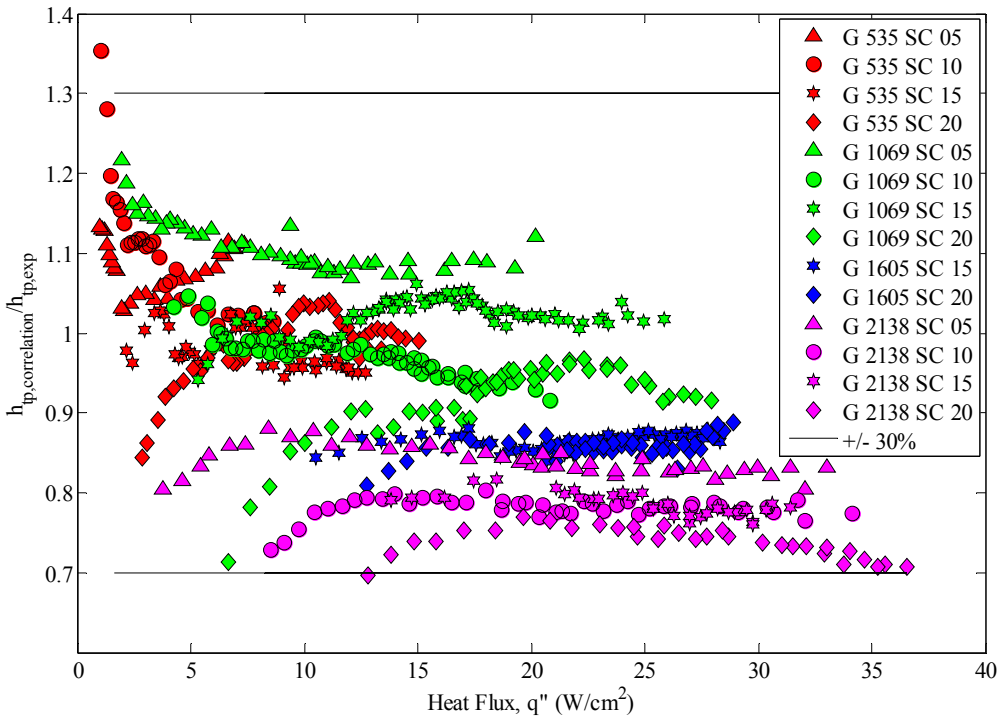

Figure 4.22 Heat transfer coefficient predictions of the correlations presented in the current study

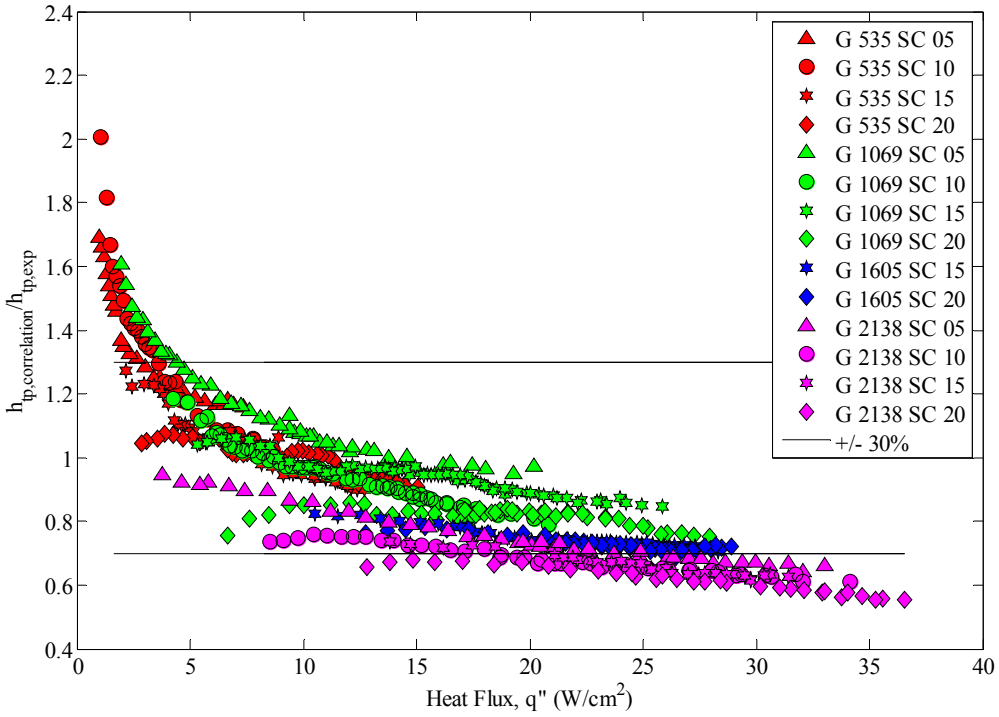

Figure 4.23 Heat transfer coefficient predictions of Kosar et al. [29]

From Figure 4.22, it can be noted that Equation 4.17 predicts 80% of data within 20% error. Interestingly, the nucleate boiling correlation of Kosar et al. [29] predicts the data well in many cases although the working fluid in those experiments was water which would normally result in higher heat transfer coefficient. This might be attributed to the efficiency of the re-entrant cavities in promoting bubble nucleation.

Although equations of the form as reported in Equation 4.17 have been found to predict the nucleate boiling heat transfer coefficient to good accuracy, the effects of number of other parameters such as surface tension, channel size and fluid properties which play a significant role in micro scale flow boiling heat transfer is not represented adequately and hence may not always represent the heat transfer characteristics [65]. Large numbers of flow boiling studies in the recent past, both micro and macro, have

resulted in correlations and models representing all or some of the parameters aforementioned. The following section is aimed at validating the application of some of these correlations for flow boiling of FC72 in microchannels using the available experimental data. The correlations studied are listed in Table 4.2 and the vast majority of correlations or models listed are for nucleate boiling since much of this study focuses on subcooled nucleate boiling.

Among the correlations, only the study conducted by Xie et al. [40] was for microchannels and Warrier et al. [34] for minichannels, while the rest were for much larger channels. Correlations of Shah [66], Liu and Winterton [67], and Warrier et al. [34] will be of special interest since they were developed for subcooled flow boiling conditions which are same as the conditions prevailing in the current study. The predicted heat transfer coefficient values by the some of the important correlations in Table 4.2 Correlations for average two-phase heat transfer coefficient are plotted in Figure 4.24 - Figure 4.28.

Table 4.2 Correlations for average two-phase heat transfer coefficient

	Reference	Fluid	Geometry/ Flow regime	Correlation
1	Lazerek and Black [68]	R 113	Circular, d_h = 3.15 mm/ Nucleate boiling	$h_{tp} = 30 Re_{LO}^{0.857} Bo^{0.714} \frac{k_f}{D_h};\ Bo = Boiling\ number.$
2	Kandlikar [69]	Water	Nucleate boiling	$h_{tp} = \left(.6683 Co^{-0.2} \left(1 - x_e\right)^{0.8} h_{lo} + 1058 Bo^{0.7} \left(1 - x_e\right)^{0.8} h_{lo}\right)$ $h_{lo} = 0.023 \mathrm{Re}_f^{0.8} Pr_f^{0.4} \frac{k_f}{D_h}; Co = Convection\ number.$
3	Kandlikar [69]	Water	Convective boiling	$h_{tp} = \left(1.136 Co^{-0.9} \left(1 - x_e\right)^{0.8} h_{lo} + 667.2 Bo^{0.7} \left(1 - x_e\right)^{0.8} h_{lo}\right)$ $h_{lo} = 0.023 \mathrm{Re}_f^{0.8} Pr_f^{0.4} \frac{k_f}{D_h}$
4	Yu et al. [70]	Water	Small horizontal tube, D = 2.98 mm / Nucleate boiling	$h_{tp} = 6.4 \times 10^6 \left(Bo^2 We_f\right)^{0.24} \left(\frac{\rho_f}{\rho_g}\right)^{-0.2}$
5	Tran et al. [65]	R 12, R 13	Horizontal rectangular channel, d_h = 2.4 mm/ Nucleate boiling	$h_{tp} = 8.4 \times 10^5 \left(Bo^2 We_f\right)^{0.3} \left(\frac{\rho_f}{\rho_g}\right)^{-0.4}$
6	Tran et al. [65]	R 134 a	Horizontal rectangular channel, d_h = 2.4 mm/ Nucleate boiling	$h_{tp} = 770 \left(BoRe_l N_{conf}\right)^{0.62} \left(\frac{\rho_g}{\rho_f}\right)^{0.297} \left(\frac{k_f}{D_h}\right)$

7	Warrier et al. [34]	FC 84	5 parallel rectangular channels/ Nucleate boiling	$h_{tp} = \left(1 + 6Bo^{1/16} - 5.3\left(1 - 855Bo\right)x_e^{0.65}\right)h_{sp}$ $h_{sp} = 8.235\begin{pmatrix}1 - 2.042\beta + 3.085\beta^2 - \\ 2.477\beta^3 + 1.058\beta^4 - 0.186\beta^5\end{pmatrix}\frac{k_f}{D_h}$
8	Liu and Winterton[67]	Pr_f = 0.83 to 9.1	Nucleate and convective boiling	$h_{tp}^2 = \left(Fh_{lo}\right)^2 + \left(Sh_{pool}\right)^2$ $F = \left[1 + x_e Pr_f\left(\frac{\rho_f}{\rho_g} - 1\right)\right]0.35; S = 1\Big/\left(1 + 0.055F^{0.1}Re_{lo}^{0.16}\right)$ $h_{lo} = 0.023Re_f^{0.8}Pr_f^{0.4}\frac{k_f}{D_h}$ $h_{pool} = 55\left(\frac{p}{p_{cr}}\right)^{0.12}\left(-\log_{10}\left(\frac{p}{p_{cr}}\right)\right)^{-0.55}M^{-0.5}q''^{0.67}$
9	Shah, MM [66]	Water, R11, R12, R22	Subcooled boiling	$h_{tp} = h_l\psi\left(\frac{T_w - T_{sat}}{T_w - T_{f,m}}\right)$ $\psi = \psi_o + \left(\frac{T_{sat} - T_{f,m}}{T_w - T_{sat}}\right)$
10	Xie et al. [40]	FC 72	19 parallel microchannels, dh = 0.33 -0.54mm / Nucleate boiling	$h_{tp} = 0.02472Re^{0.6399}Pr_f^{-3.5104}\left(\frac{Pr_f}{Pr_w}\right)^{-0.0872}\left(\frac{D_h}{L}\right)^{-2.0960}\left(\frac{H}{W_c}\right)^{0.}$
11	Current Study	FC 72	19 microchannels/ Subcooled Nucleate boiling	$h_{tp} = 0.15\,q''^{0.82}_{eff}$

From Table 4.2, it can be noted that there are very few correlations available in the literature which would suit the conditions of the current study such as subcooled nucleate boiling of a low contact angle fluid in surface augmented microchannels. Hence, most of the correlations listed [2-5,7-8] in Table 4.2 which were primarily developed for saturated flow boiling conditions significantly over predict the heat transfer.

Comparing the saturated flow boiling correlation (#3) proposed by Kandlikar [69] with the experimental heat transfer coefficient, significant over prediction was observed as shown in Figure 4.24 Heat transfer predictions of correlation#3. Similarly other convection dominant boiling correlations such as Lazerek and Black [68] over predicted by a large margin.

However, even the correlations (#4 and 5) developed for nucleate boiling dominant heat transfer due to flow in small channels by Yu et al. [70] and Tran et al. [65], over estimated the heat transfer coefficient under all operating conditions as shown in Figure 4.25. The Tran et al [65] correlation over predicted the experimental data by a factor of eight, but the error reduced significantly at high heat flux values as the correlation was developed for a quality range of $0.2 < x < 0.8$, which could also be a reason for the over estimation at other conditions.

Figure 4.26 and Figure 4.27 show the predictions of subcooled flow boiling correlations developed for nucleate boiling dominant heat transfer, which are of special interest because of similar conditions of the current study, proposed by Warrier et al. [34] (#7), and Shah [66] (#9). Warrier et al. [34] correlation is dependent only upon boiling number (Bo) and subcooling number (Sc) and valid for $0.00014 \le Bo \le 0.00089$, $0 \le Sc \le 0.80$. It can be noted that the predictions of correlation # 7over estimate the

results by a factor of two at low heat flux and predicts it well within a band of ±30% of experimental results at higher heat flux. The predictions exceeded the experimental results by a factor of two or three at low mass flux in the case of Shah [66] which however demonstrated better accuracy at higher mass flux. The deviation in prediction can also be attributed to the size and type of test sections tested. Warrier et al. [34] conducted tests on mini channels using FC84 and Shah [66] on pipes and annuli. The correlation of Liu and Winterton [67] proposed for conventional channels, is based on the Chen model where the heat transfer coefficient is split into the individual contributions by nucleate and convective boiling. The nucleate boiling contribution was estimated by Cooper [71] pool boiling correlation and the convective component using Dittus Boelter [44] correlation. The predictions of this correlation however were significantly higher than the experimental values. The correlation proposed by Xie et al. [40], was formulated for a test section which whose specifications were very close to those tested in the current study such as flow boiling of FC72 in 19 parallel microchannels with similar aspect ratios. However, from Figure 4.28, it can be noted that the correlation under predicts the two-phase heat transfer which illustrates the heat transfer enhancing abilities of re-entrant cavities that were used in the current study.

Hence, it can be noticed that the predictions of all the correlations listed deviate by a large margin from the experimental data set and illustrates the need for system specific models. However, the simple empirical nucleate boiling correlations proposed by Kosar et al. [29] and current study which were obtained by curve fitting predicts the data to good accuracy, although it does not sufficiently represent the factors influencing the heat transfer.

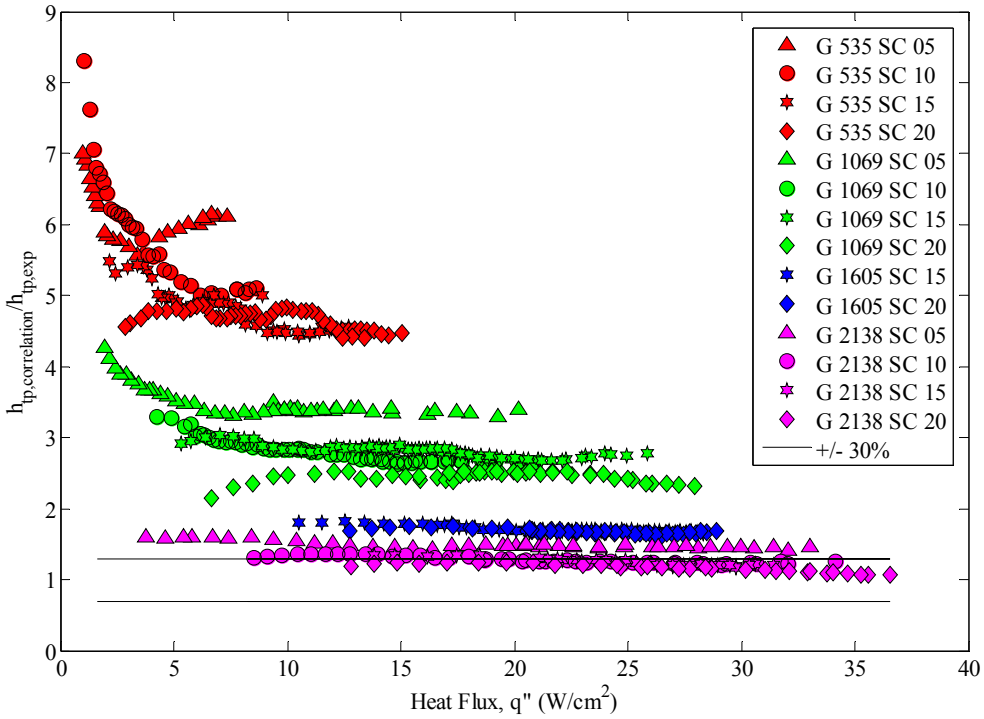

Figure 4.24 Heat transfer predictions of correlation#3

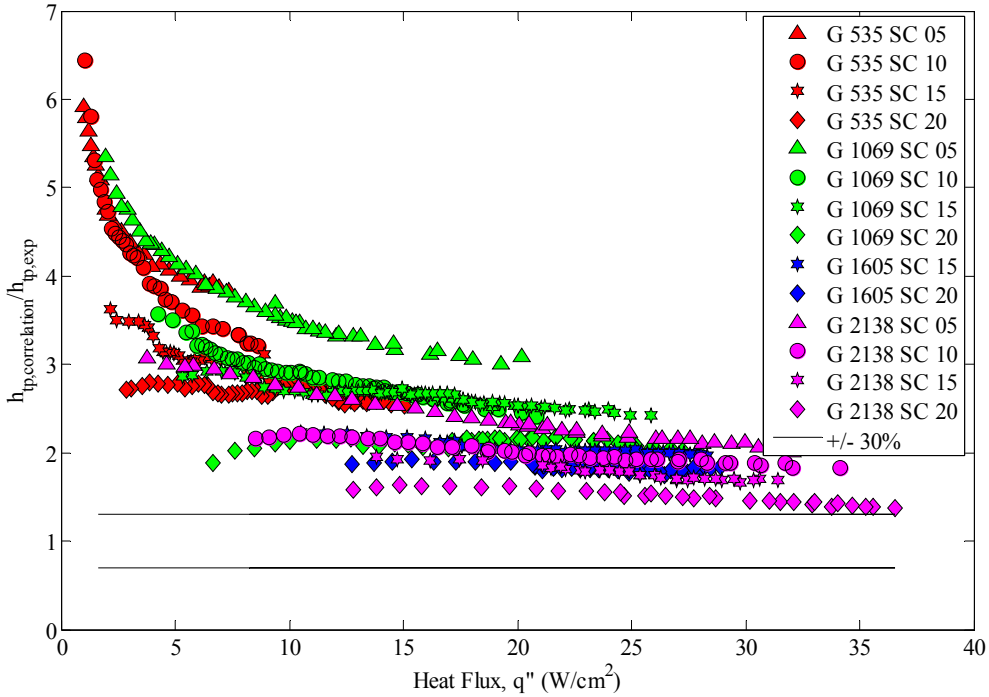

Figure 4.25 Heat transfer coefficient predictions of correlation#5

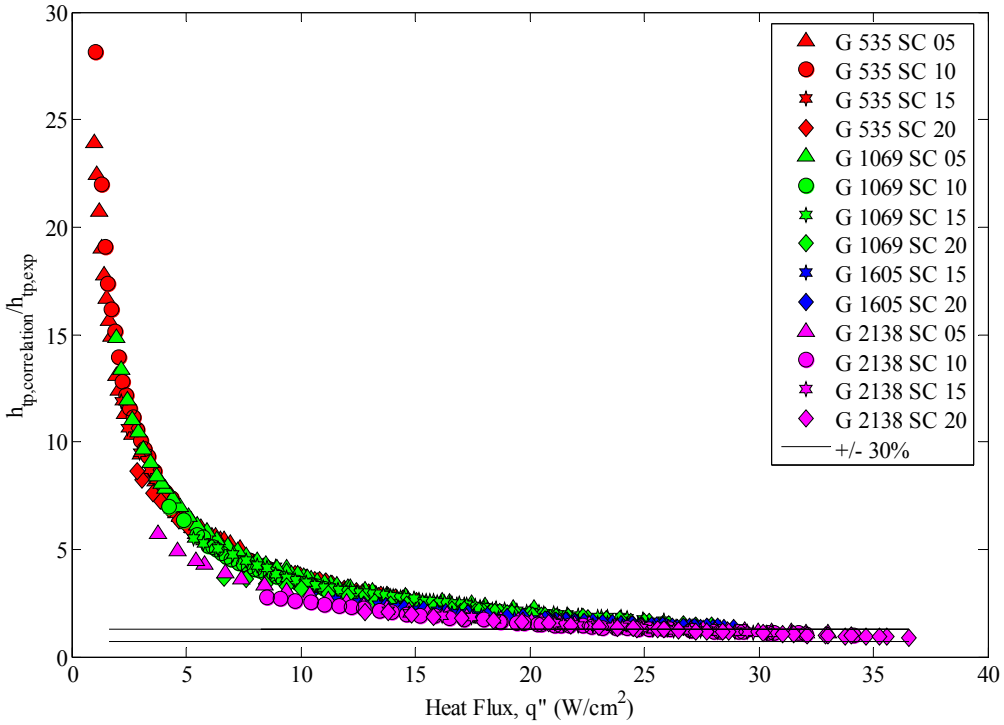

Figure 4.26 Heat transfer predictions of correlation#7

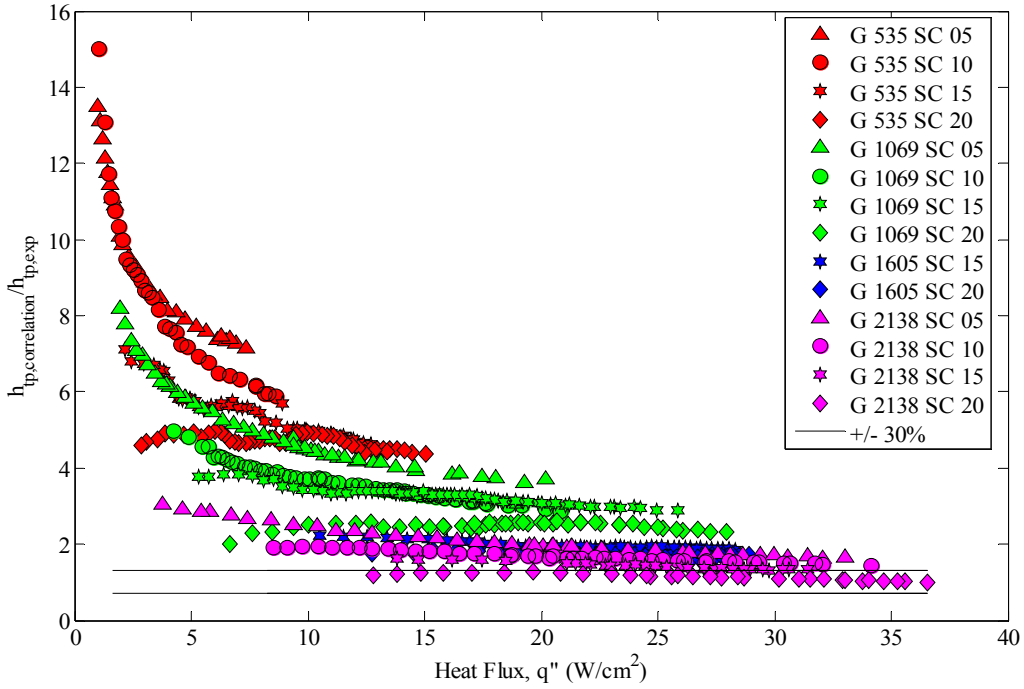

Figure 4.27 Heat transfer coefficient predictions of correlation#9

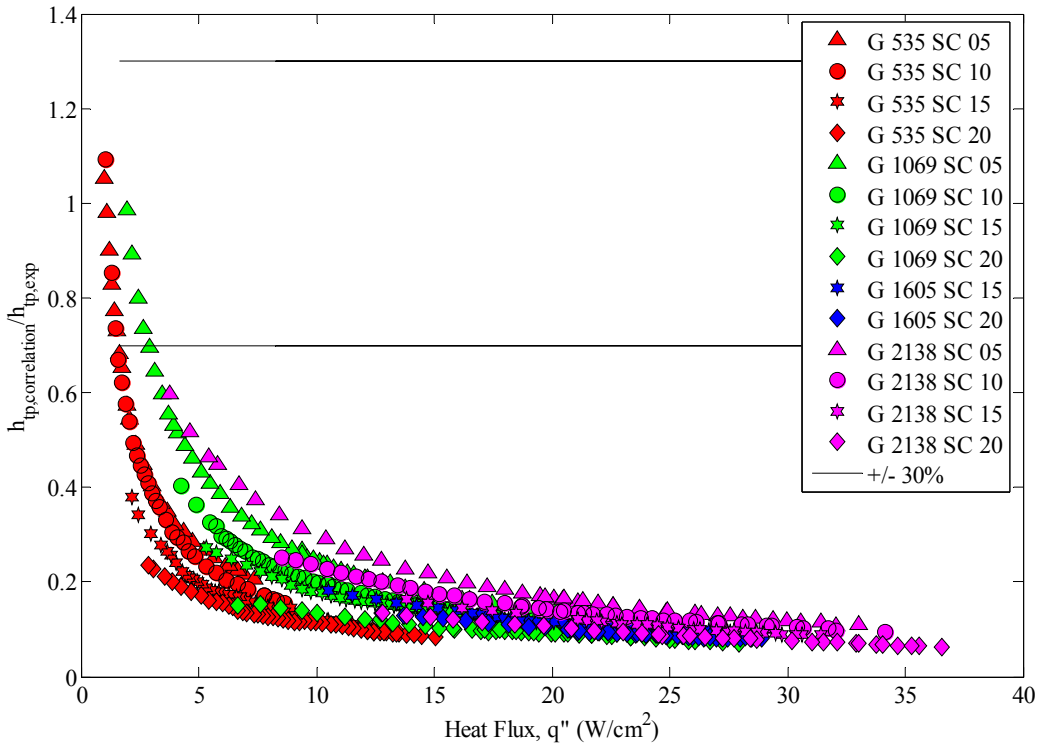

Figure 4.28 Heat transfer coefficient predictions of correlation#10

4.3 Pressure drop characteristics

This section investigates the variation of measured pressure drop between the inlet and the exit of the microchannels with increasing heat flux. The influence of parameters such as inlet liquid subcooling and mass flux has also been reported. As pointed out in the earlier sections, the literature and hence models available for subcooled flow boiling is very limited and the limitations only increase when considering the flow of a fluorocarbon such as FC72. The obtained experimental results were compared with models developed for large channel two-phase flows and small channel two-phase flows to validate the applicability of macrochannel theories to microchannels.

4.3.1 Experimental results for multi-channel configuration

The experimental pressure drop was measured using the pressure transducer measurements at the inlet and the exit. The experimental pressure drop is given by,

$$\Delta p_{total} = p_{in} - p_{out} \tag{4.18}$$

However, since the pressure measurements were made at locations away from the inlet and exit of the microchannels, the measured pressure drop also includes the pressure losses experienced at the various bends, flow contractions and expansions. Hence Equation 4.18 can be modified as,

$$\Delta p_{total} = \Delta p_{losses} + \Delta p_{microchannel} \tag{4.19}$$

The estimation of pressure losses in the various sections upstream and downstream of the microchannel has been explained in Appendix B. The estimated pressure drop in the microchannels has been plotted in Figures 4.34 – 4.41 as a function of heat flux at different operating conditions and different microchannel configurations.

It can be noticed in Figure 4.35 that in the single phase flow regime, as the heat flux increases, the pressure drop remains constant or shows a slight decrease in magnitude. Further increase in heat flux leads to the transition from single phase to subcooled nucleate boiling which is marked by a sudden jump in the pressure drop curve owing to the increase in void fraction along the channel. As heat flux is increased further, the acceleration effects increase and leads to an increase in pressure drop. When the heat flux was reduced, the pressure drop reduced and in the vicinity of ONB, the jump initially noticed was absent the pressure drop curve merged smoothly with the single phase pressure drop. This hysteresis phenomenon, as pointed out in the earlier sections, can be

attributed to the highly wetting nature of FC72 which causes a delay in ONB while the heat flux is increased.

The sections below portray the influence of independent parameters such as inlet subcooling and mass flux.

a) Effect of inlet subcooling

As inlet liquid subcooling increases, at a given heat flux and mass flux, the wall superheat reduces and consequently, less vapor fraction in the channel. This leads to a reduction in pressure drop which is clearly evident in Figures 4.29 – 4.31. This observed trend is consistent with the microchannel study reported by Jones et al. [22] and some of the earliest studies on subcooled boiling in large channels by Buchberg et al. [72] and Reynolds [73].

b) Effect of mass flux

As discussed earlier in the preceding sections, increasing the mass flux causes increases the forced convection effects and hence leads to an increase in pressure drop which is trend as shown in Figures 4.32. However, at higher heat flux, as the mass flux in increased the increase in convection effects leads to a reduction in wall superheat and hence tends to suppress the bubble nucleation at the cavities. This leads to a reduction in the rate of increase of pressure drop at higher heat flux as evident in Figures 4.32 - 4.35.

The pressure drop plots also reveal the fluctuation of pressure drop observed due to flow reversal, noted as unstable regions as marked in Figure 4.35. These unstable regions will be analyzed in detail later in the flow instabilities section.

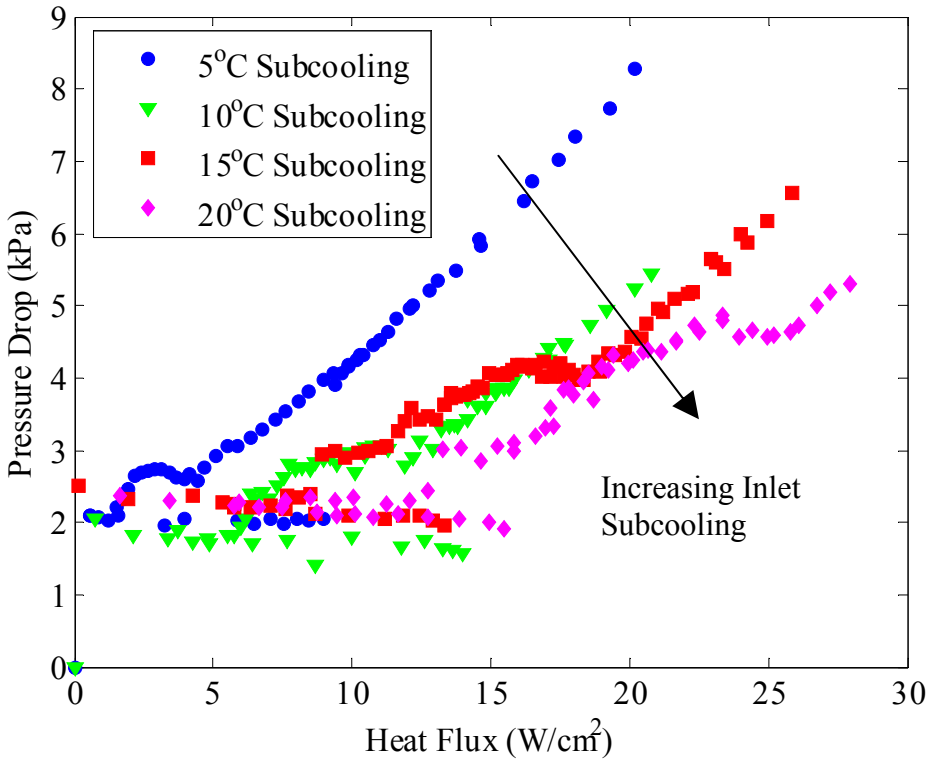

Figure 4.29 Effect of inlet subcooling on pressure drop at G=1069kg/m^2 s

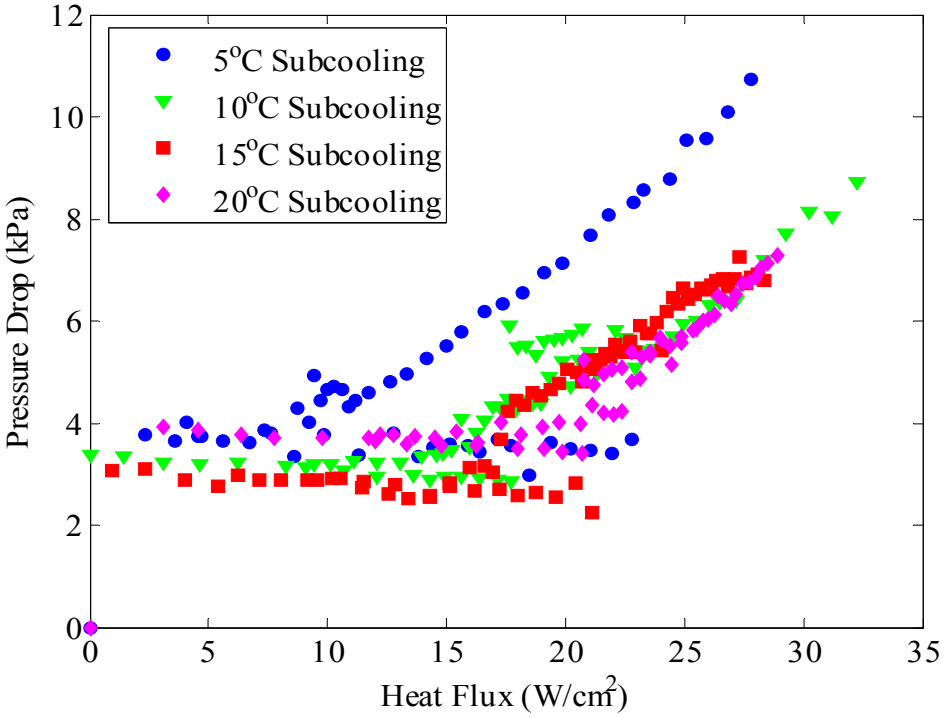

Figure 4.30 Effect of inlet subcooling on pressure drop at G=1605kg/m^{2}s

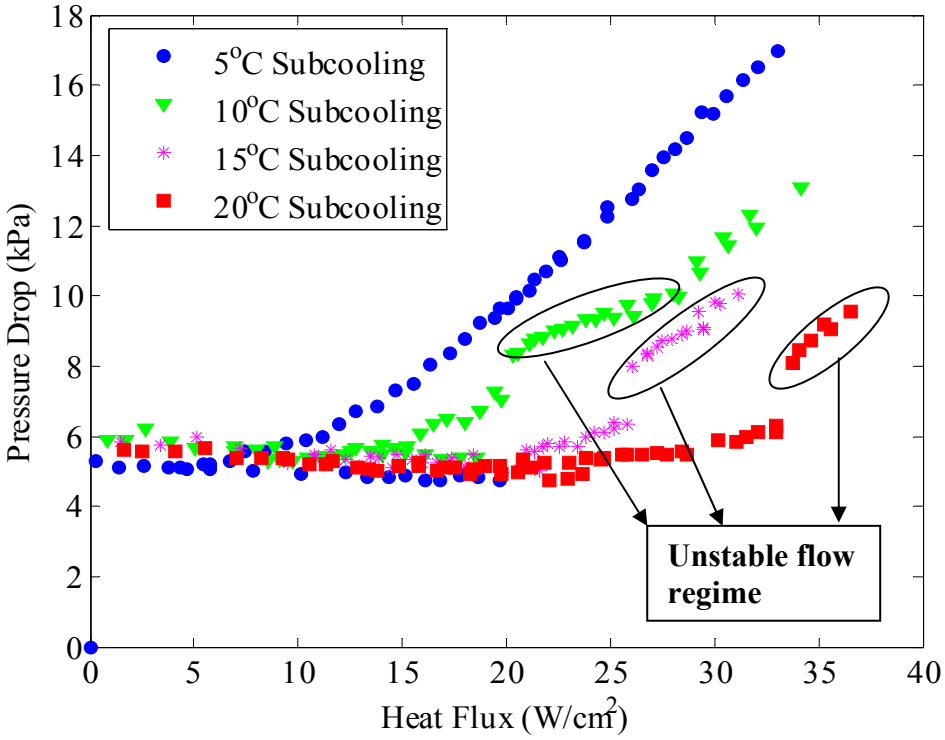

Figure 4.31 Effect of inlet subcooling on pressure drop at G=2138kg/m^{2}s

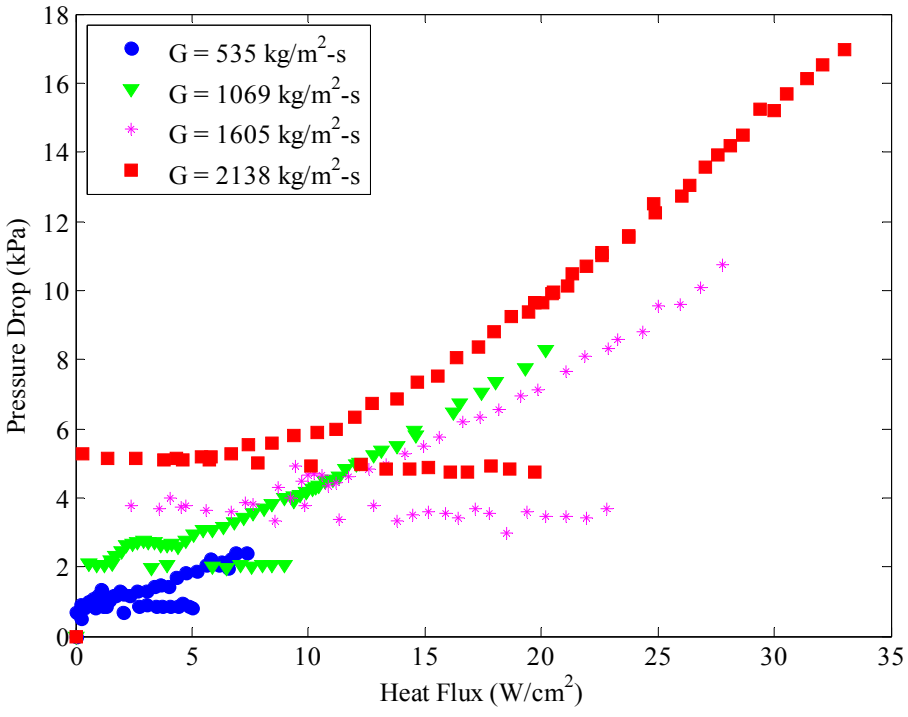

Figure 4.32 Effect of mass flux on pressure drop at 5°C inlet subcooling

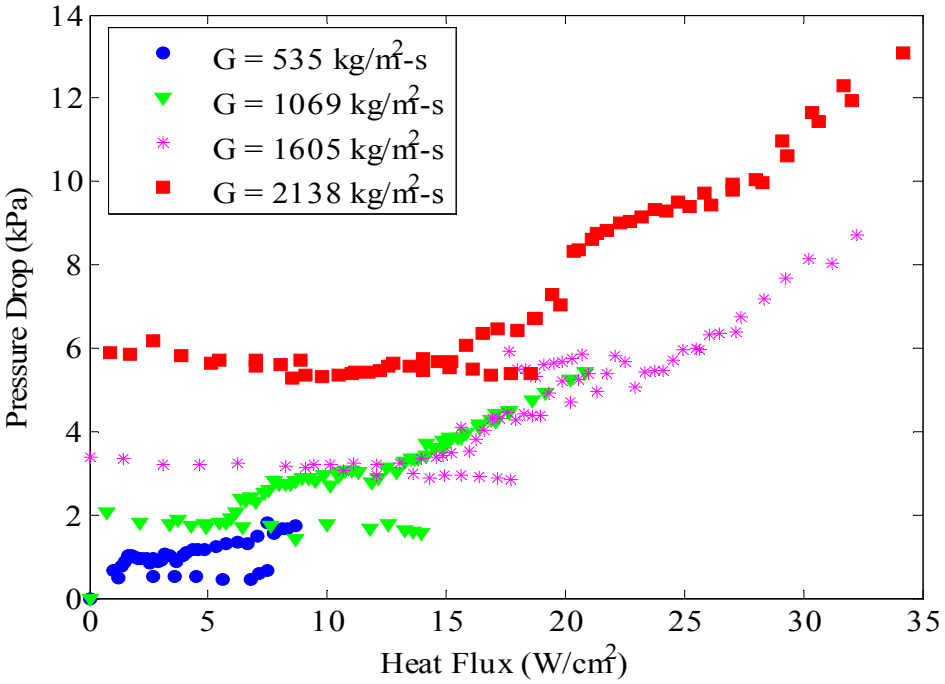

Figure 4.33 Effect of mass flux on pressure drop at 10°C inlet subcooling

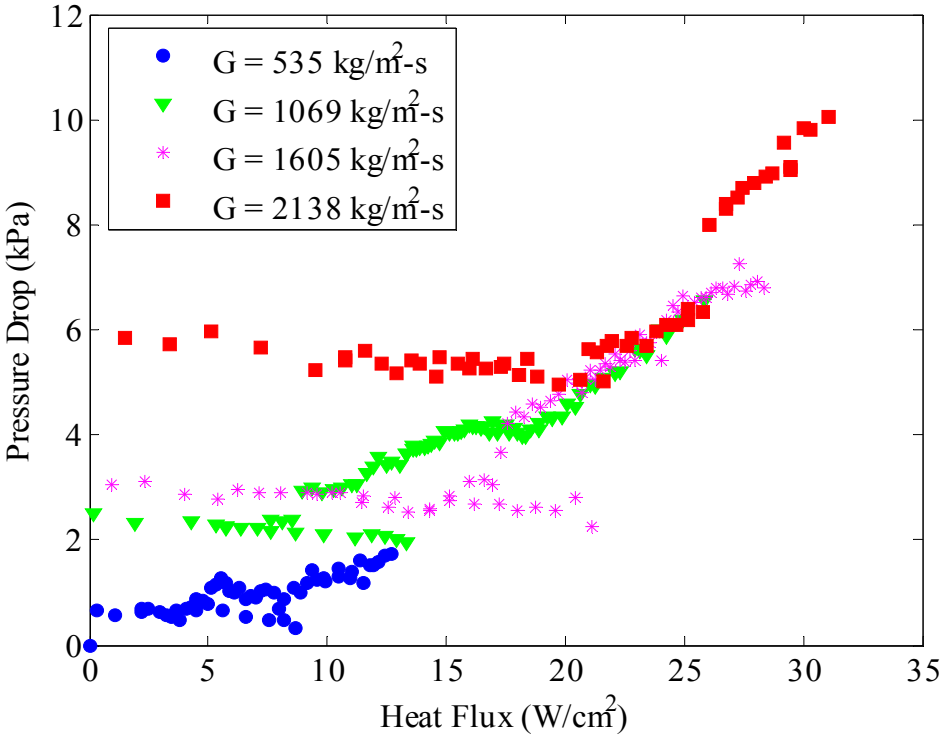

Figure 4.34 Effect of mass flux on pressure drop at 15°C inlet subcooling

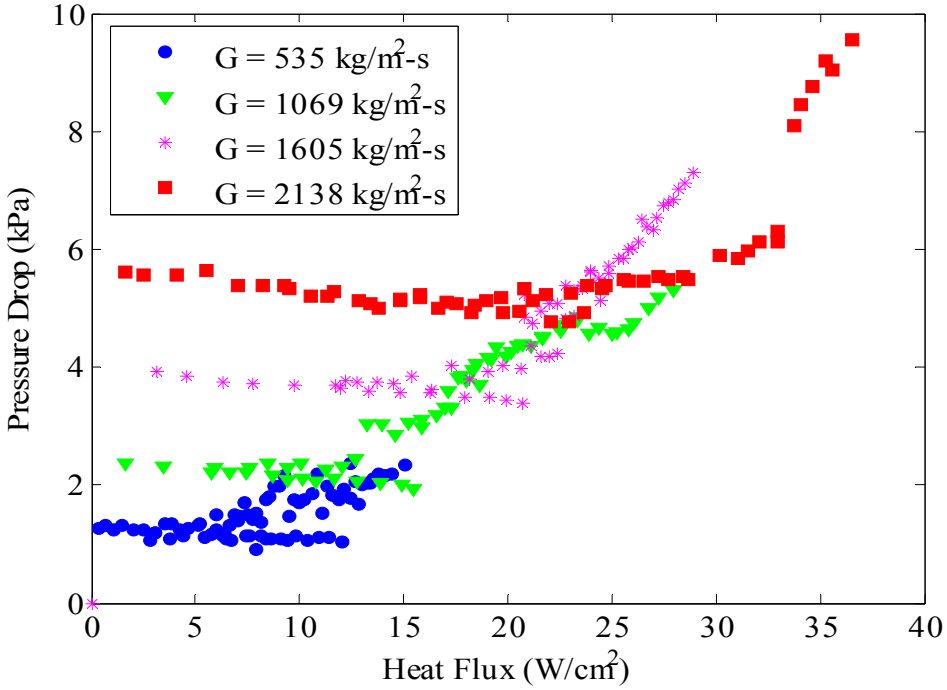

Figure 4.35 Effect of mass flux on pressure drop at 20°C inlet subcooling

4.3.2 Experimental pressure drop in a single channel

The experimental pressure drop in a single microchannel was measured in the same way as multichannel configuration. The experimental pressure drop is the difference in pressure measured by the transducers at the exit and inlet and the losses were accounted in a similar manner.

In Figure 4.36, in single phase, as the heat flux is increased, the pressure drop remains constant or shows a slight decrease in magnitude. Further increase in heat flux leads to the transition from single phase to subcooled nucleate boiling which is marked by a sudden jump in the pressure drop curve owing to the increase in void fraction along the channel. Under some conditions, this discontinuity in pressure drop was not observed as in the case of 15°C inlet subcooling in Figure 4.36, and instead, it happened under saturated conditions at the exit when there were hints of flow reversal or vapor bubbles

seen at the channel inlet. This may be due to the transition from bubbly flow to annular flow which accompanies high vapor production. As the heat flux is reduced, the pressure drop curve followed a different path, and this hysteresis can be attributed to the highly wetting nature of FC72 which causes a delay in ONB while the heat flux is increased.

a) Effect of inlet subcooling and mass flux

Figure 4.36 shows the effect of inlet subcooling on pressure drop at a constant mass flux of 1069 kg/m^{2}s for the 155μm test section with two cavities (SC 100-2). The single phase pressure drop will not be affected as it is controlled only by the mass flux. The two phase pressure drop curve shifts to the right as the inlet subcooling increases, owing to the lower wall superheat at higher subcooling at a heat flux, which also leads to a higher incipient heat flux. This observed trend confirms with those observed for the multichannel test device, MC 200-2.

Figure 4.37 shows the effect of mass flux on pressure drop at a constant inlet subcooling of 10°C. As expected an increase in single phase pressure drop was observed. As mass flux increases, it can be noticed that the incipient flux increases due to lower wall superheats and causes the two phase pressure drop curve to shift to the left.

b) Effect of number of cavities

Experiments were also conducted to investigate the effects of number of cavities on the pressure drop. Two different configurations were tested – one with two cavities equally spaced along the length of the channel and the other with six cavities, also equally spaced. Although the pressure drop was expected to differ from that of two cavity sections due to the increased number of nucleation sites, the pressure drop curves showed very little difference as no significant increase in vapor production was observed as seen in Figure 4.38.

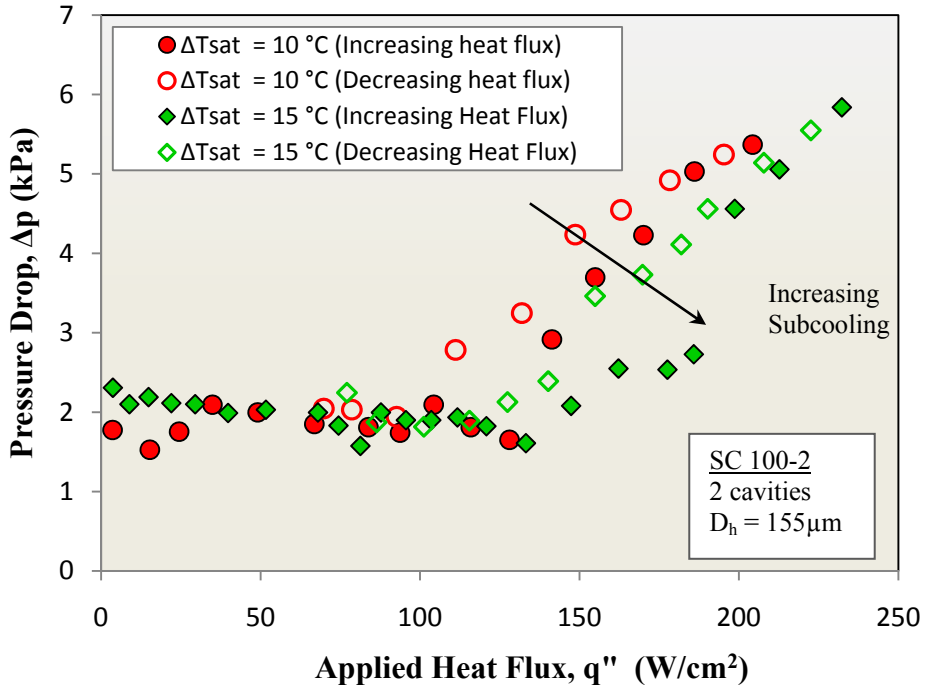

Figure 4.36 Effect of inlet subcooling on pressure drop at G=1069kg/m^{2}s

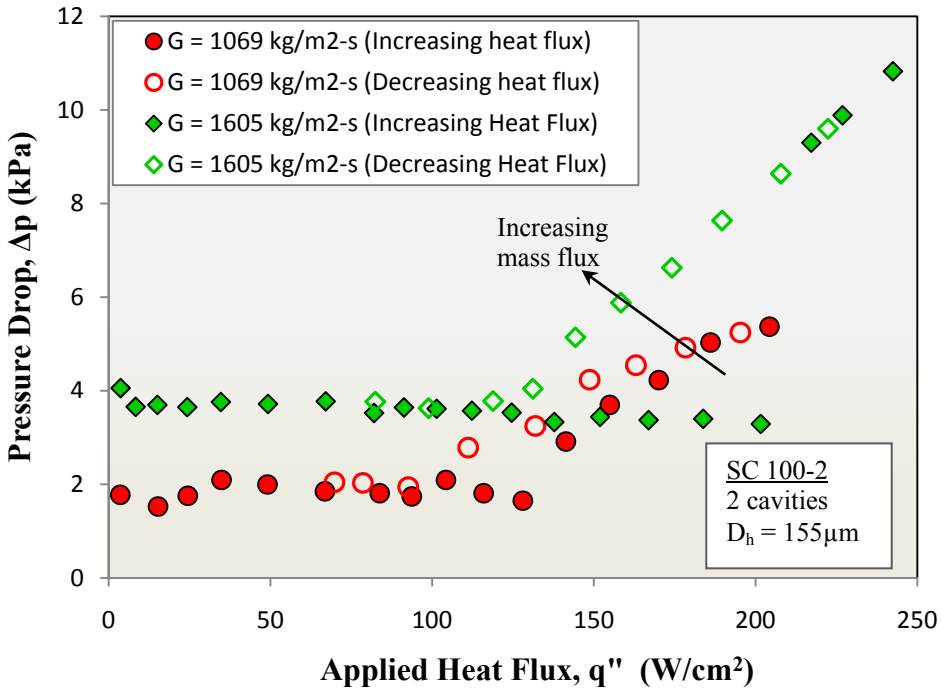

Figure 4.37 Effect of mass flux on pressure drop at 10°C inlet subcooling

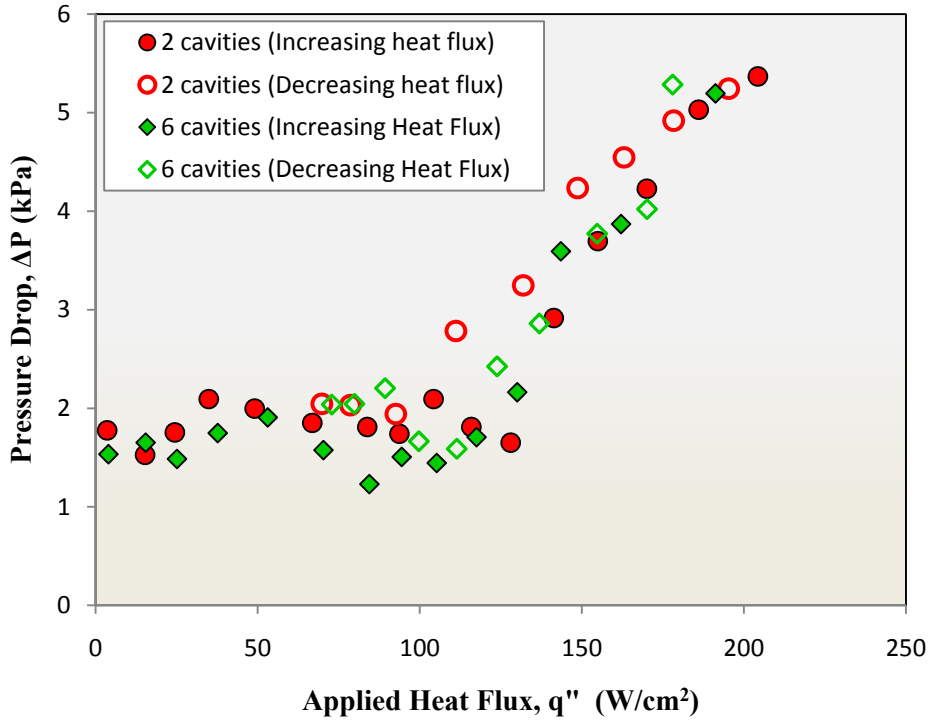

Figure 4.38 Effect of number of cavities on pressure drop at inlet subcooling of 10°C and G=1069kgm^{2}s

4.3.1 Theoretical Models

The purpose of this section is to analyze the predictive ability of classical models developed for the two-phase pressure gradients and investigate its validity for flow in microchannels. The models developed for pressure drop based on the momentum balance approach mainly fall into two categories – Homogeneous model and Separated flow model.

Homogeneous model assumes [74]

a. equal liquid and vapor phases velocity

b. thermodynamic equilibrium between the phases

c. use of single-phase friction factor for two-phase flow

From high speed visualization of the flow boiling process of FC72 in microchannels, the main flow regime, especially in the range of operating conditions

tested, was bubbly flow which involves the movement of individual vapor bubbles along with the liquid. This makes the first assumption of homogeneous flow very attractive as it can be applied for estimating two-phase pressure gradient in the current study. Bowers and Mudawar [36] showed that satisfactory prediction can be achieved using this model for the flow boiling of a R113 which has properties similar to that of FC72 such as low surface tension and a very low contact angle.

Separated flow, on the other hand ,models the flow as phases moving in layers.This model is well suited for flow regimes involving stratified flow. Comparing it to the homogeneous model, it assumes [74] constant but not necessarily equal velocity of liquid and vapor phases.

The experimental pressure drop data obtained at various operating conditions were compared with the homogeneous and four separated flow models. In all the models, the two-phase pressure drop is expressed as a sum of the frictional and acceleration pressure gradients.

$$\Delta p_{tp} = \Delta p_{tp,fr} + \Delta p_{tp,a} \tag{4.20}$$

The frictional and acclerational pressure drop components can be estimated using the models described in the table (only the two phase components).

The average two-phase viscosity used in the above calculations was estimated by using the McAdams [53] two-phase mixture viscosity model,

$$\mu_{tp} = \left[\frac{x_e}{\mu_g} + \frac{(1 - x_e)}{\mu_f} \right]^{-1} \tag{4.21}$$

In all the previous sections, it can be observed that a negative exit quality usually represents subcooled flow regime during which vapor does exist at the channel exit. To represent this vapor present under subcooled conditions, the definition of exit quality has been modified . The modified exit quality can be expressed as,

$$x_e = x_{e,mod} = \begin{cases} \frac{q_{wall} - q_{ONB}}{\dot{m} h_{fg}}, & T_{out} < T_{sat} \\ \frac{q_{wall} - q_{ONB}}{\dot{m} h_{fg}} + \frac{q_{wall} - \dot{m} C_p (T_{sat} - T_{in})}{\dot{m} h_{fg}}, & T_{out} \geq T_{sat} \end{cases} \quad (4.22)$$

Table 4.3 Two-phase pressure drop correlations

#	Model/ Reference	Pressure drop equation
1	Homogeneous model [62]	$\Delta p_{tp,fr} = \frac{2 f_{tp} G^2 L_{tp} \upsilon_f}{D_h}\left[1+\left(\frac{x_e}{2}\frac{\upsilon_{fg}}{\upsilon_f}\right)\right];$ $\Delta p_{tp,a} = G^2 \upsilon_f x_e$
2	Separated flow/ Lockhart Martineli (Laminar liquid – laminar vapor) [62,75]	$\Delta p_{tp,fr} = \frac{2 f_f G^2 L_{tp} \upsilon_f (1-x_{avg})}{D_h}\phi_f^2$ $f_f Re_f = 24\left(1-1.355\beta+1.947\beta^2-1.701\beta^3+0.956\beta^4-0.254\beta^5\right)$ $Re_f = \frac{G(1-x_e)D_h}{\mu_f}$ $\phi_f^2 = 1+\frac{C}{X_{vv}}+\frac{1}{X_{vv}^2}; C = 5.$ $X_{vv} = \left(\frac{\mu_f}{\mu_g}\right)^2\left(\frac{1-x_e}{x_e}\right)^{0.5}\left(\frac{\upsilon_f}{\upsilon_g}\right)^{0.5}$ $\Delta p_{tp,a} = G^2\upsilon_f\left[\frac{x_e^2}{\alpha_e}\left(\frac{\upsilon_f}{\upsilon_g}\right)+\frac{(1-x_e)^2}{1-\alpha_e}-1\right]$ $\alpha_e = 1-\frac{1}{\sqrt{1+\frac{20}{X_{vv,e}}+\frac{1}{X_{vv,e}^2}}}$
3	Separated flow/ Lockhart Martineli (Laminar liquid – turbulent vapor) [62,75]	$\Delta p_{tp,fr} = \frac{2 f_f G^2 L_{tp} \upsilon_f (1-x_{avg})}{D_h}\phi_f^2$ $\phi_f^2 = 1+\frac{C}{X_{vt}}+\frac{1}{X_{vt}^2}; C = 12;$ $X_{vt} = \left(\frac{f_f \,\mathrm{Re}_g^{0.25}}{0.079}\right)^2\left(\frac{1-x_e}{x_e}\right)\left(\frac{\upsilon_f}{\upsilon_g}\right)^{0.5}; Re_g = \frac{G x_e D_h}{\mu_g};$ $\Delta p_{tp,a} = G^2\upsilon_f\left[\frac{x_e^2}{\alpha_e}\left(\frac{\upsilon_g}{\upsilon_f}\right)+\frac{(1-x_e)^2}{1-\alpha_e}-1\right]$ $\alpha_e = 1-\frac{1}{\sqrt{1+\frac{20}{X_{vv,e}}+\frac{1}{X_{vv,e}^2}}}$

4	Separated flow/ Mishima and Hibiki [76]	$\Delta p_{tp,fr} = \dfrac{2 f_f G^2 L_{tp} \upsilon_f (1 - x_{avg})}{D_h} \phi_f^2$ $\phi_f^2 = 1 + \dfrac{C}{X_{vt}} + \dfrac{1}{X_{vt}^2}; C = 21\left[1 - \exp\left(-319 D_h\right)\right];$ $X_{vv} = \left(\dfrac{\mu_f}{\mu_g}\right)^{0.5} \left(\dfrac{1 - x_e}{x_e}\right)^{0.5} \left(\dfrac{\upsilon_f}{\upsilon_g}\right)^{0.5}$ $\Delta p_{tp,a} = G^2 \upsilon_f \left[\dfrac{x_e^2}{\alpha_e}\left(\dfrac{\upsilon_g}{\upsilon_f}\right) + \dfrac{(1 - x_e)^2}{1 - \alpha_e} - 1\right]$ $\alpha_e = 1 - \dfrac{1}{1 + \left(\dfrac{1 - x_e}{x_e}\right)\left(\dfrac{\upsilon_f}{\upsilon_g}\right)^{2/3}}$
5	Separated flow/ Lee and Lee [77]	$\Delta p_{tp,fr} = \dfrac{2 f_f G^2 L_{tp} \upsilon_f (1 - x_{avg})}{D_h} \phi_f^2$ $\phi_f^2 = 1 + \dfrac{C}{X_{vt}} + \dfrac{1}{X_{vt}^2}; C = 6.185 \times 10^{-2} Re_{lo}^{0.726};$ $X_{vt} = \left(\dfrac{f_f \, \mathrm{Re}_g^{0.25}}{0.079}\right)^2 \left(\dfrac{1 - x_e}{x_e}\right)\left(\dfrac{\upsilon_f}{\upsilon_g}\right)^{0.5}; Re_g = \dfrac{G x_e D_h}{\mu_g};$ $\Delta p_{tp,a} = G^2 \upsilon_f \left[\dfrac{x_e^2}{\alpha_e}\left(\dfrac{\upsilon_g}{\upsilon_f}\right) + \dfrac{(1 - x_e)^2}{1 - \alpha_e} - 1\right]$ $\alpha_e = 1 - \dfrac{1}{1 + \left(\dfrac{1 - x_e}{x_e}\right)\left(\dfrac{\upsilon_f}{\upsilon_g}\right)^{2/3}}$
6	Separated flow/ Chisholm [78]	$\Delta p_{tp,fr} = \dfrac{2 f_{fo} G^2 L_{tp} \upsilon_f}{D_h x_e} \phi_{fo}^2$ $\phi_{fo}^2 = 1 + \left(\Gamma^2 - 1\right)\left[B x_{avg}^{0.5}\left(1 - x_{avg}\right) + x_{avg}\right];$ $\Gamma = \left(\dfrac{\mu_g}{\mu f}\right)^{0.5} \left(\dfrac{\upsilon_g}{\upsilon_f}\right)^{0.5}$

$$\Delta p_{tp,a} = G^2 \upsilon_f \left[\frac{x_e^2}{\alpha_e} \left(\frac{\upsilon_g}{\upsilon_f} \right) + \frac{\left(1 - x_e\right)^2}{1 - \alpha_e} - 1 \right]$$

$$\alpha_e = 1 - \frac{1}{\sqrt{1 + \frac{20}{X_{vv,out}} + \frac{1}{X_{vv,out}^2}}}$$

7 Separated flow/ Friedel [74]

$$\Delta p_{tp,fr} = \frac{2 f_{fo} G^2 L_{tp} \upsilon_f}{D_h x_e} \phi_{fo}^2$$

$$\phi_{fo}^2 = A_1 + \frac{3.34 A_2 A_3}{Fr_H^{0.045} Fr_H^{0.035}};$$

$$A_1 = \left(1 - x_{avg}\right)^2 + x_{avg}^2 \left(\frac{\mu_g}{\mu_f} \right) \left(\frac{\upsilon_g}{\upsilon_f} \right); A_2 = x_{avg}^{0.78} \left(1 - x_{avg}\right)^{0.234};$$

$$A_3 = \left(\frac{\mu_g}{\mu_f} \right)^{0.19} \left(\frac{\upsilon_g}{\upsilon_f} \right)^{0.91} \left(1 - \frac{\mu_g}{\mu_f} \right)^{0.7}$$

$$\Delta p_{tp,a} = G^2 \upsilon_f \left[\frac{x_e^2}{\alpha_e} \left(\frac{\upsilon_g}{\upsilon_f} \right) + \frac{\left(1 - x_e\right)^2}{1 - \alpha_e} - 1 \right]$$

$$\alpha_e = 1 - \frac{1}{\sqrt{1 + \frac{20}{X_{vv,out}} + \frac{1}{X_{vv,out}^2}}}$$

8 Separated flow/ Tran et al. [79]

$$\Delta p_{tp,fr} = \frac{2 f_{fo} G^2 L_{tp} \upsilon_f}{D_h x_e} \phi_{fo}^2$$

$$\phi_{fo}^2 = 1 + \left(4.3\Gamma^2 - 1\right) \left[N_{conf} x_{avg}^{0.875} \left(1 - x_{avg}\right)^{0.875} + x_{avg}^{1.75} \right];$$

$$\Gamma = \left(\frac{\mu_g}{\mu f} \right)^{0.5} \left(\frac{\upsilon_g}{\upsilon_f} \right)^{0.5}; N_{conf} = \frac{\left[\frac{\sigma}{g\left(\rho_f - \rho_g\right)} \right]^{0.5}}{D_h}$$

$$\Delta p_{tp,a} = G^2 \upsilon_f \left[\frac{x_e^2}{\alpha_e} \left(\frac{\upsilon_g}{\upsilon_f} \right) + \frac{\left(1 - x_e\right)^2}{1 - \alpha_e} - 1 \right]$$

$$\alpha_e = 1 - \frac{1}{1 + \left(\frac{1 - x_e}{x_e} \right) \left(\frac{\upsilon_f}{\upsilon_g} \right)^{2/3}}$$

9	Separated flow/ Qu and Mudawar [80]	$\Delta p_{tp,fr} = \dfrac{2 f_f G^2 L_{tp} \upsilon_f (1 - x_{avg})}{D_h} \phi_f^2$ $\phi_f^2 = 1 + \dfrac{C}{X_{vt}} + \dfrac{1}{X_{vt}^2}; C = 21\left[1 - \exp\left(-319 D_h\right)\right]\left(0.00418G + 0.0613\right);$ $X_{vv} = \left(\dfrac{\mu_f}{\mu_g}\right)^{0.5} \left(\dfrac{1 - x_e}{x_e}\right)^{0.5} \left(\dfrac{\upsilon_f}{\upsilon_g}\right)^{0.5}$ $\Delta p_{tp,a} = G^2 \upsilon_f \left[\dfrac{x_e^2}{\alpha_e}\left(\dfrac{\upsilon_g}{\upsilon_f}\right) + \dfrac{\left(1 - x_e\right)^2}{1 - \alpha_e} - 1\right]$ $\alpha_e = 1 - \dfrac{1}{1 + \left(\dfrac{1 - x_e}{x_e}\right)\left(\dfrac{\upsilon_f}{\upsilon_g}\right)^{2/3}}$
10	Separated flow/ Zhang and Webb[81]	$\Delta p_{tp,fr} = \dfrac{2 f_{fo} G^2 L_{tp} \upsilon_f}{D_h x_e} \phi_{fo}^2$ $\phi_{fo}^2 = \left(1 - x_{avg}\right)^2 + 2.87 x_{avg}^2 \left(\dfrac{P^{-1}}{P_c}\right) + 1.68 x_{avg}^{0.80} \left(1 - x_{avg}\right)^{0.25} \left(\dfrac{P}{P_c}\right)^{-1.64};$ $\Delta p_{tp,a} = G^2 \upsilon_f \left[\dfrac{x_e^2}{\alpha_e}\left(\dfrac{\upsilon_g}{\upsilon_f}\right) + \dfrac{\left(1 - x_e\right)^2}{1 - \alpha_e} - 1\right]$ $\alpha_e = 1 - \dfrac{1}{1 + \left(\dfrac{1 - x_e}{x_e}\right)\left(\dfrac{\upsilon_f}{\upsilon_g}\right)^{2/3}}$

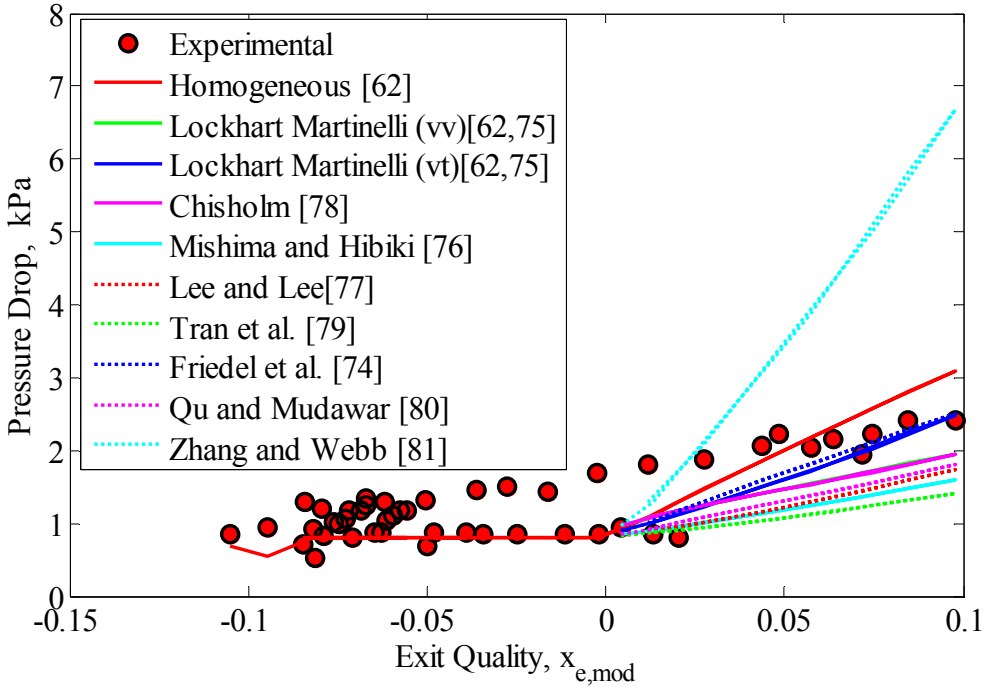

Figure 4.39 Pressure drop presictions at G=535kg/m^{2}s and ΔT_{sat}=5°C

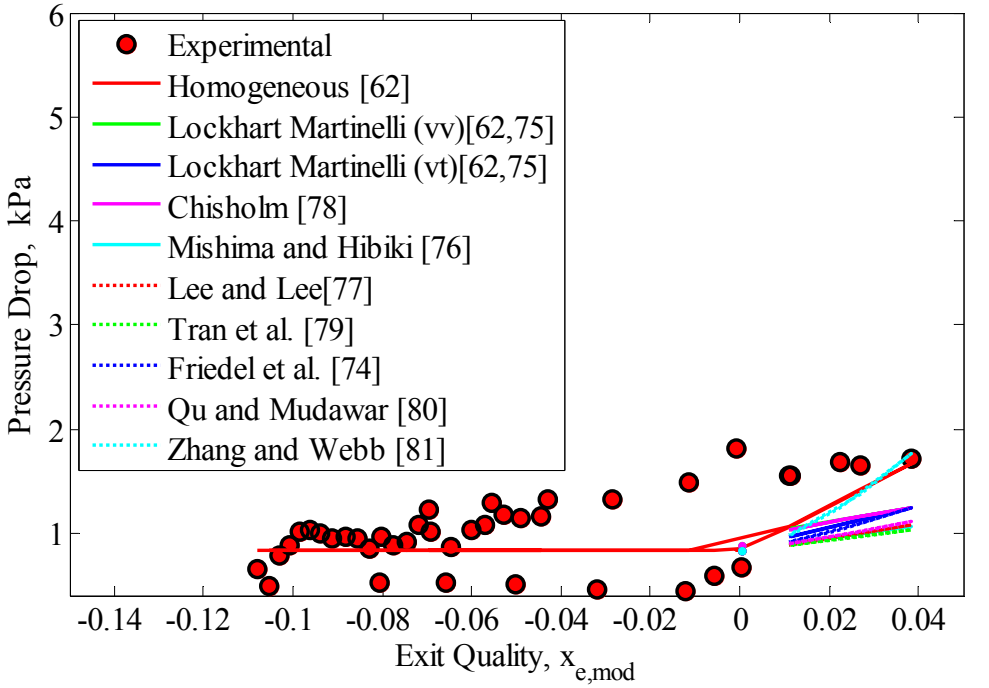

Figure 4.40 Pressure drop predictions at G=535 kg/m^{2}s and ΔT_{sat}=10°C

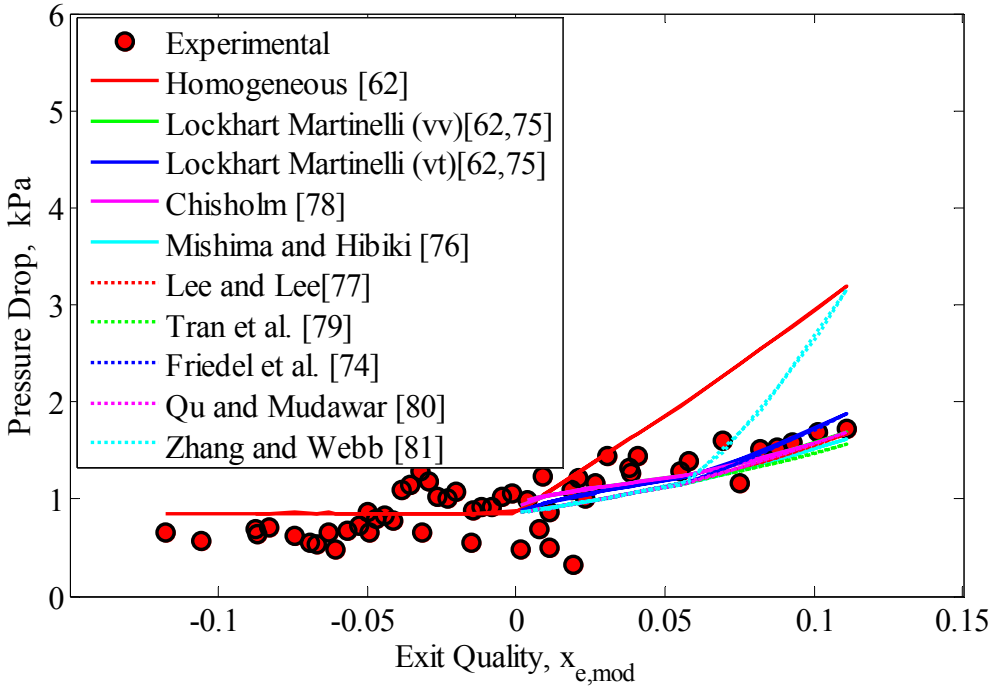

Figure 4.41 Pressure drop predictions at G=535kg/m^{2}s and ΔT_{sat}=15°C

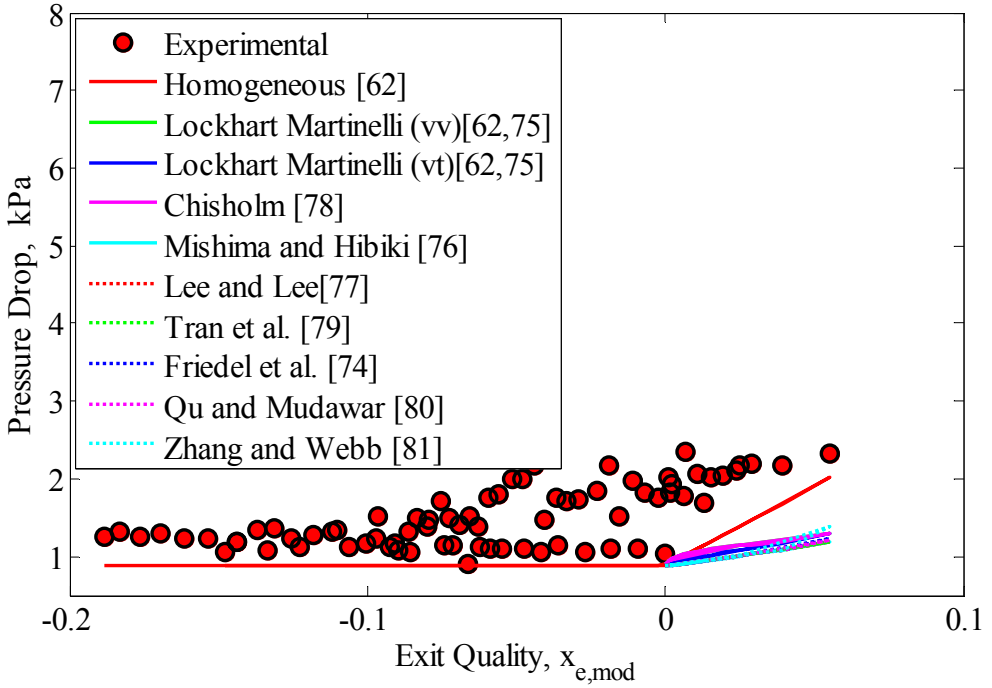

Figure 4.42 Pressure drop predictions at G=535kg/m^{2}s and ΔT_{sat}=20°C

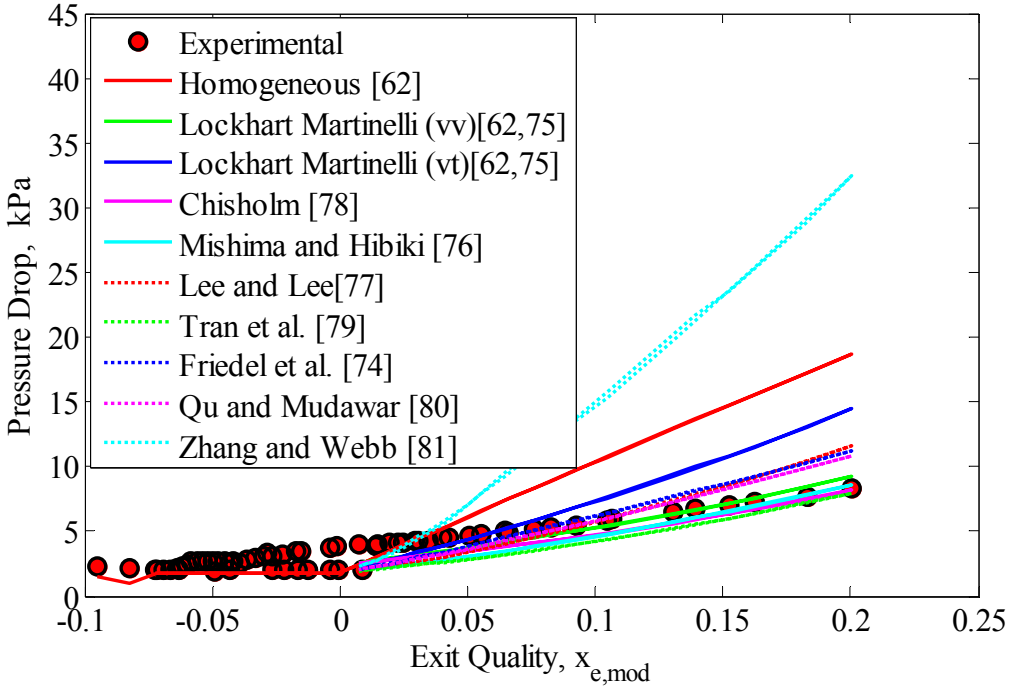

Figure 4.43 Pressure drop predictions at G=1069 kg/m^{2}s and ΔT_{sat}=5°C

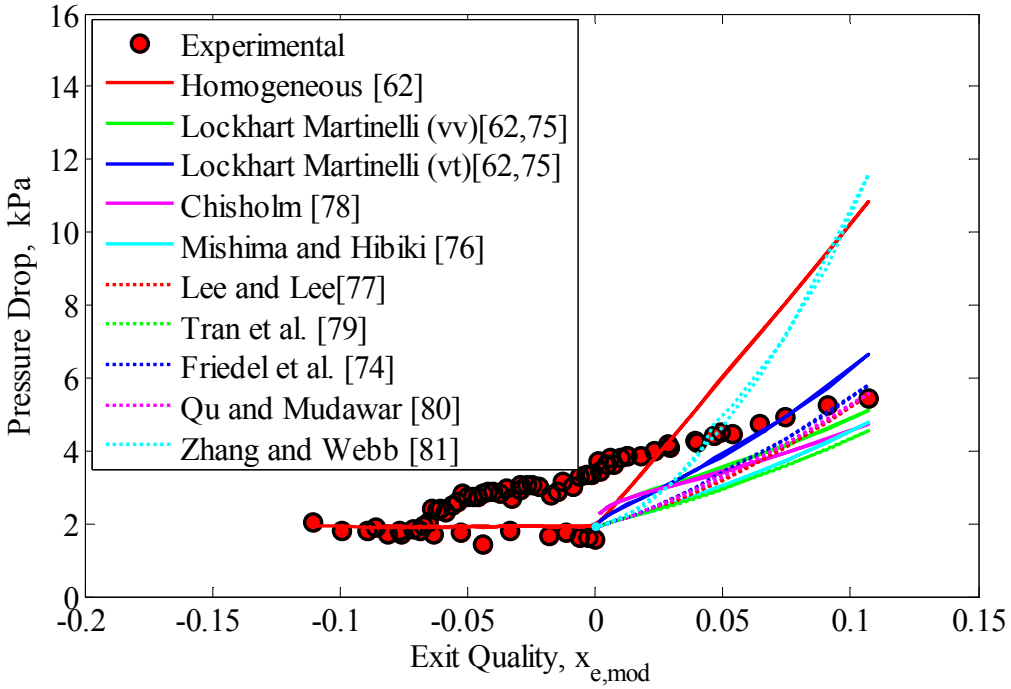

Figure 4.44 Pressure drop predictions at G=1069 kg/m^{2}s and ΔT_{sat}=10°C

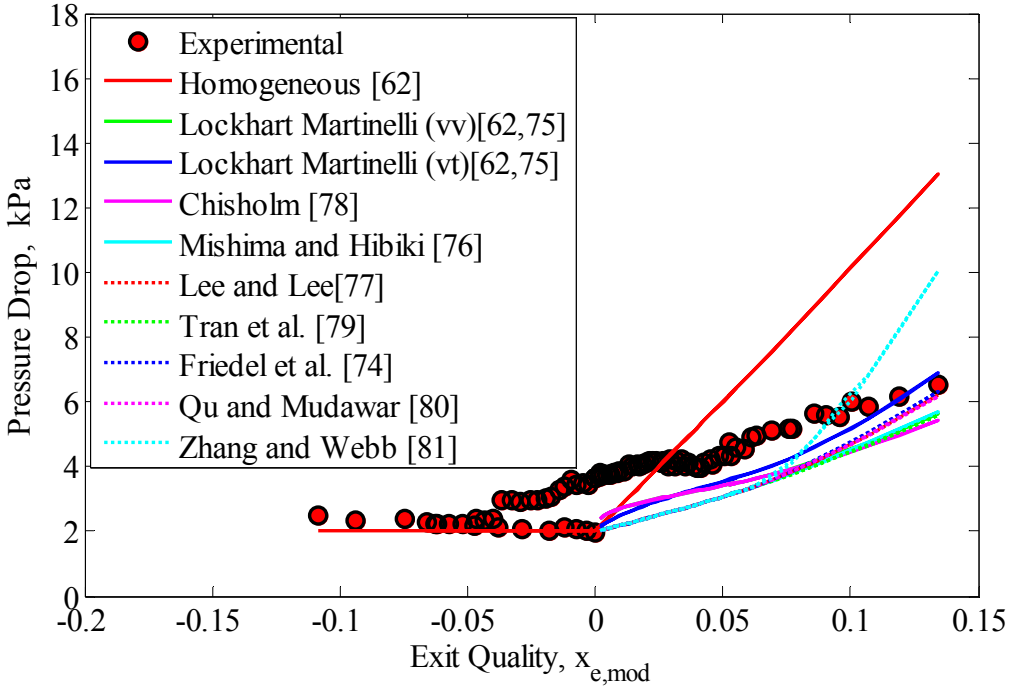

Figure 4.45 Pressure drop predictions at G=1069kg/m^{2}s and ΔT_{sat}=15°C

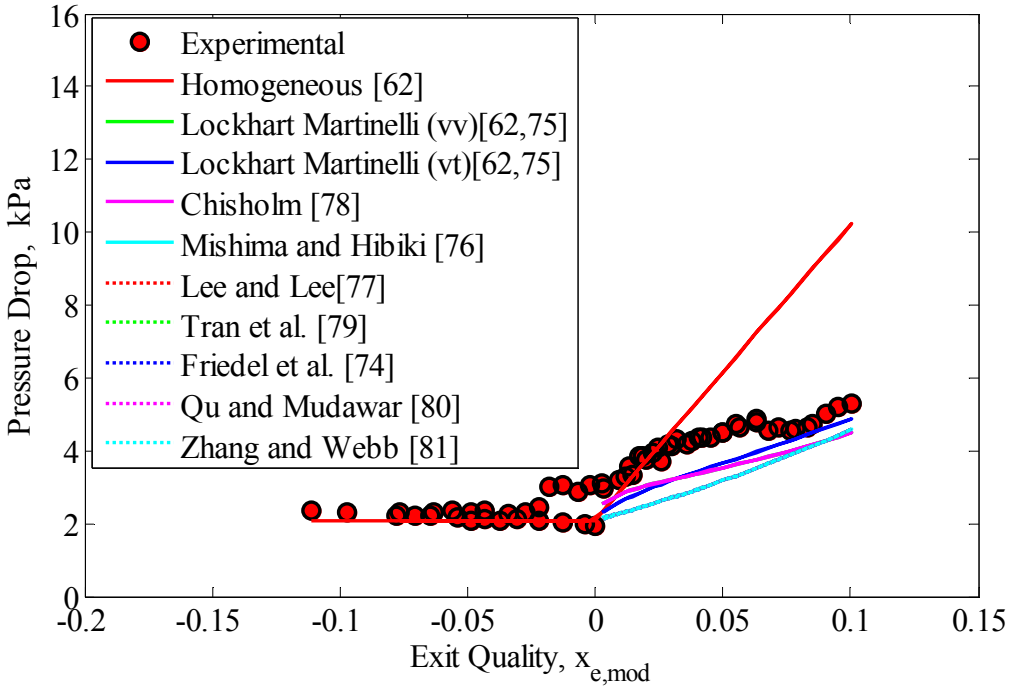

Figure 4.46 Pressure drop predictions at G=1069 kg/m^{2}s and ΔT_{sat} = 20°C

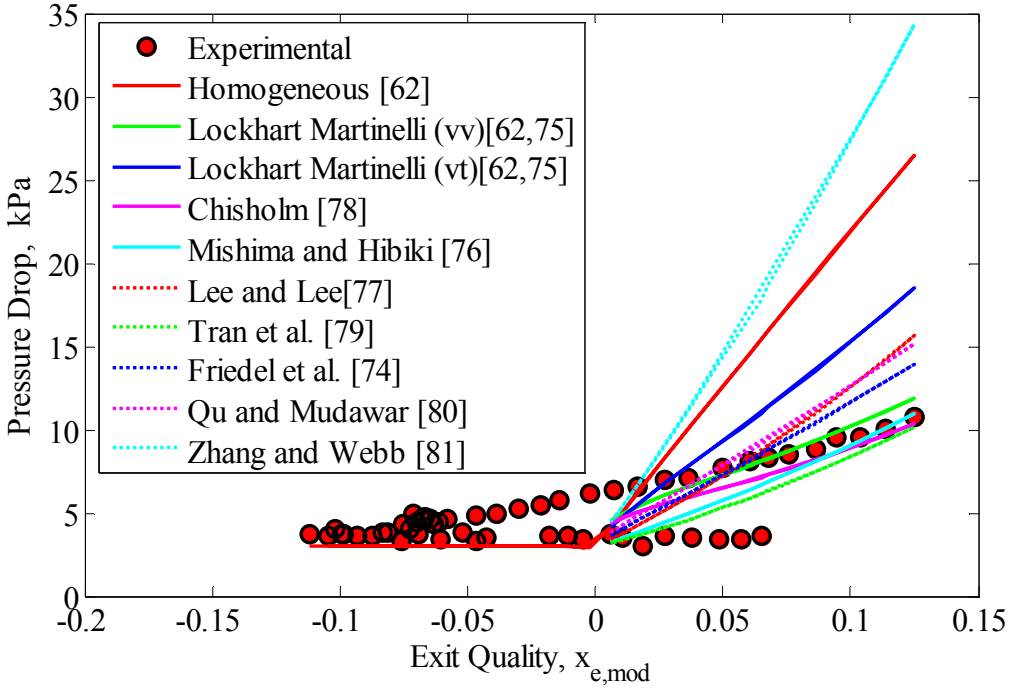

Figure 4.47 Pressure drop predictions at G=1605 kg/m^{2}s and ΔT_{sat}=5°C

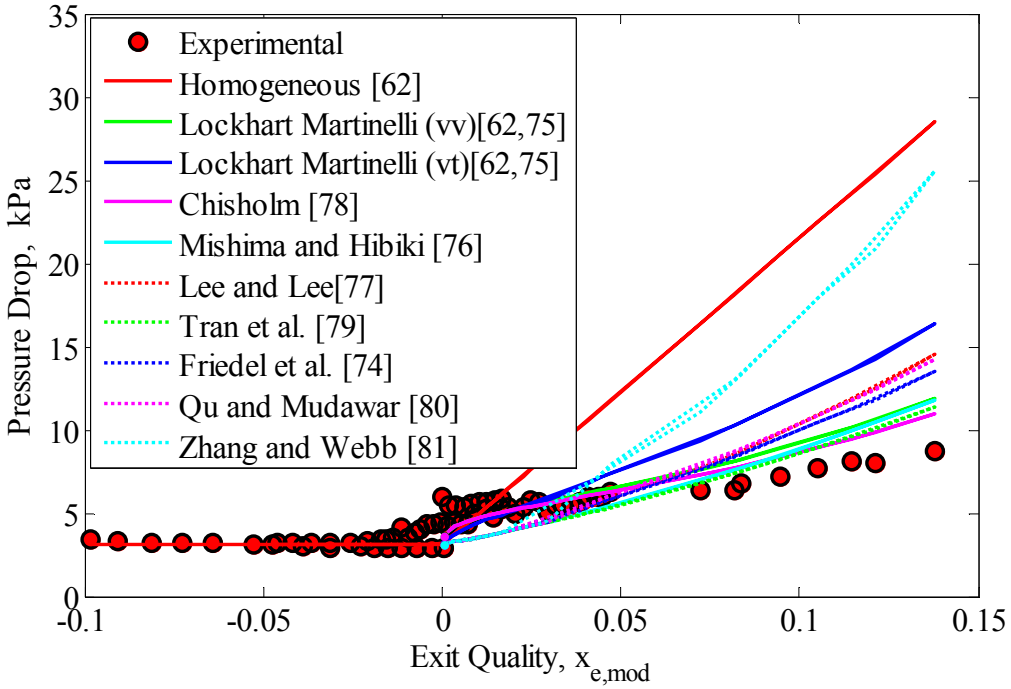

Figure 4.48 Pressure drop predictions at G=1605 kg/m^{2}s and ΔT_{sat}=10°C

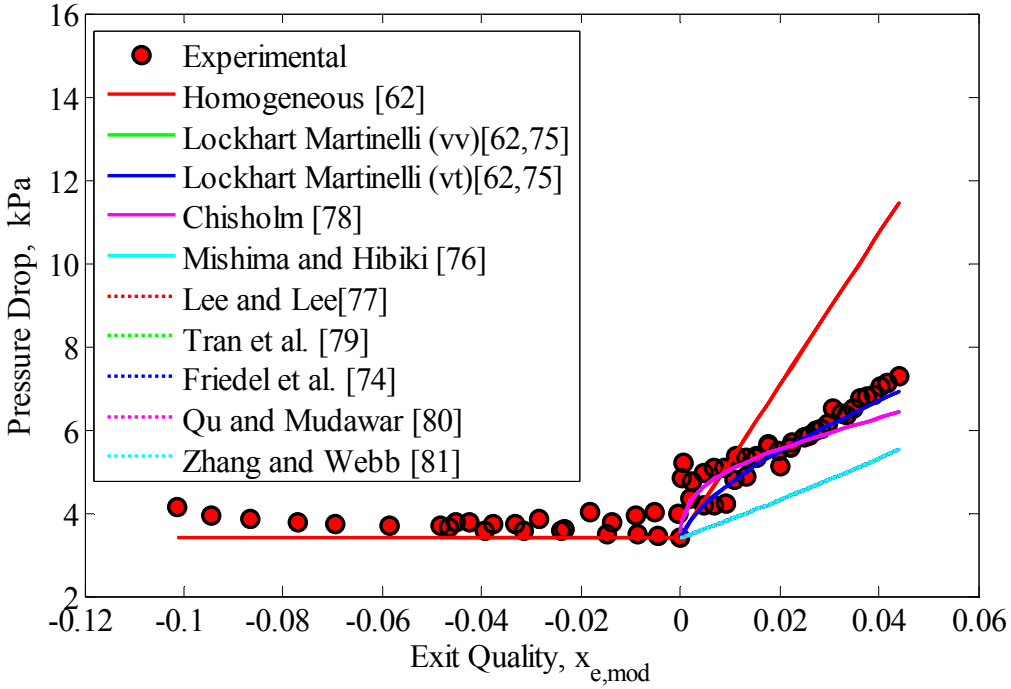

Figure 4.49 Pressure drop predictions at G=1605kg/m^{2}s and ΔT_{sat}=15°C

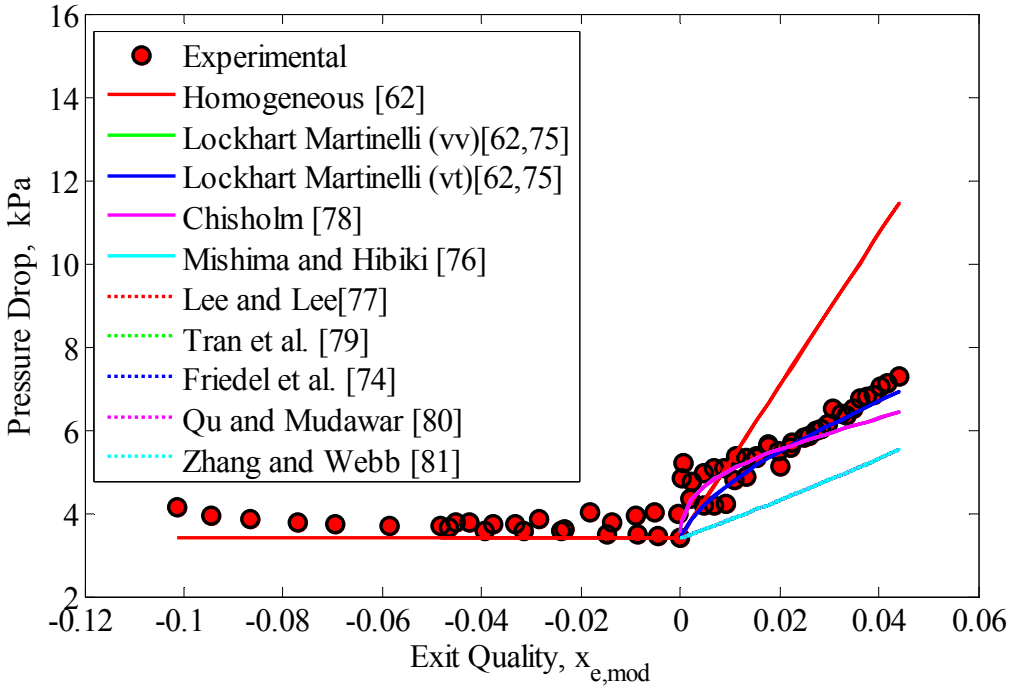

Figure 4.50 Pressure drop predictions at G=1605kg/m^{2}s and ΔT_{sat}=20°C

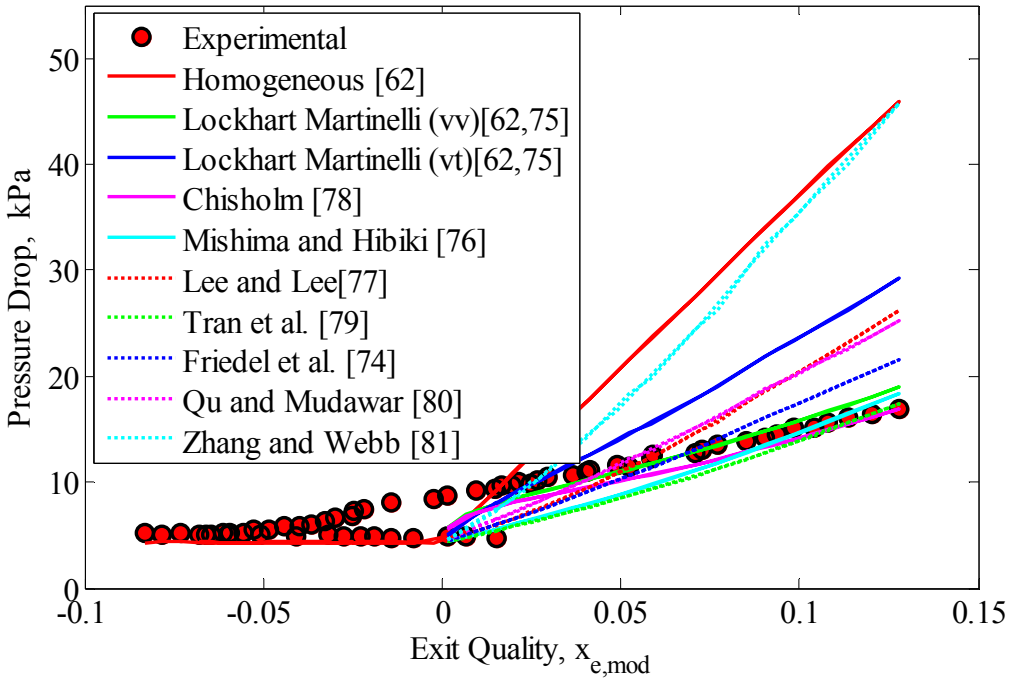

Figure 4.51 Pressure drop predictions at G=2138kg/m^{2}s and ΔT_{sat} = 5°C

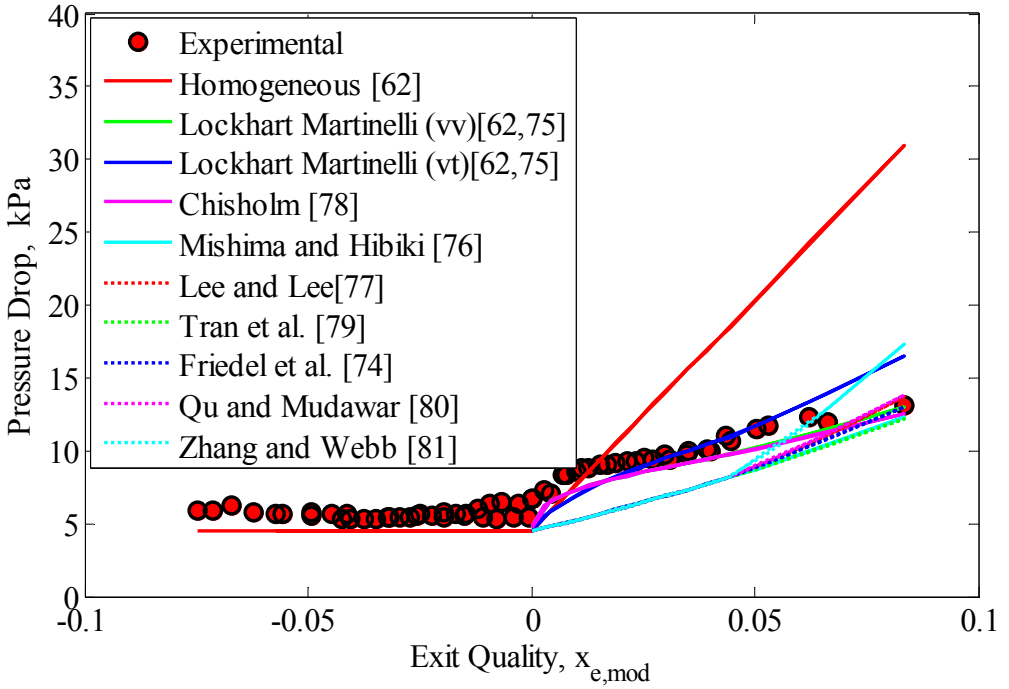

Figure 4.52 Pressure drop predictions at G=2138 kg/m^{2}s and ΔT_{sat}=10°C

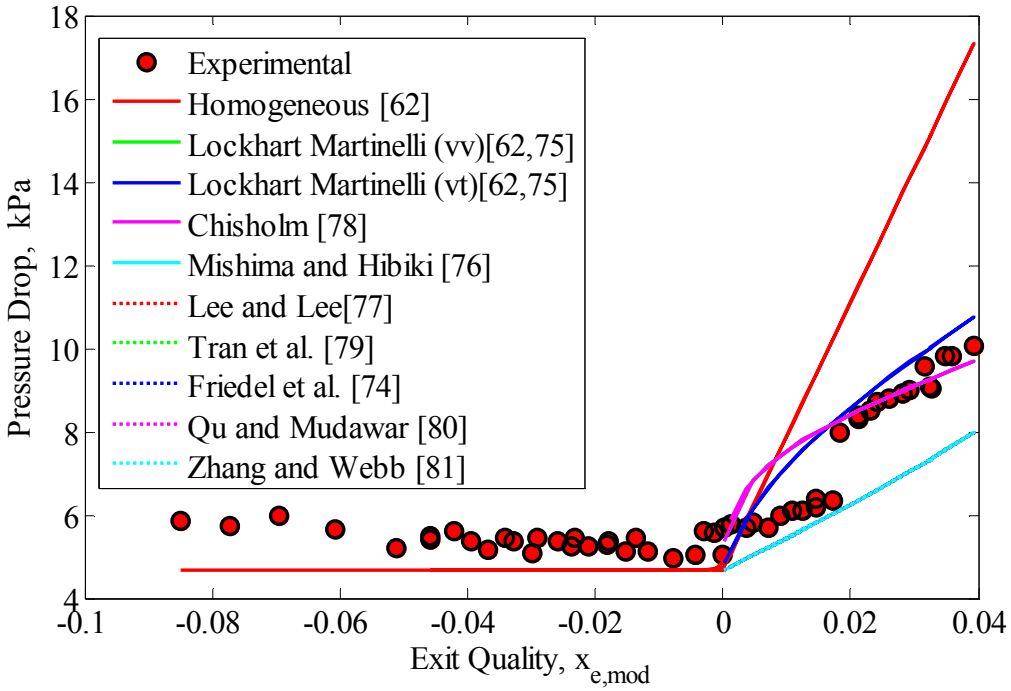

Figure 4.53 Pressure drop predictions at G=2138kg/m^{2}s and ΔT_{sat}=15°C

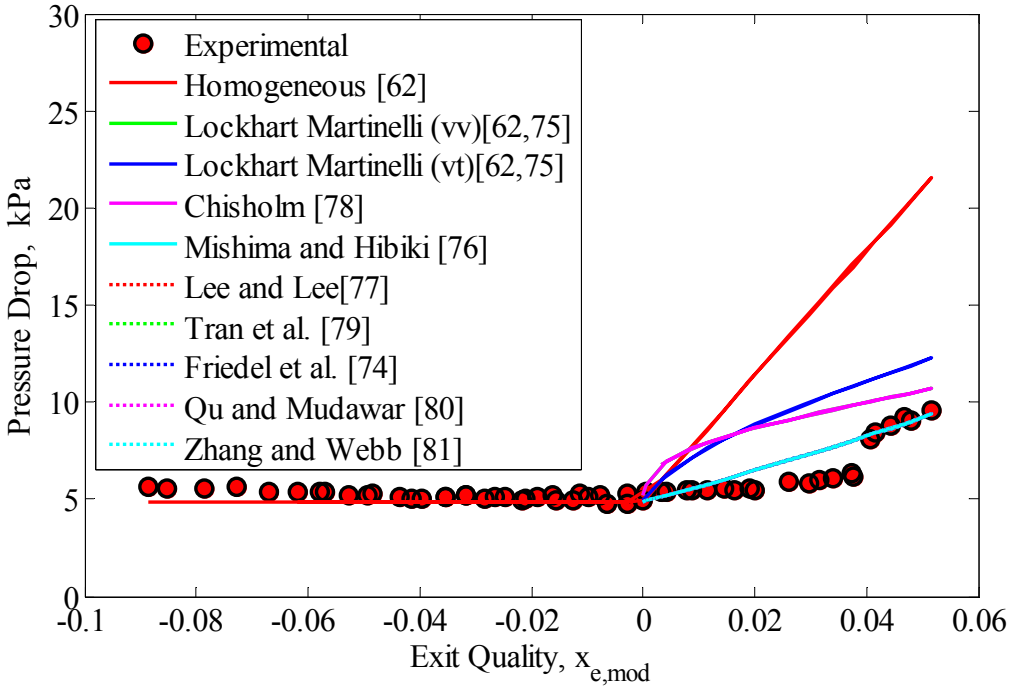

Figure 4.54 Pressure drop predictions at G=2138kg/m^{2}s and ΔT_{sat} =20°C

From Figures 4.39-4.54, it can be noticed that the separated flow correlations predict the experimental data to good accuracy. The homogeneous model which was expected to produce reasonable estimates, over predicts the experimental data for moderate to high mass flux range at high heat flux values. However, it predicts the data well at high heat flux range at low mass flux and low subcooling when the flow is mostly saturated (Figures 4.39 – 4.40). At low subcooling for all mass flux range, the separated flow models of Lockhart-Martinelli (Laminar liquid; laminar vapor)[62,75], Mishima and Hibiki [76], and Tran et al. [79] predict the pressure drop well. It has to be noted that the correlations of Mishima and Hibiki [76] and Tran et al. [65] were developed for mini/microchannels. As the subcooling increases the Lockhart-Matinelli (Laminar liquid-turbulent vapor) [62,75] correlation predicts the experimental data consistently. The macrochannel correlation proposed by Chisholm [82] predicts the pressure drop consistently well across all tested conditions to good accuracy further indicating that conventional macrochannel pressure drop theories do apply to flow boiling microchannel.

However, all the correlations under predict the data for decreasing heat flux at low quality. One of the reasons for the deviation is that, none of the correlations were developed for subcooled flow boiling where the qualities are so low. Tran et al. [79] suggested that the reason for the failure of large-tube correlations could be due to the difference in bubble mechanics observed in small channels. It was postulated that the pressure drop was higher in smaller channels than the predictions due to additional friction that would result from the confined elongated bubble movement. It can also be proposed that the quality be defined differently for increasing and decreasing heat flux to capture the subcooled boiling regime more accurately. The current scheme of exit quality

represents the subcooled boiling regime well for increasing heat flux, but for decreasing heat flux, it does not capture the subcooled boiling regime below the incipient heat flux. Hence for decreasing heat flux, the flux at which all the cavities are *snuffed out* (q_{snuff}) will have to be taken into account. However, since this is a prediction technique, it has to be understood that there is not enough data or models to predict $q_{snuff.}$

4.4 Flow instabilities

Flow instabilities are one of the principal deterrents to the implementation of liquid microchannel cooling. As discussed in the literature review section, the various types of instabilities include static instabilities (Ledinegg [46]), instability due to upstream compressible volume [49], pressure drop oscillations, and parallel channel instability [30] arising due to slug formation in the microchannel. This section explores the types of instabilities observed in the multichannel test device and also analyzes the frequency and amplitude of the instabilities. Instability pattern maps demarcating the flow conditions based on the stability of the flow were constructed to identify the stable conditions of operation for effective operation of the microchannel heat sink. This discussion is followed by the study of instabilities in a single microchannel and observed patterns will be compared with the multi channel flow instabilities.

Two-phase flow instabilities are of great concern in microchannel boiling as they cause large scale pressure fluctuations and temperature oscillations. However, in the current study, the presence of cavities in the channel was instrumental in promoting controlled release of bubbles, thereby preventing any slug formation, which in turn, prevents the instabilities caused by flow restriction. The cavities were very effective in suppressing the instabilities for all combinations of flow rate, inlet subcooling, and heat

flux tested as long the outlet conditions were saturated. However, instabilities do exist under some conditions when the exit is still at subcooled conditions. Such instabilities under subcooled exit conditions were observed as fluctuations in pressure drop. As will be detailed in the discussion that follows, these are attributed to the rapid condensation of vapor in the subcooled pool of liquid that prevails further downstream in the channel and also due to the vapor bubbles coming in contact with the cooler top pyrex wall. This results in a pressure reversal in the channels, thus leading to flow reversal. A similar phenomenon observed in the study conducted by Wang et al.[83], termed as *boiling onset oscillations*, were observed at the onset of nucleate boiling. Like the observations of the current study the instabilities disappeared at high heat flux and low subcooling when the conditions at the exit were suitable to sustain two-phase flow. In a study conducted by Liu and Peng [60] it was observed that the instabilities in subcooled liquid were due to interface oscillation fueled by subcooled conditions experienced by the vapor at the exit when it comes in contact with cooler Pyrex top wall at the exit. A high speed image of the condensing vapor from the same study is shown in Figure 4.55. It was observed by the authors that dropwise condensation first appeared at the interface between hot liquid and low temperature pyrex wall (Figure 4.55a). This was followed by the coalescence of liquid droplets to form a thin film as shown in Figure 4.55b. The condensation process increased leading to an increase in film thickness moving from Figure c through d until the elongated vapor bubble is broken into two in Figure e. In this fashion, condensation of vapor plays an important role in promoting the flow instabilities observed in microchannel flows.

Thus an alteration in the design of exit plenum to include a heating mechanism at the exit to prevent the condensation or redesigning the inlet plenum to accommodate flow restrictors that increase the pressure at the inlet, might aid in suppressing the flow oscillations. However, the latter would lead to a significant rise in pressure drop which makes the option less attractive.

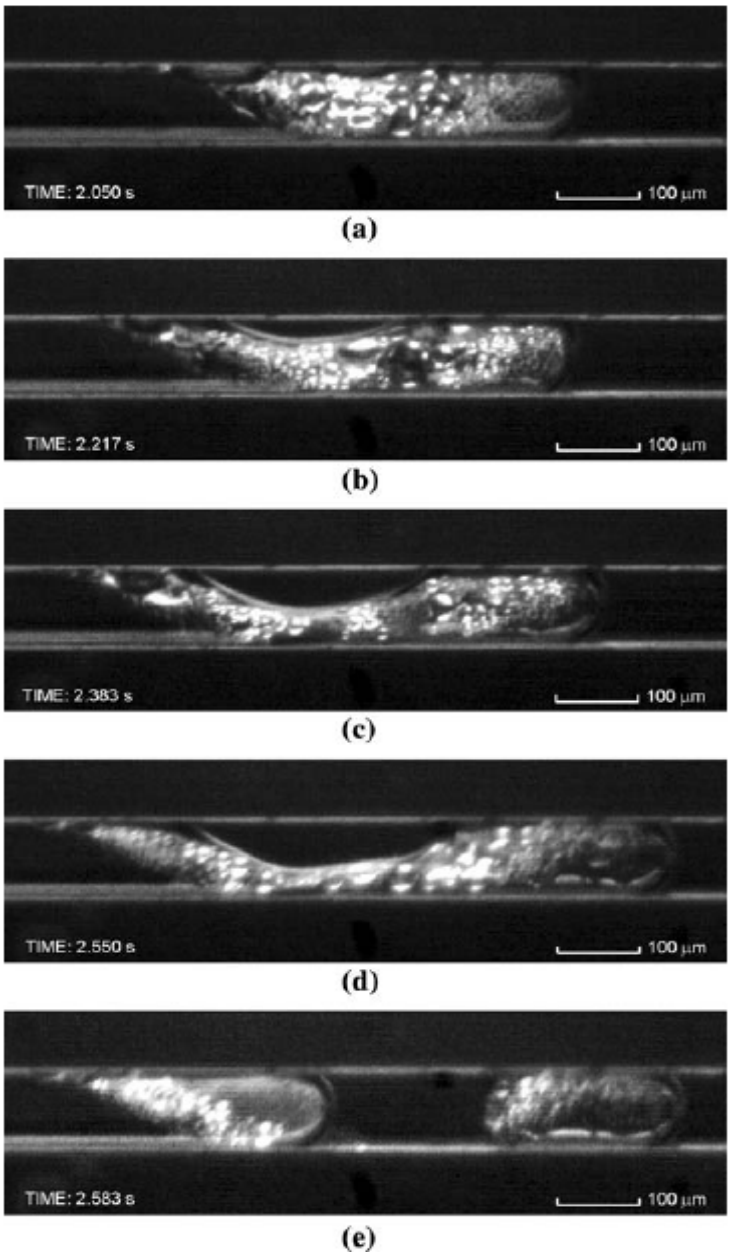

Figure 4.55 Condensation of vapor in microchannels (Liu and Peng [60])

In the study conducted on the multi channel test devices (MC 200-2), analysis of flow instabilities was performed using high-speed photography and pressure drop signals recorded by the pressure transducers at the inlet and exit of the microchannel array. Typical fluctuations in pressure signals are shown in Figures 4.56 (a) and 4.56 (b). It is very evident from figures that two regimes of instabilities exist; the first characterized by high frequency and the second characterized by a much lower frequency. The signals shown were recorded at G=2138 kg/m^2-s and inlet subcooling 10°C.

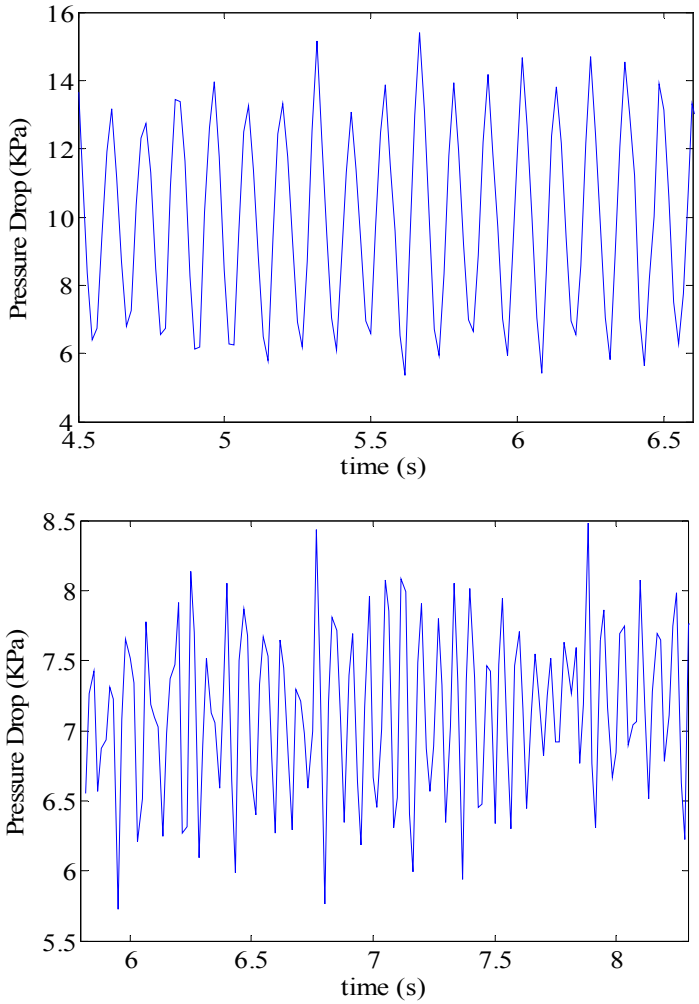

Figure 4.56 Pressure drop fluctuation at G=2138kg/m^{2}s and inlet subcooling 10°C a) high frequency instability b) low frequency instability

Figure 4.57 shows high speed images of one cycle of flow reversal observed at subcooled exit conditions at G = 1605 kg/m^2-s and inlet subcooling of 15°C in the multi channel test device MC 200-2. The images shown were captured at an interval of 0.005 seconds and the liquid flows from the right to the left in all the figures. Figure 4.57a shows a stable flow with liquid leaving the microchannels subcooled along with the vapor. In the subsequent images (Figures b through d) significant reduction in vapor volume can be observed, which is hypothesized to be due to its condensation as shown in Figure 4.55. This condensation process causes a pressure differential to reverse and hence causes the flow to reverse which is seen as vapor leaving the inlet into the subcooled pool of liquid at the inlet plenum in Figure 4.57f through g. Due to the subcooled conditions, the vapor condenses back to the liquid which is pushed back into the channels due to the presence of an external pump acting against the reversing flow. This cycle repeats itself at a frequency as high as ~25Hz under highly subcooled conditions. It will be shown in the next section that the frequency of oscillation reduces as the inlet subcooling reduces owing to the low condensation at higher temperature of the liquid. These high frequency oscillations are very different from parallel channel instabilities observed by Balasubramaniam and Kandlikar [84] where the observed frequency of oscillation was 1-2Hz . The section which follows discusses the variation of the frequency with changes in heat flux, mass flux and inlet subcooling .

Flow direction

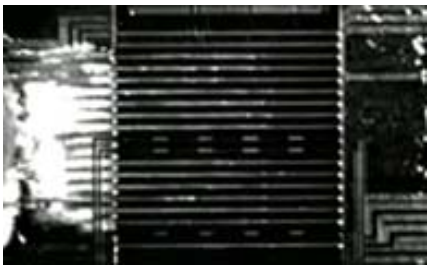

(a) 0.0 s

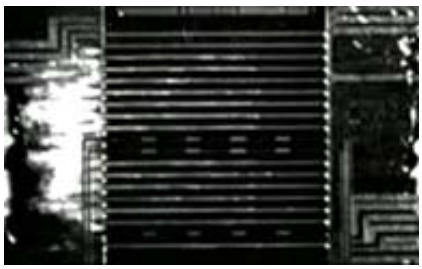

(b) 0.005 s

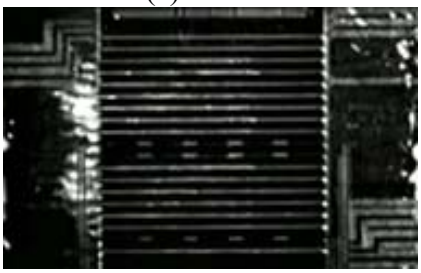

(c) 0.01 s

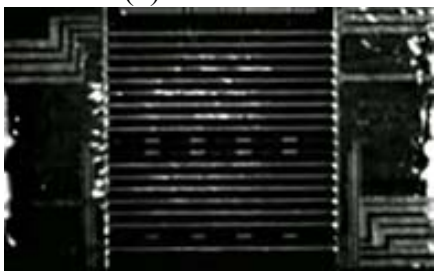

(d)0.015 s

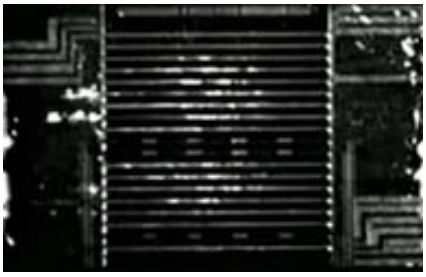

e) 0.02 s

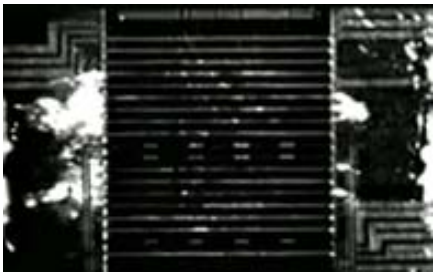

(f) 0.025

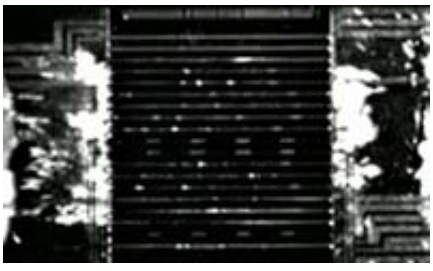

(g) 0.03 s

(h) 0.035 s

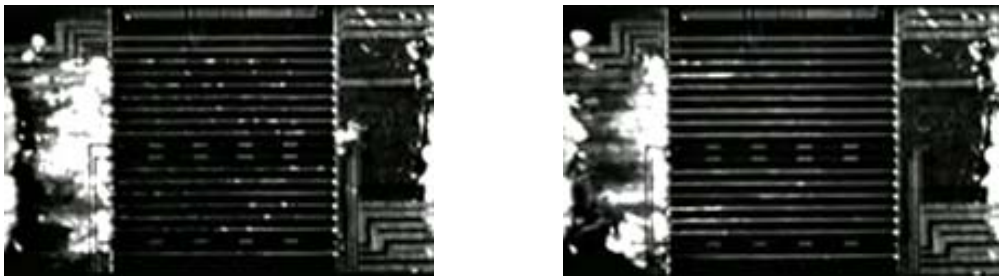

(i) 0.04 s (j) 0.045 s

Figure 4.57 Flow oscillations in a multichannel test section recorded at intervals of 0.005 seconds

4.4.1 Frequency of oscillations

The frequency of the instabilities was determined by a Fast Fourier Transform of pressure drop data obtained from experiments conducted on the multi channel test device MC200-2. Figures 4.58 and 4.60 represent the variation of frequency with heat flux while figures 4.59 and 4.61 correspond to variation of frequency with exit quality. It was observed that, at low heat fluxes, the instabilities prevail as high frequency oscillations and as the heat flux increases, a sudden transition of instabilities to low frequency oscillations was observed. It is postulated that the high frequency instability manifests itself when the vapor volume is low (due to high subcooling, high mass flux or low heat flux). Bubbles at these low vapor volume conditions are more conducive to complete collapse at the exit plenum which experiences greater subcooled conditions, thus leading to stronger instabilities propagating from the exit. As the vapor volume increases (due to low subcooling or high heat flux), this mechanism is somewhat diminished and leads to a sudden transition to low frequency oscillations. The above findings are evident in figures 4.51 through 4.54.The aforementioned hypothesis supported by the observations made by Wang et al. [83] who reported a dynamic instability at ONB. It was observed that the instability was due to the transition of two-phase flow to single phase flow at the exit due

to the prevailing subcooled conditions. It was reported that, as the heat flux increased, the boiling moved further upstream and at the exit two-phase flow always prevailed constantly, hence causing the system to return to a stable state. These findings agree well with those made in the current study. The observations of interface oscillation due to condensation, reported by Liu and Peng [60] which was explained using high speed images from the study in the previous section, further substantiates the hypothesis presented here.

a) Effect of inlet subcooling

Figure 4.58 (i) through (iv) show the effect of subcooling on the frequency at mass fluxes of 535, 1069, 1605 and 2138 kg/m^2-s. It is quite evident that the unstable region increases with increasing inlet subcooling. Recalling the hypothesis presented earlier, at low inlet subcooling and low heat flux, the vapor quality is high and hence the bubbles are less vulnerable to collapse, and hence the frequency of oscillations will be low and high frequency oscillation were rarely observed, which is very evident at all mass fluxes. At a given mass flux, as the inlet subcooling increases, the *onset of instability* (OFI) shifts to higher qualities and hence low vapor qualities are never experienced, thereby reducing the low frequency oscillations and increasing the high frequency oscillations.

An attempt to study the effect of exit quality on the flow instabilities proved that the frequency of oscillation is a stronger function of exit quality than wall heat flux. With 4.59 (i) through (iv) supporting the theory postulated for flow instabilities, another interesting feature was that, at high inlet subcooling and low mass flux, all the instabilities were encompassed within a range of exit quality and frequency, and the transition from high to low frequency occurring at the same quality, x_e = -0.1 for all

conditions. However, the same was not observed at higher mass fluxes or lower inlet subcooling conditions. It was also observed that for $x_e = 0$ (saturated conditions), the flow was stable. Similar trends were observed by Wang et al. [83], where instabilities were found to decrease with increasing inlet subcooling.

b) Effect of mass flux

Figures 4.60 (i) through (iv) show the variation of the frequency with heat flux at constant subcooling and variable mass flux. It is known that as the boiling regime moves from partial to fully developed nucleate boiling, the convective effects will gradually diminish. Hence, the main effect of mass flux is to delay the onset of instability, leading to the inference that the unstable region decreases with increasing mass flux which is evident in the plots and will also be elaborated in detail in the flow pattern instability maps. Also at a given heat flux and inlet subcooling, higher mass flux will lead to low vapor volume and hence according to the hypothesis will produce high frequency instabilities at low inlet subcooling which is evident in Figure 4.60 and Figure 4.61 .

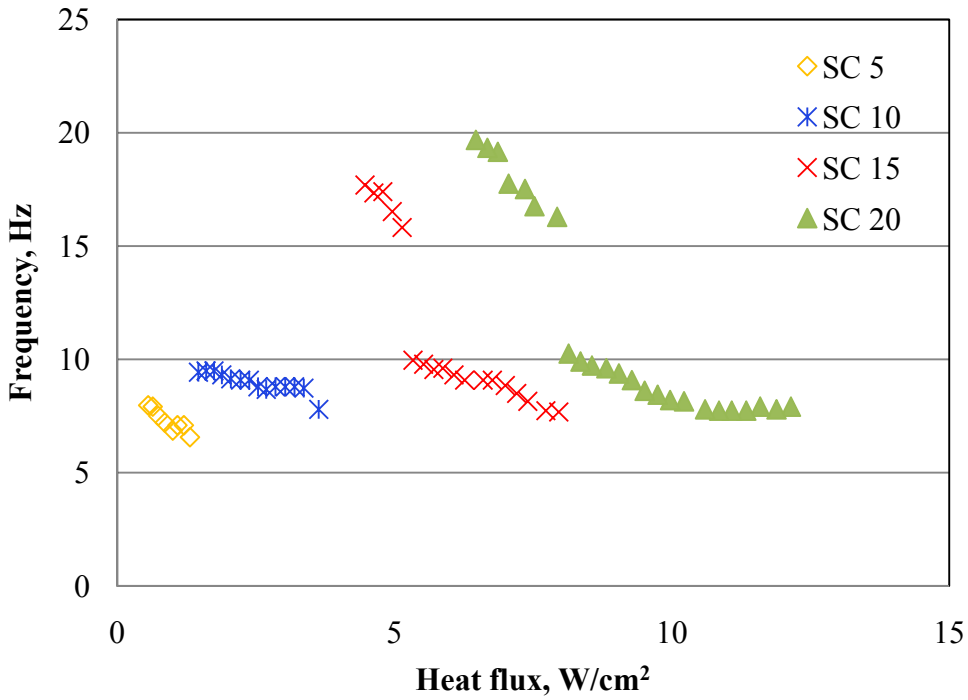

(i) G =535 kg/m^{2}s

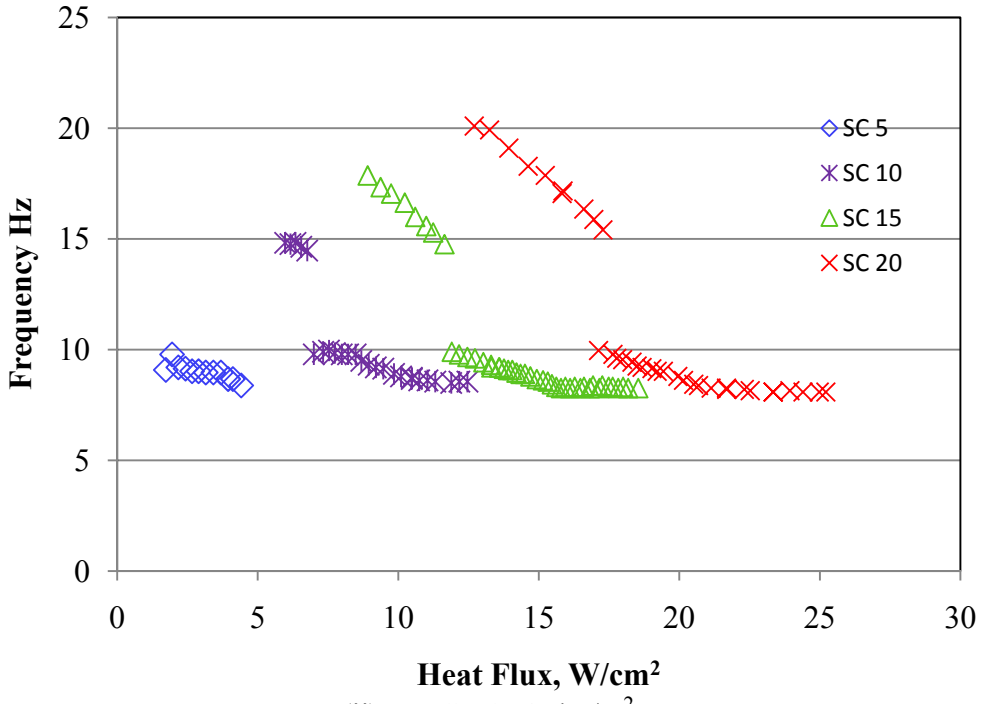

(ii) G =1069 kg/m^{2}s

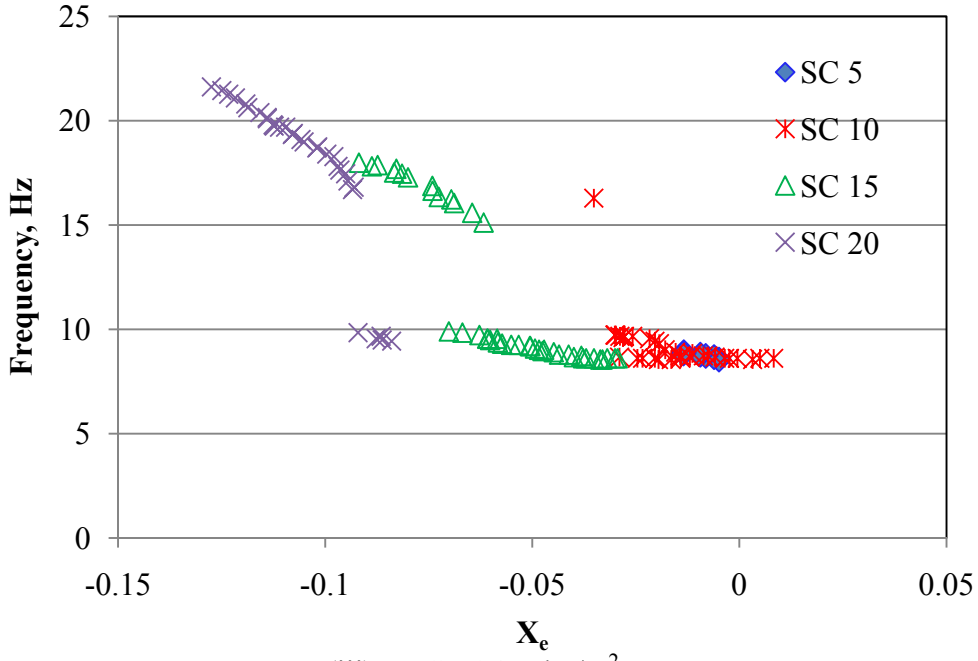

(iii) G =1605 kg/m^{2}s

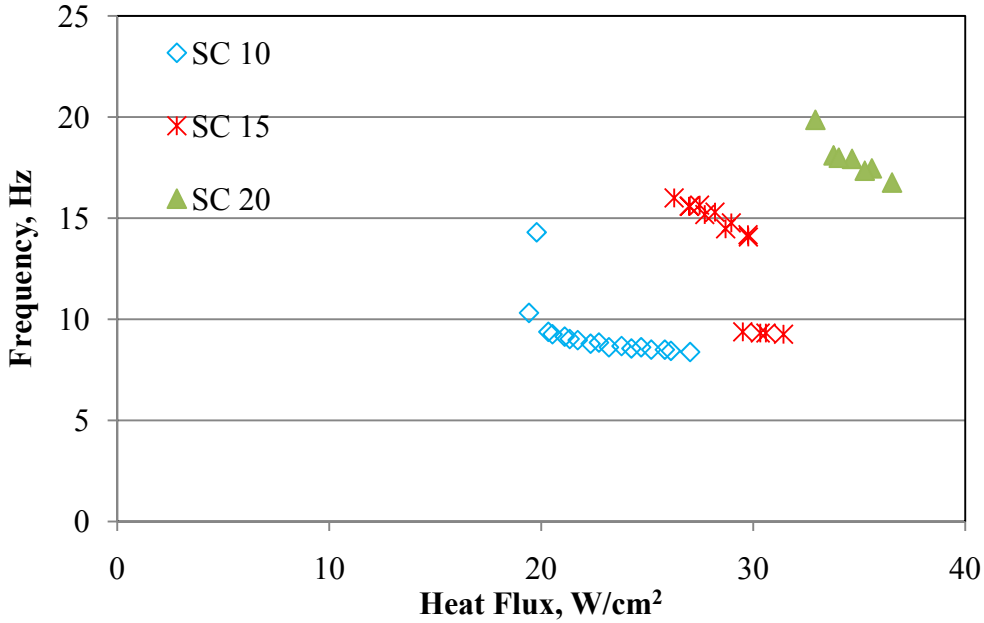

(iv) G =2138 kg/m^{2}s

Figure 4.58 Effect of inlet subcooling on the frequency of instability plotted as function of heat flux

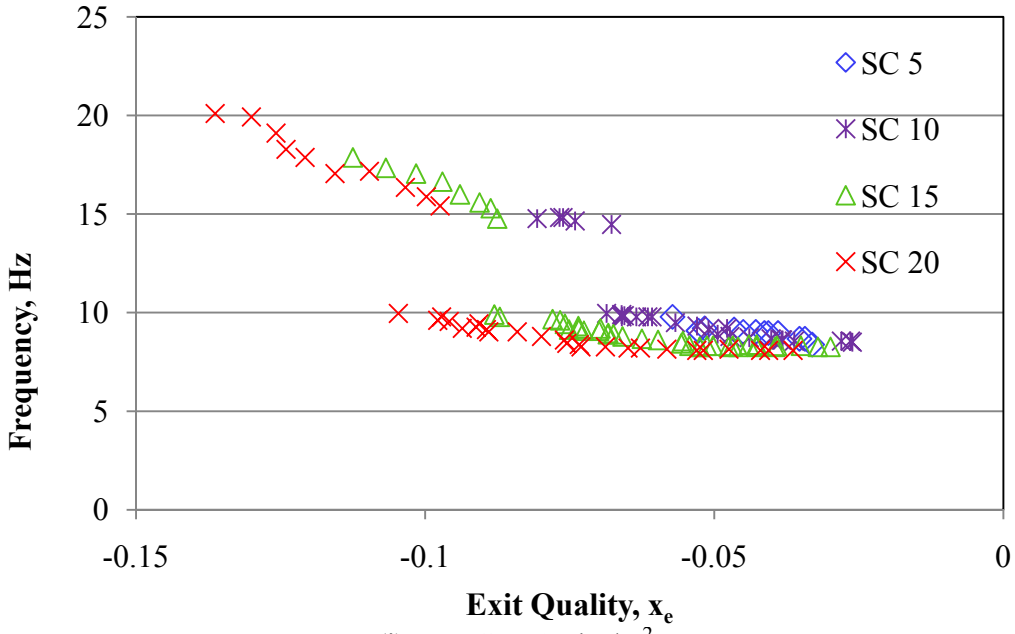

(i) G =535 kg/m^{2}s

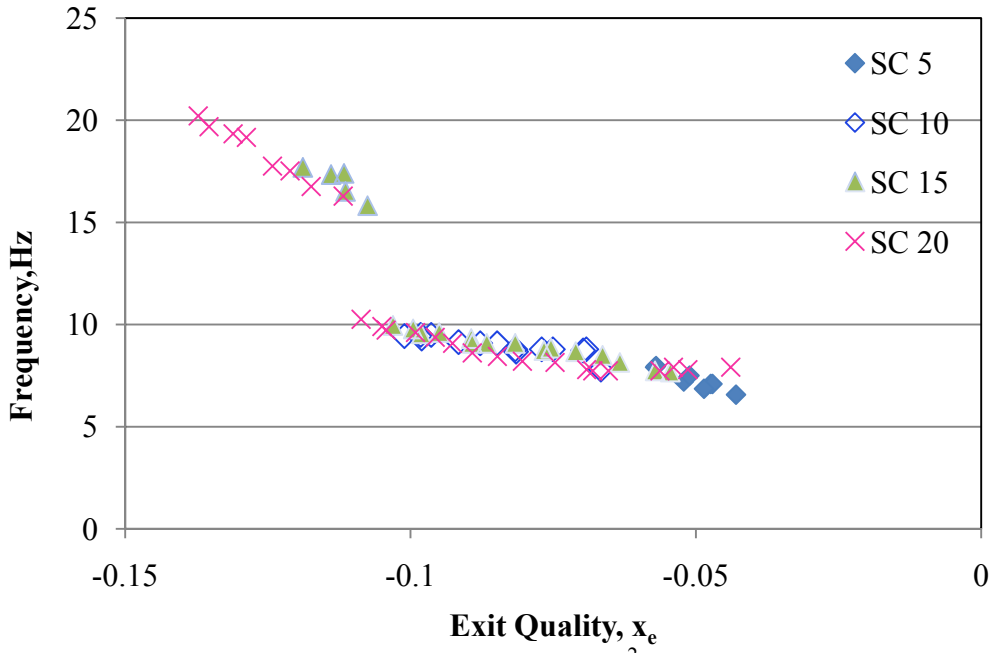

(ii) G =1069 kg/m^{2}s

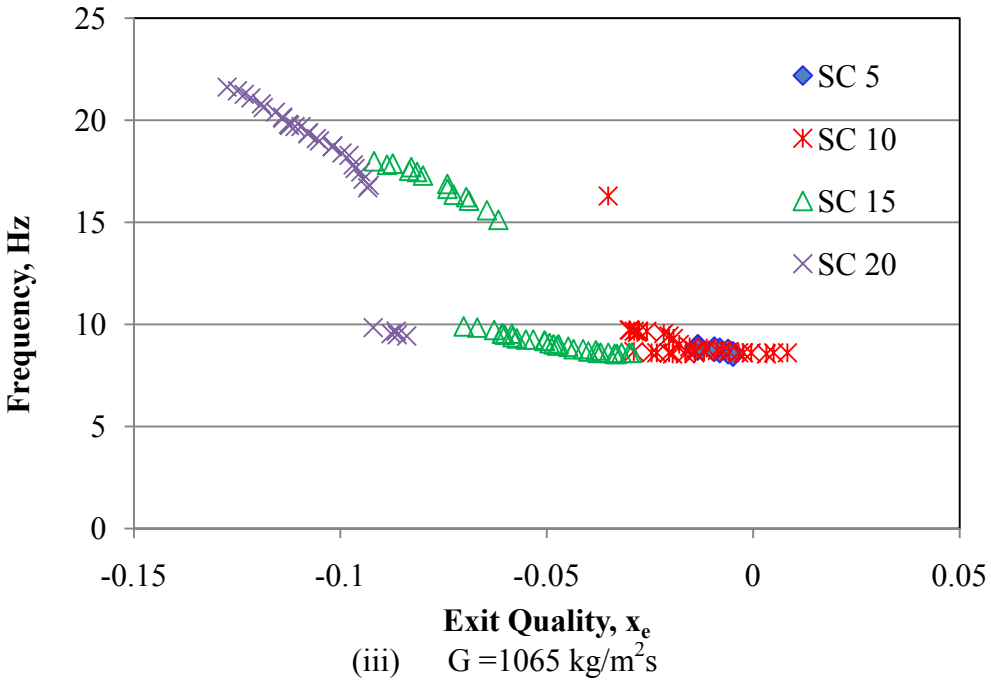

(iii) G =1065 kg/m^{2}s

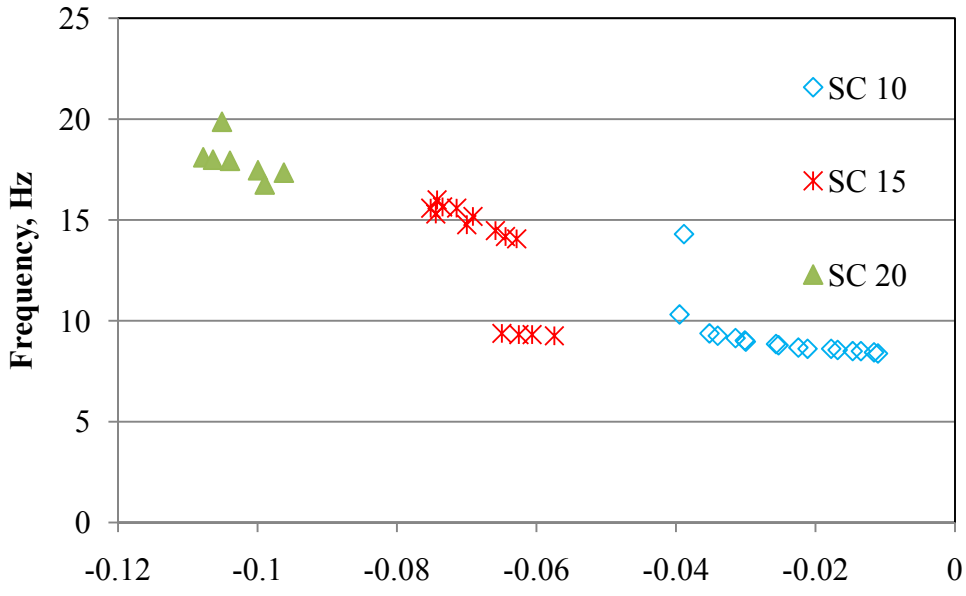

(iv) G =2138 kg/m^{2}s

Figure 4.59 Effect of inlet subcooling on the frequency of instabilities plotted as a function of exit quality

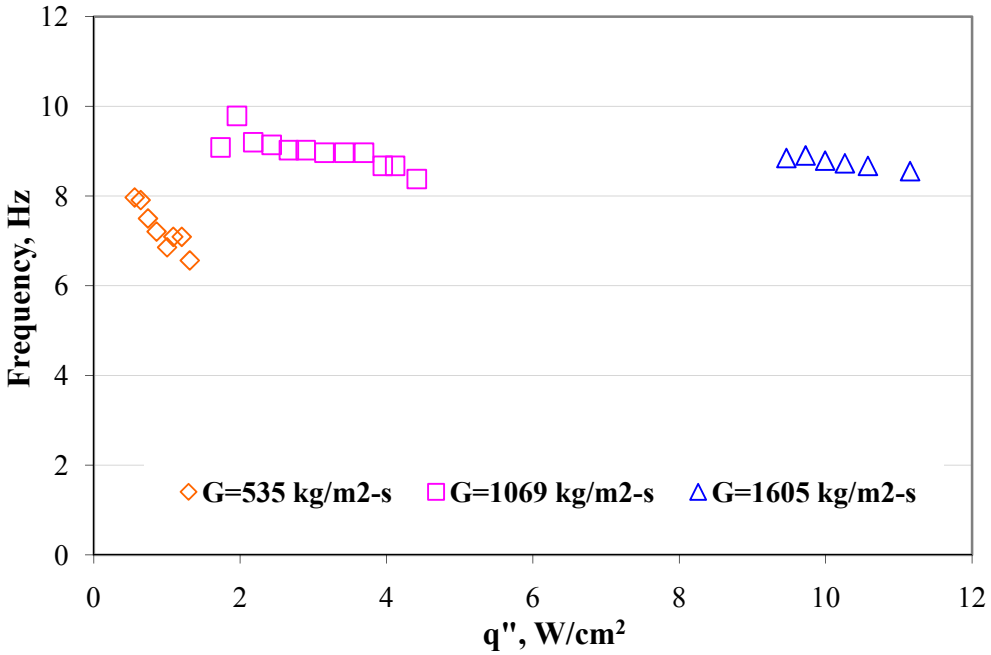

i. 5°C inlet subcooling

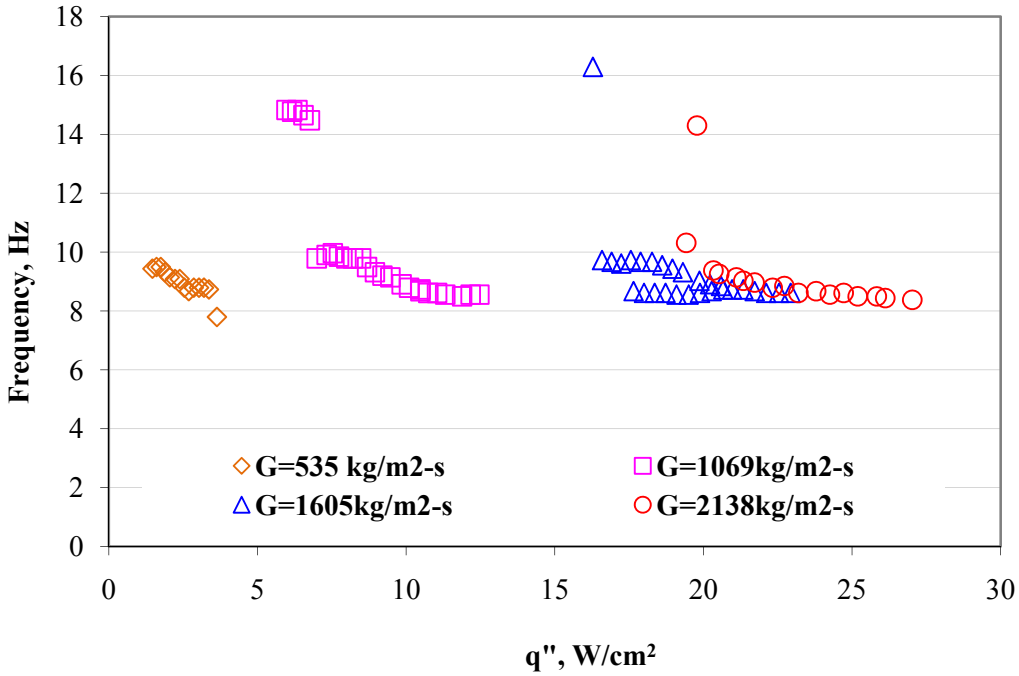

ii. 10°C inlet subcooling

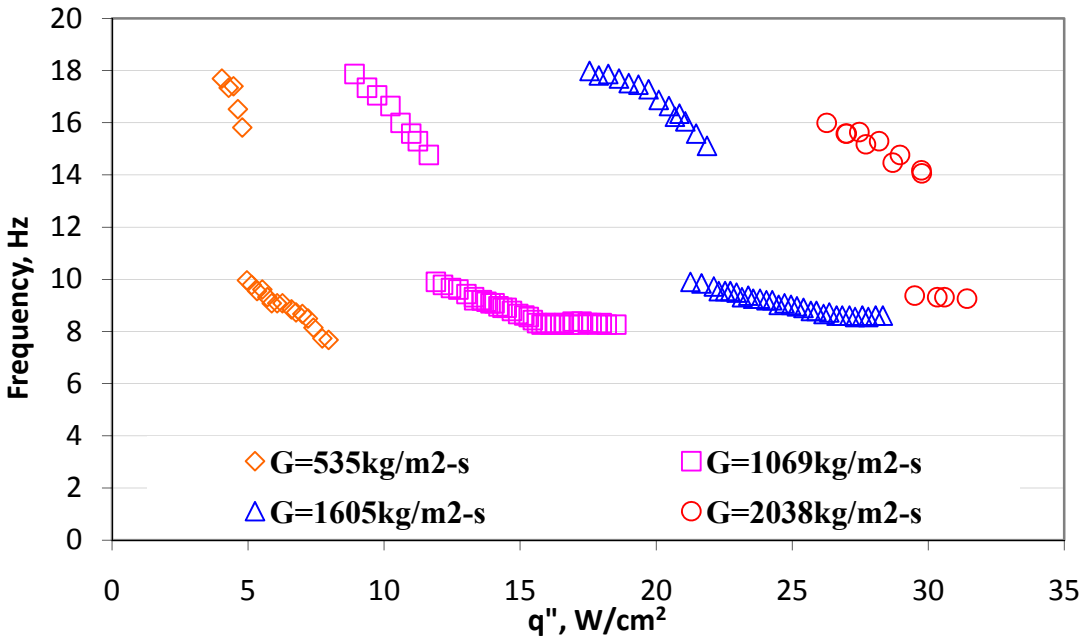

iii. 15°C inlet subcooling

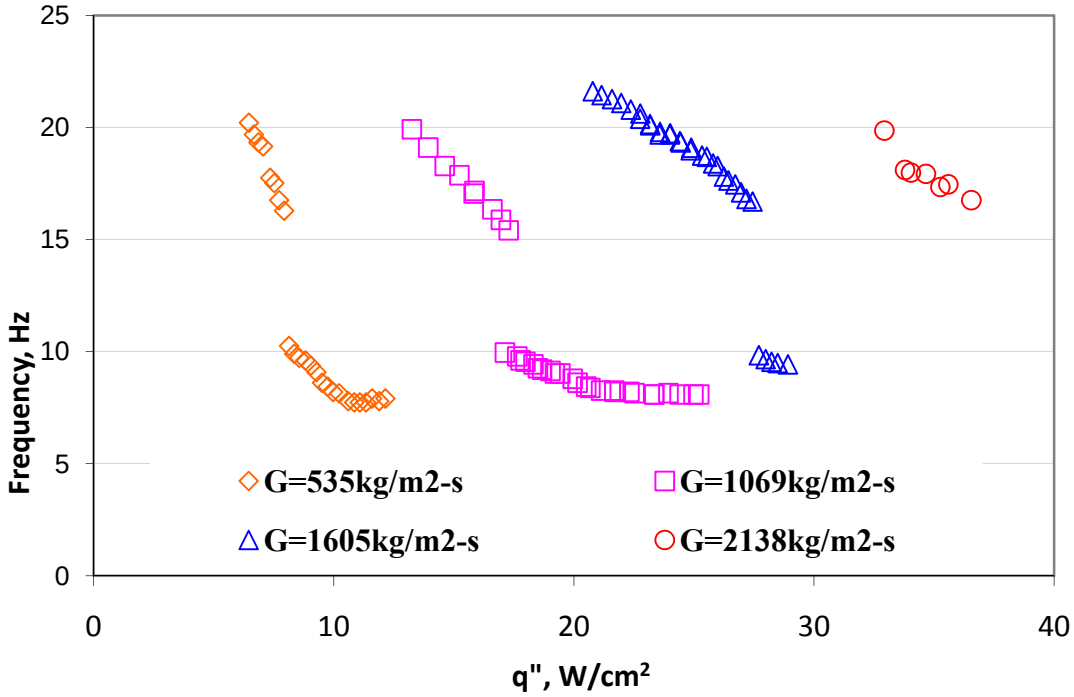

iv. 20°C inlet subcooling

Figure 4.60 Effect of mass flux on frequency of instability plotted as a function of heat flux

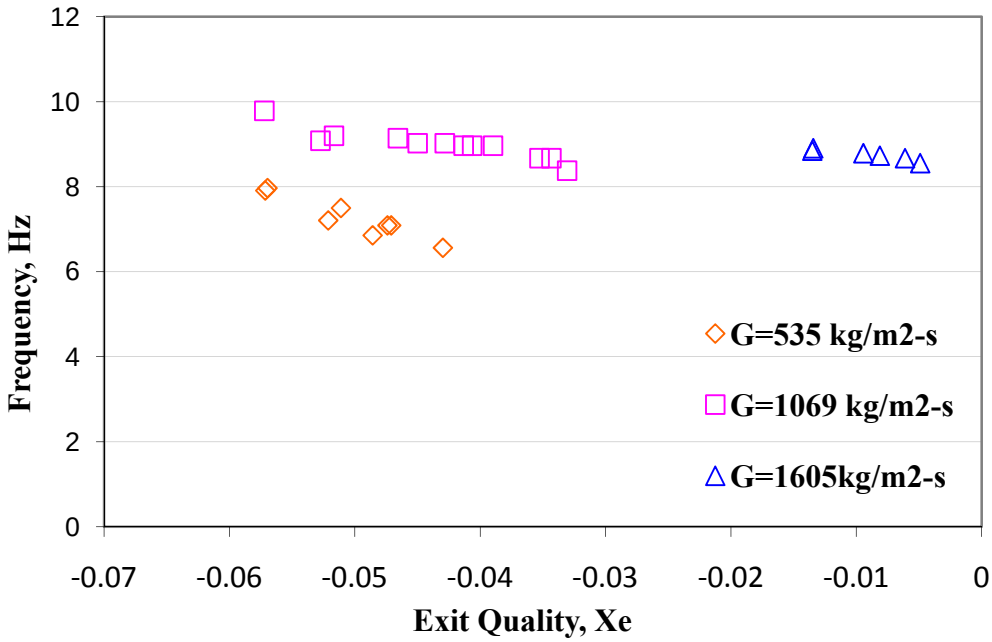

i. 5°C inlet subcooling

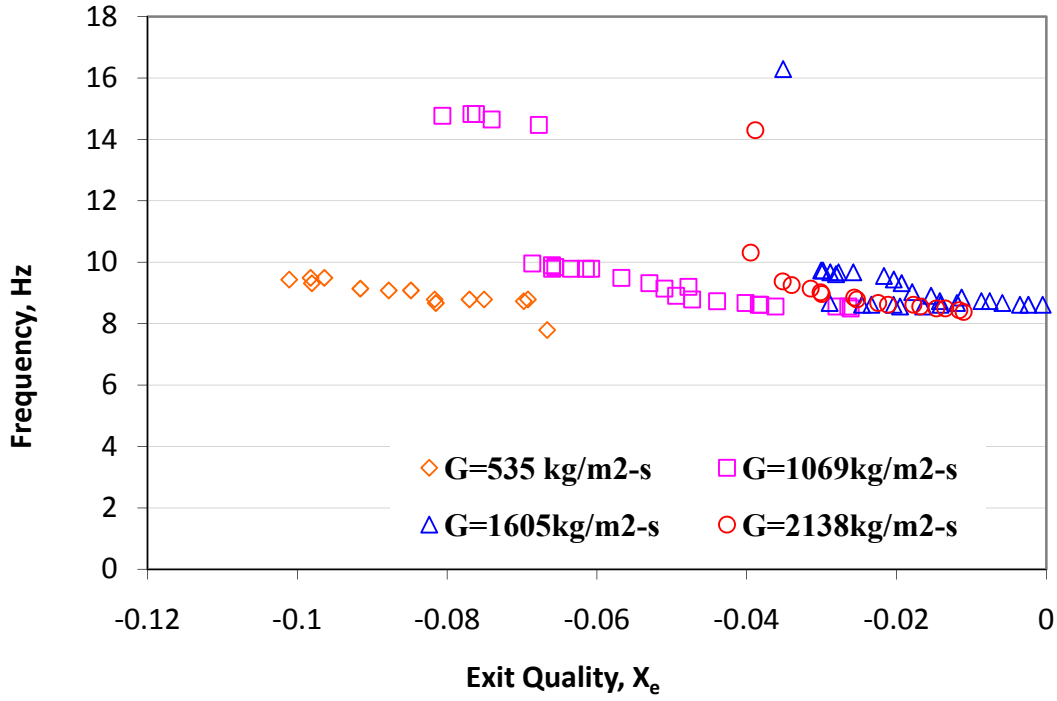

ii. 10°C inlet subcooling

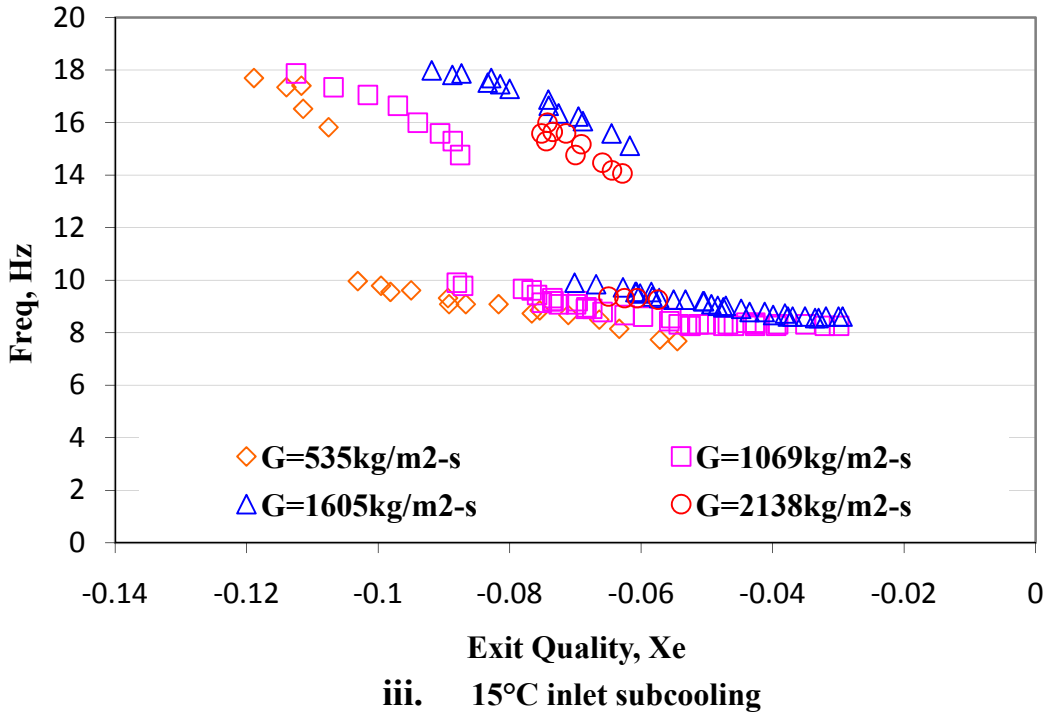

iii. 15°C inlet subcooling

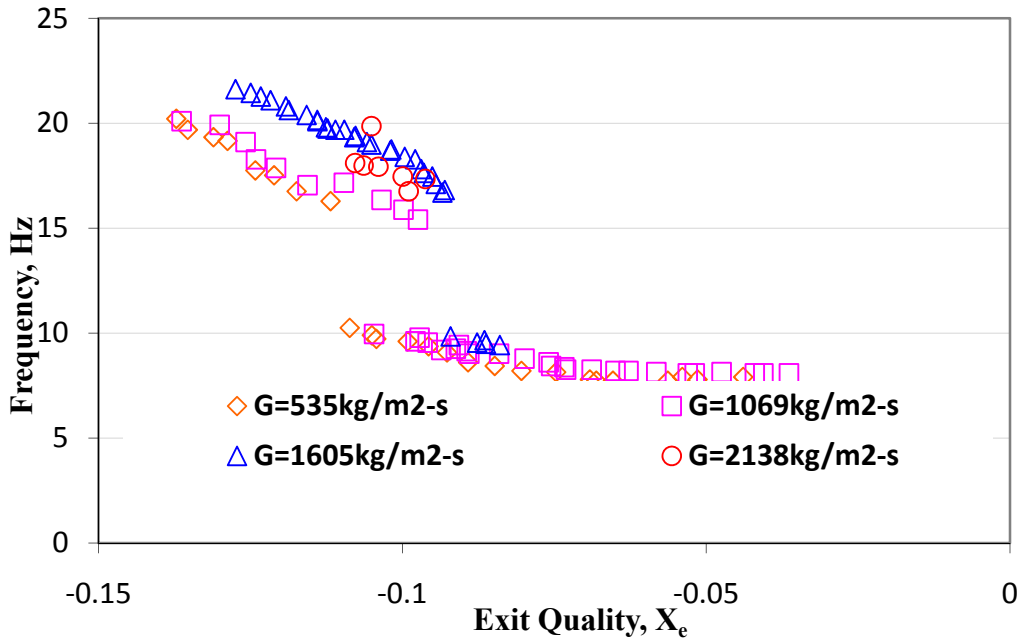

iv. 20°C inlet subcooling

Figure 4.61 Effect of mass flux on frequency of instability plotted as a function of exit quality

4.4.2 Amplitude of oscillations

The amplitude of oscillation represents the magnitude (peak-to-peak) of the fluctuation in pressure drop. It is important to keep the amplitude of oscillations as low as possible, as it can be detrimental to the system being cooled and the pumping system. Like the frequency of oscillation, the amplitude is also affected by the operating conditions such as heat flux, mass flux and inlet subcooling and it is necessary to identify the conditions which produce the oscillations of least magnitude. In Figure 4.62, the amplitude of pressure drop fluctuations is plotted against exit vapor quality. It is interesting to note that, within each regime of instability, high frequency and low frequency, the amplitude increases to reach a maximum and then decreases with increasing heat flux. Immediately after the transition to low frequency, the amplitude continues to follow the same cycle as in the case of high frequency but does not scale the same peak as attained in the high frequency regime.

The sections below investigate the effects of inlet subcooling and mass flux on the amplitude of oscillations.

a) Effect of inlet subcooling

As described earlier, the amplitude of oscillation increases and decreases with heat flux within each regime of instability. It has to be noted that amplitude of oscillation indicates the magnitude of oscillation. To further analyze the effect of inlet subcooling on the amplitude , the peak-to-peak amplitude of pressure drop oscillations are plotted versus heat flux and quality with the mass flux held constant and inlet subcooling varying from 5 - 20°C.

As the inlet subcooling increases, at a constant mass flux, the instabilities are encountered at higher heat flux. The vapor quality is highest at lower inlet subcooling and hence according to the hypothesis the strength of oscillations is low as indicated by Figure 4.63 and Figure 4.64. As the inlet subcooling increases, it can be observed that the peak amplitude attained increases and this can be attributed to the lower quality prevailing under these conditions.

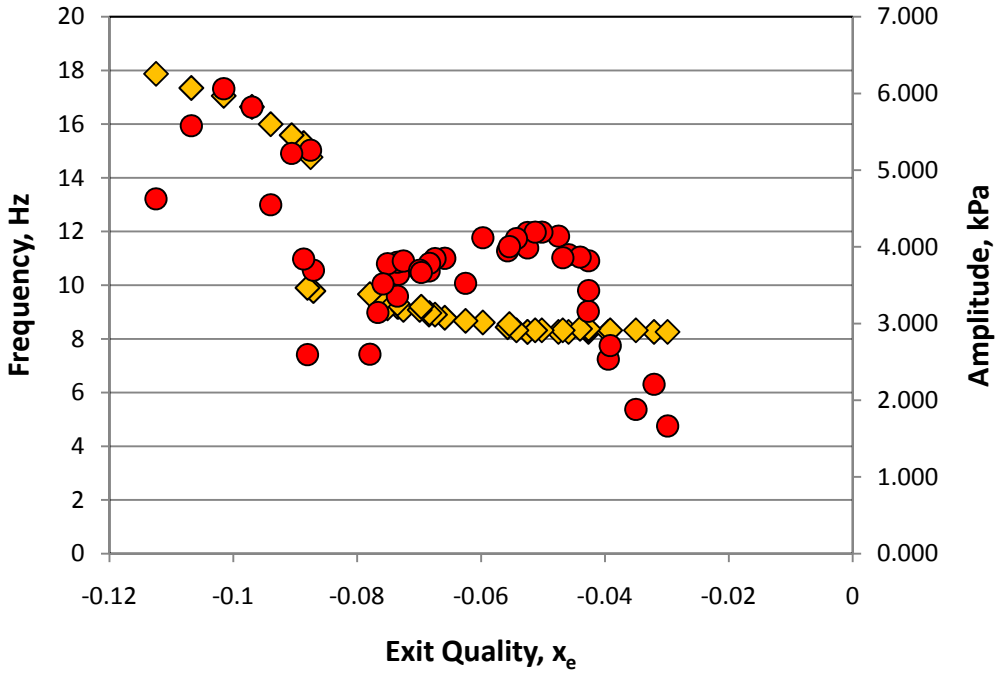

Figure 4.62 Amplitude and frequency of instability at G=1069kg/m^{2}s and ΔT_{sat}=15°C

b) Effect of mass flux

At a constant inlet subcooling, increase in mass flux would produce lower vapor quality and hence higher amplitude of oscillations. It is evident from Figure 4.65 and Figure 4.66that the peak amplitude increases as mass flux increases.

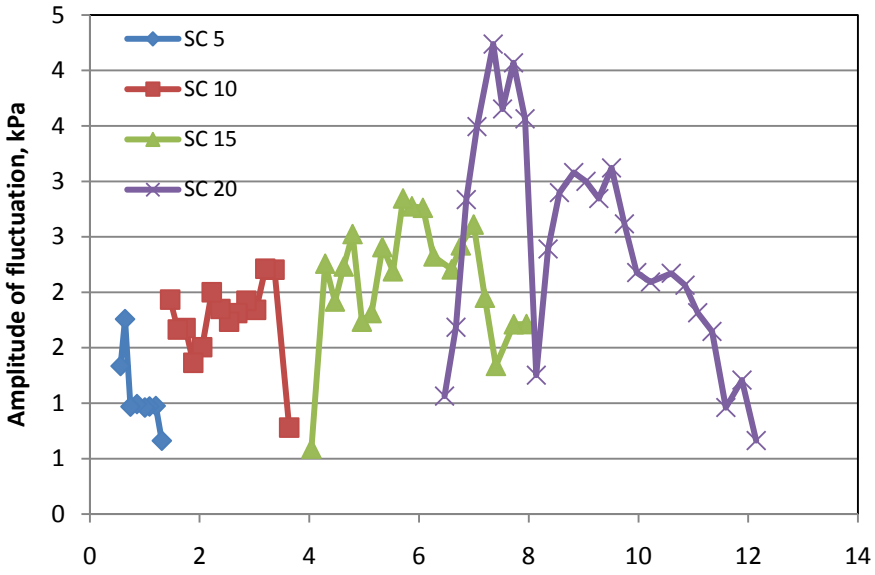

Figure 4.63 Effect of inlet subcooling on the amplitude of instability plotted as a function of heat flux at G=535kg/m^{2}s

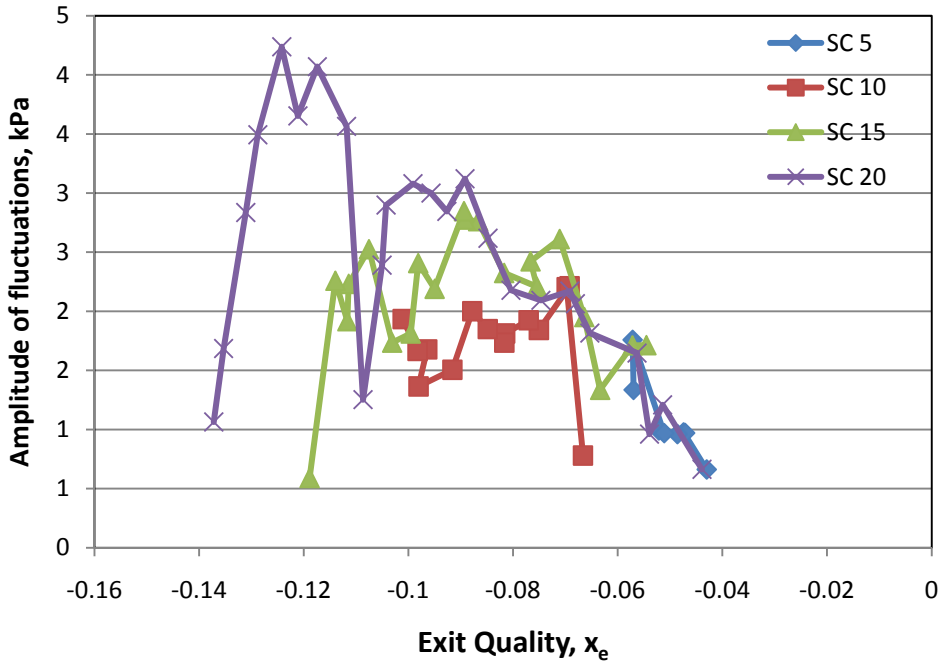

Figure 4.64 Effect of inlet subcooling on the amplitude of instability plotted as a function of exit quality at G=535 kg/m^{2}s

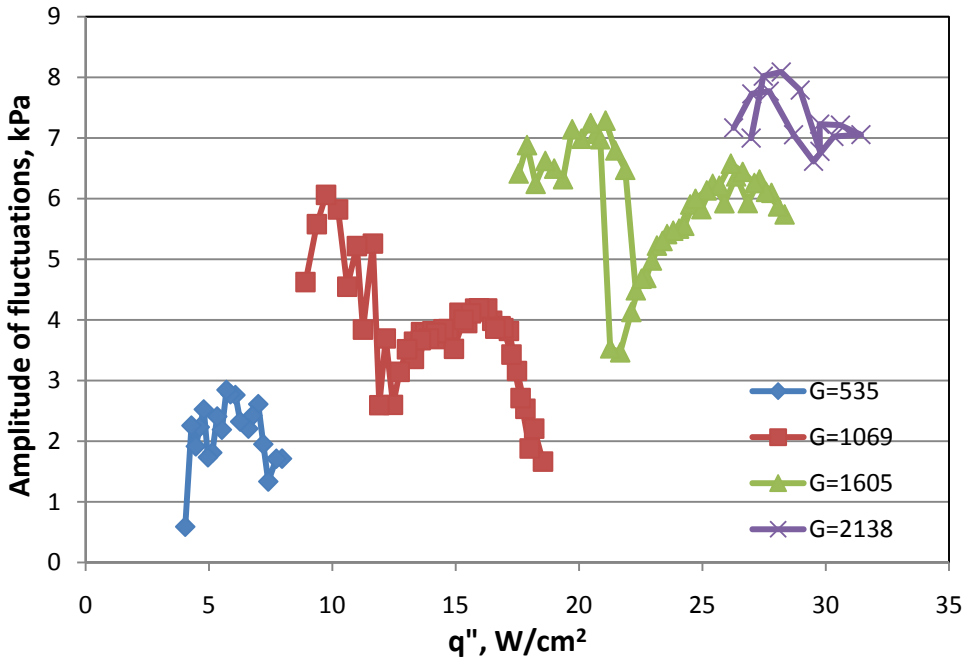

Figure 4.65 Effect of mass flux on the amplitude of instability plotted as a function of heat flux at 15°C inlet subcooling

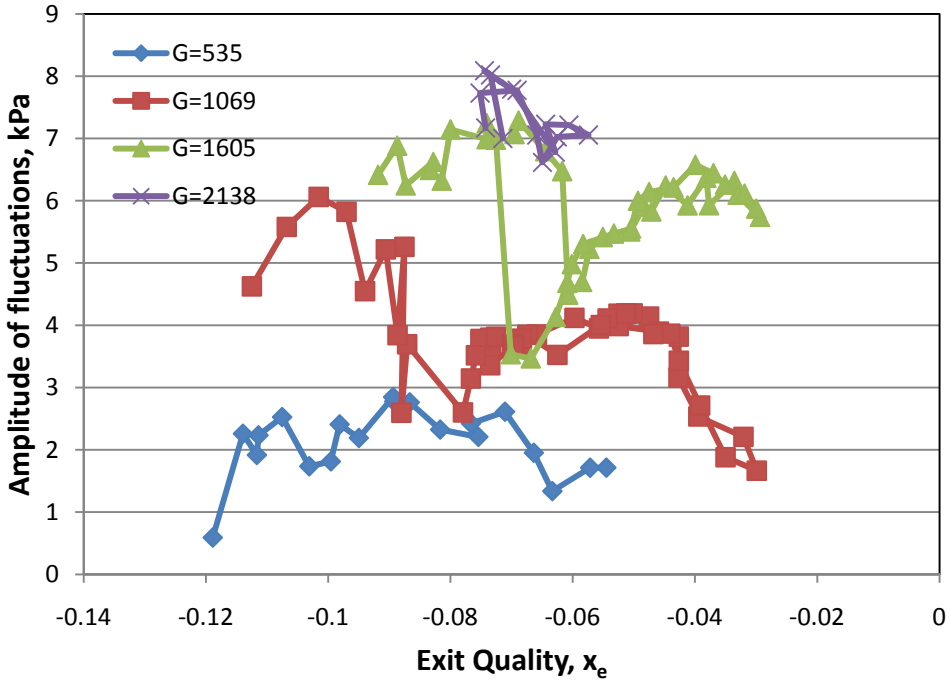

Figure 4.66 Effect of mass flux on the amplitude of instability plotted as a function of exit quality at 15°C inlet subcooling

4.4.3 Onset of Flow Instability

In the case of a static instability, the onset of flow instability (OFI) marks the minimum in the pressure drop curve plotted against mass flux. However, the OFI in the discussion to follow refers to the wall heat flux at which the instabilities cease while following the path of decreasing flux i.e. the transition from unstable to stable flow. OFI is an important parameter that deserves thorough research, since it is always of paramount importance to operate the microchannel heat sink in the stable region. Failure to predict the OFI may result in the microchannel heat sink being operated in the oscillatory regime which leads to fluctuations in wall temperature and may trigger premature critical heat flux (CHF) or dryout.

Following the path of increasing heat flux, OFI mostly follows the ONB almost immediately and prevails until the exit conditions become saturated. While decreasing the heat flux, it can be noticed that the unstable region prevails at even lower heat fluxes, before shifting to single phase. This phenomenon of instabilities following the boiling onset has been reported in number of studies in the literature such as Wang et al. [83] and Chavan et al. [57]. In the latter, perturbation analysis of flow boiling in microchannels was conducted and the unstable regions were found to follow the ONB. Kennedy et al. [56] investigated subcooled flow boiling of water in tubes of diameter 1.17 mm. It was proposed that the heat flux at onset of flow instability is 90% of the heat flux required to produce saturated flow (q''_{sat}).However, in the current study, it was observed that the heat flux at OFI as a percent of heat flux at saturated conditions (q''_{sat}) varied with increasing inlet subcooling and mass flux and was not a constant as reported by Kennedy et al. [56].

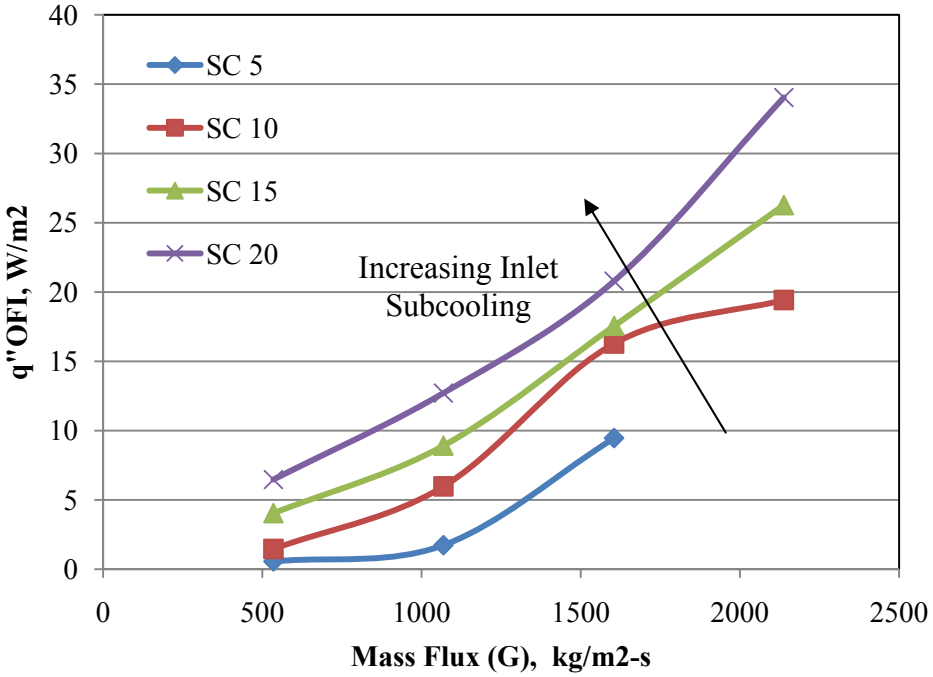

Figure 4.67 Effect of inlet subcooling and mass flux on q''_{OFI}

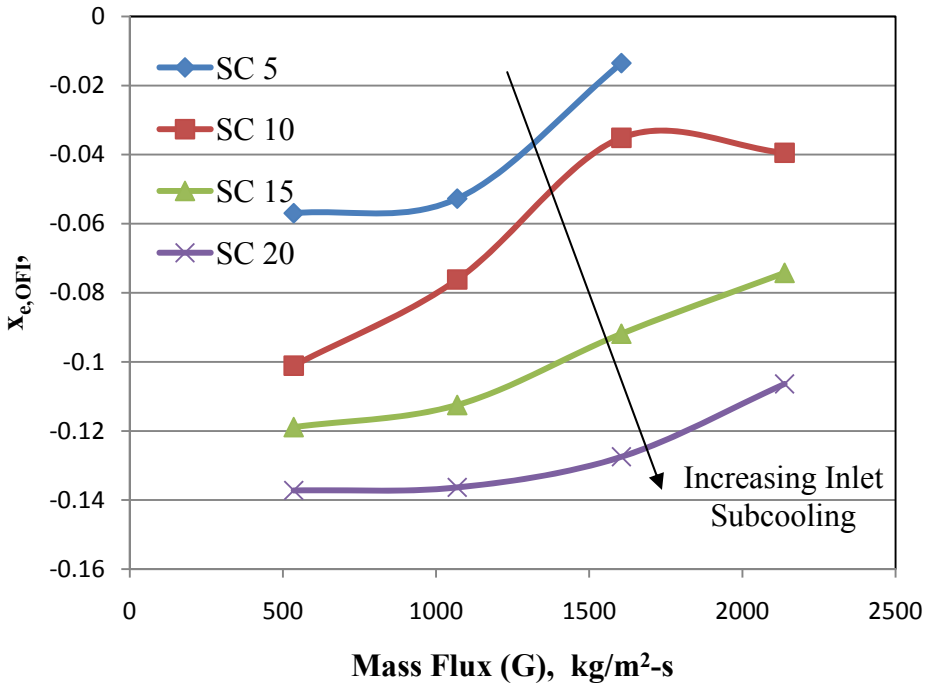

Figure 4.68 Effect of inlet subcooling and mass flux on $x_{e,OFI}$

The following discussion analyzes the effects of mass flux and inlet subcooling on heat flux at OFI (q''_{OFI}) From Figure 4.67, it can be observed that at a constant mass flux, q''_{OFI} increases with increasing inlet subcooling. At lower inlet subcooling the fact that the fluid enters microchannels at a high temperature, and so the heat flux required to initiate OFI is very low. The mass flux has a similar effect on OFI. It is evident from Figure 4.68 that the OFI increases with increasing mass flux at a constant inlet subcooling.

4.4.4 Flow instability pattern maps

To summarize all the aforementioned frequency and amplitude of oscillations and to demarcate the various flow patterns observed in the experiments conducted on the multi channel test device, and even more so to identify the stable conditions of operation for a microchannel heat sink flow pattern maps were constructed which depict the various flow patterns as a function of heat flux, mass flux and inlet subcooling. Different regimes that were observed for decreasing heat flux are: (i) single phase regime (pink colored in the flow maps) (ii) regime of stable subcooled exit (orange colored) (iii) regime of unstable subcooled exit, which can be further subdivided into high frequency (green colored) and low frequency unstable regions (blue colored) (iv) saturated exit regime (entire region in white above q''_{sat}) . Similar flow maps were obtained from the study by Jones et al. [55], but without the distinction between high and low frequency instabilities. The flow maps can also be used to identify the stable regions of operation of a microchannel heat sink, as a function of heat flux, mass flux, and inlet subcooling.

In all the flow maps (Figure 4.69 through Figure 4.76), it is to be noted that the saturated exit regime is stable for any given operating condition, which can be attributed to the controlled nucleation promoted by the cavities . As the wall heat flux decreases

below q''_{sat}, the flow instabilities prevail as low frequency oscillations, which later transform to high frequency oscillations at lower heat flux values. Further decrease in heat flux results in conditions where the vapor bubble produced condenses in the cooler fluid medium immediately after inception resulting in a stable subcooled exit. Further reduction in wall heat flux results in a stable single phase flow regime. Flow maps plotted for a constant mass flux and variable inlet subcooling (Figure 4.69 through Figure 4.72) show that the stable region decreases as the flow rate decreases. Similarly, flow maps plotted for a constant subcooling and variable mass flux (Figure 4.73 through

Figure 4.76 shows that the stable region decreases with increasing inlet subcooling. Figure 4.73 also reveals that no instabilities were encountered at a mass flux of 2138 kg/m^2-s and an inlet subcooling of 5°C. Similar conclusions were reported by Chavan et al. [57] who conducted a perturbation analysis on flow boiling in microchannels.

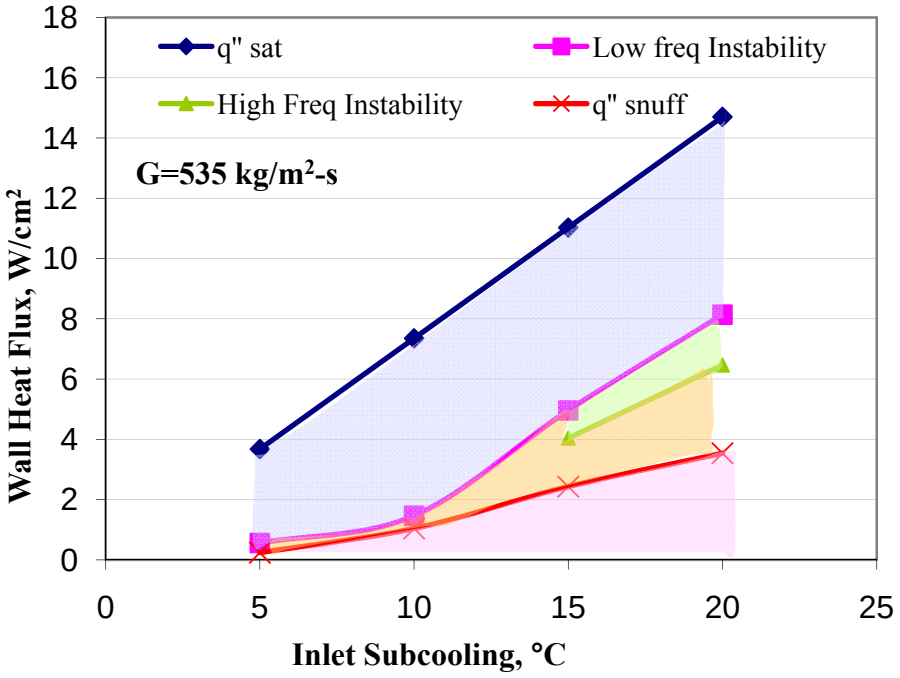

Figure 4.69 Flow pattern map at G = 535 kg/m^{2}s

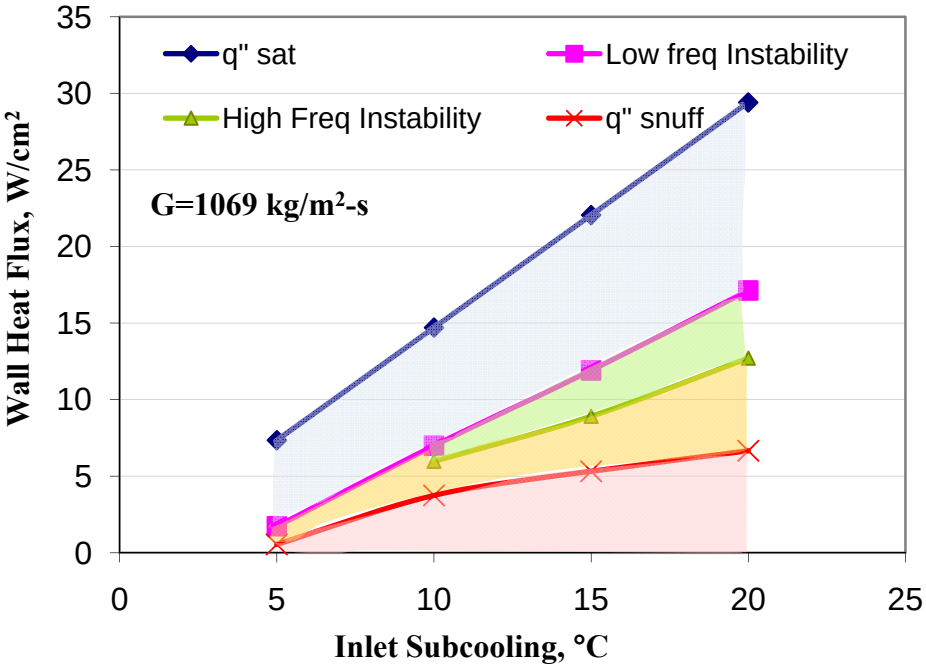

Figure 4.70 Flow pattern map at G = 1069 kg/m^{2}s

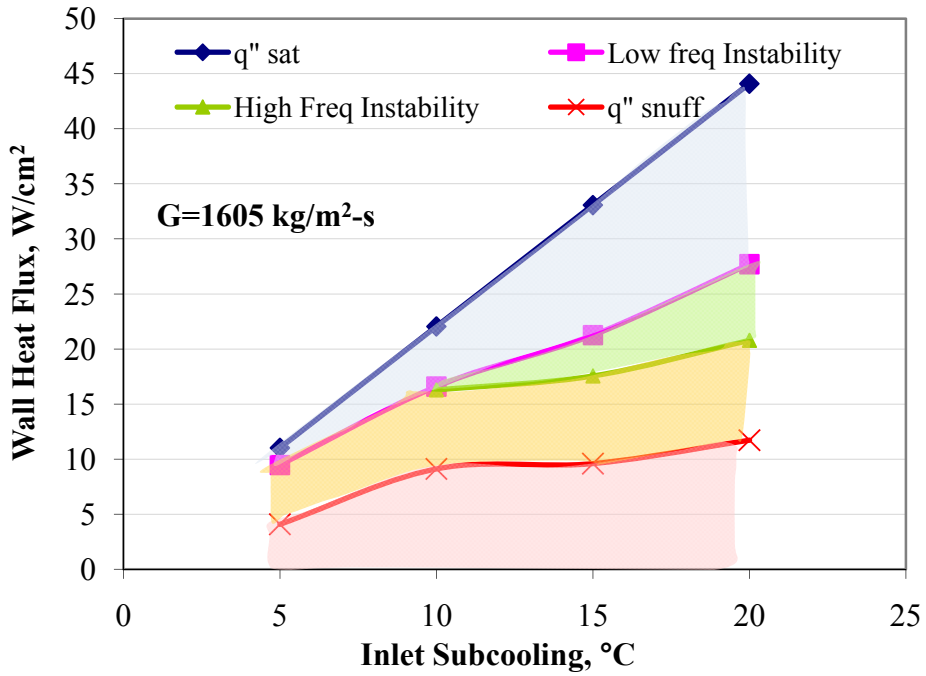

Figure 4.71 Flow pattern map at G = 1605kg/m^{2}s

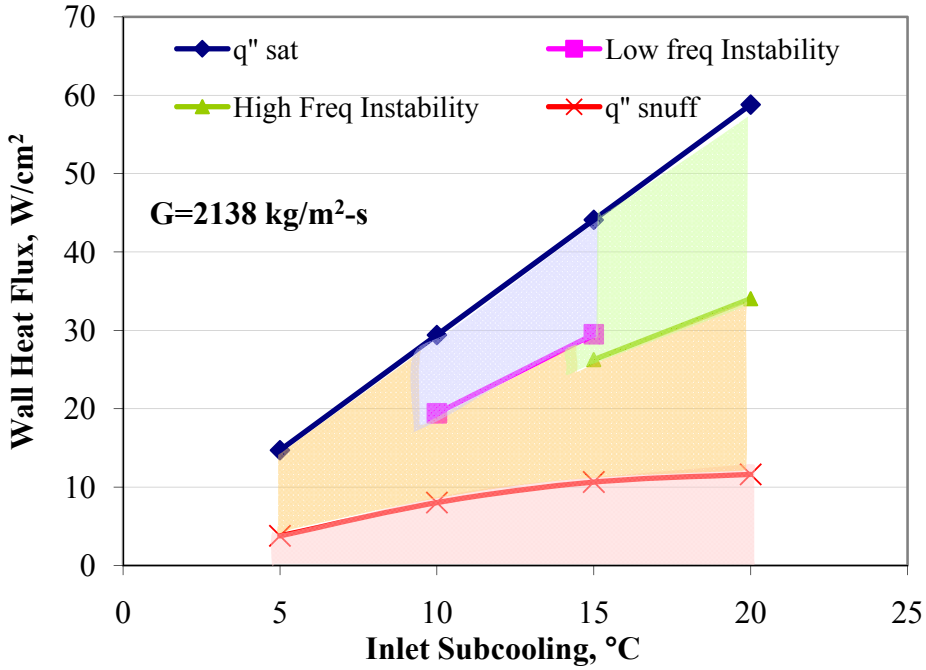

Figure 4.72 Flow pattern map at G = 2138 kg/m^{2}s

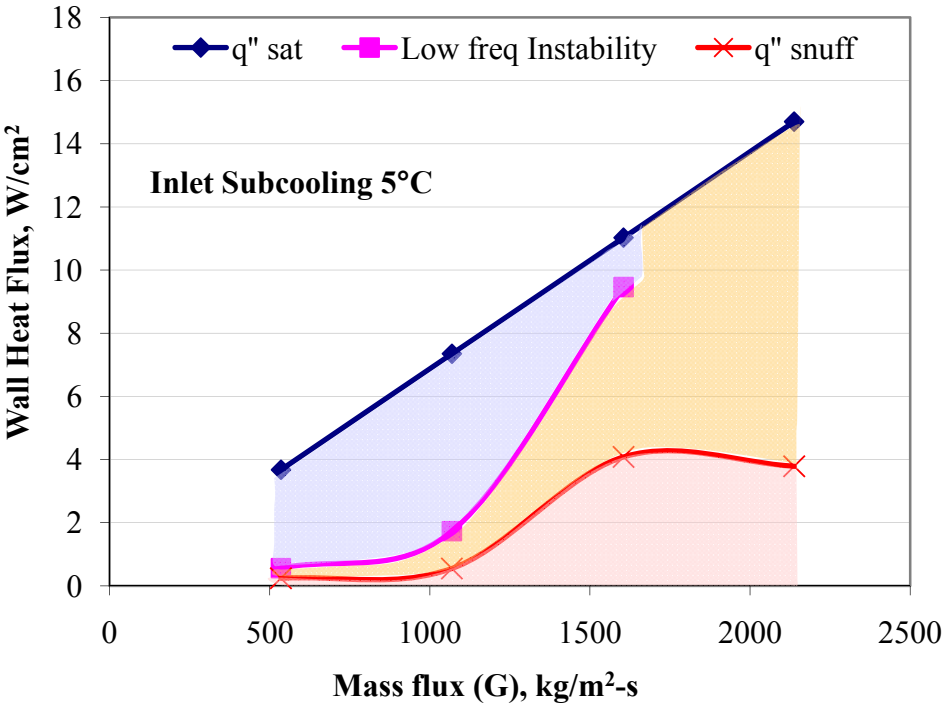

Figure 4.73 Flow pattern map at 5°C inlet subcooling

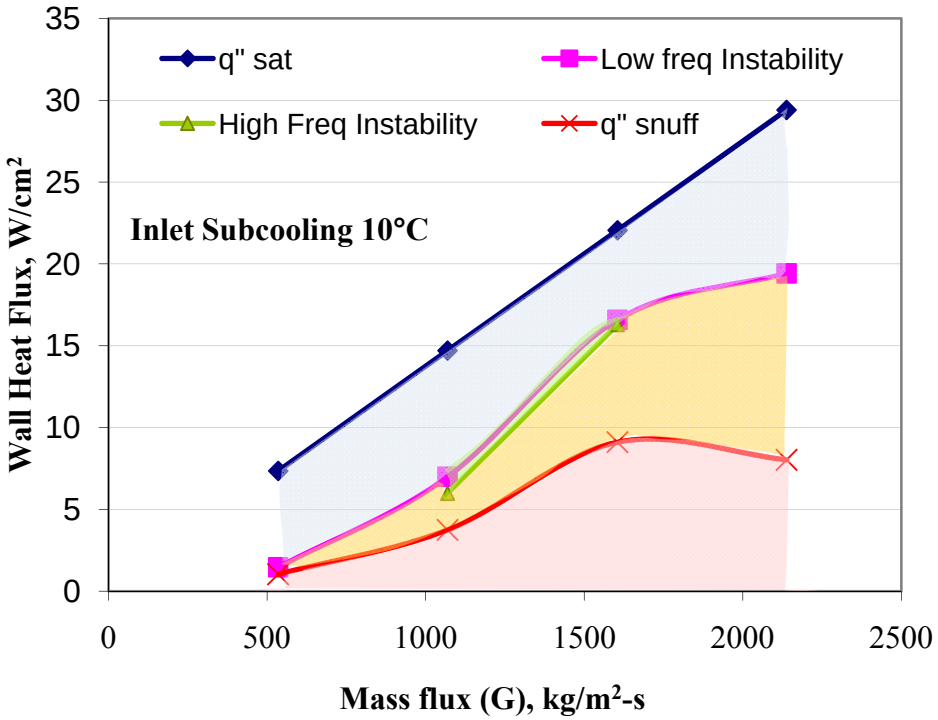

Figure 4.74 Flow pattern map at 10°C inlet subcooling

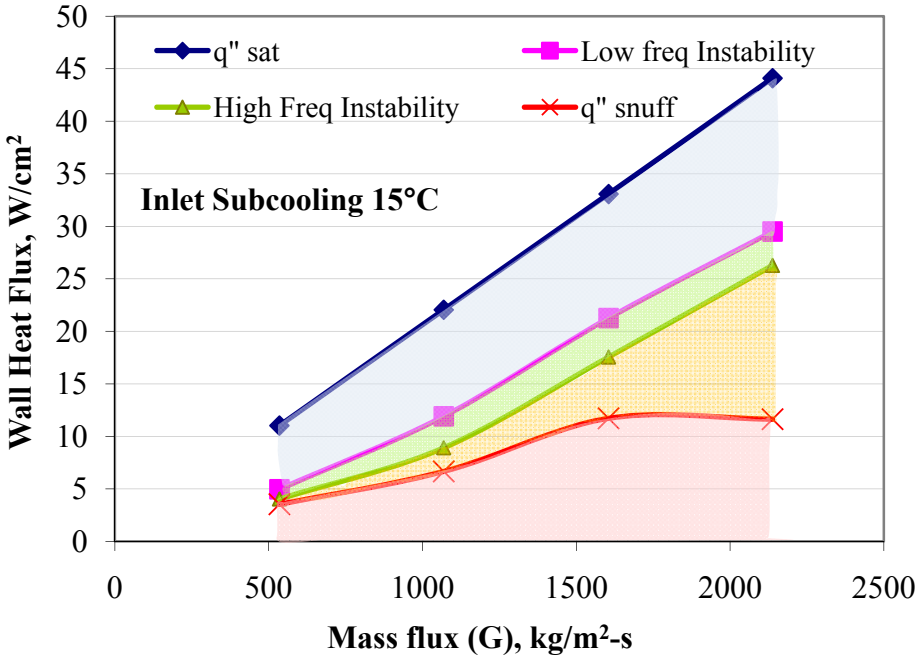

Figure 4.75 Flow pattern map at 15°C inlet subcooling

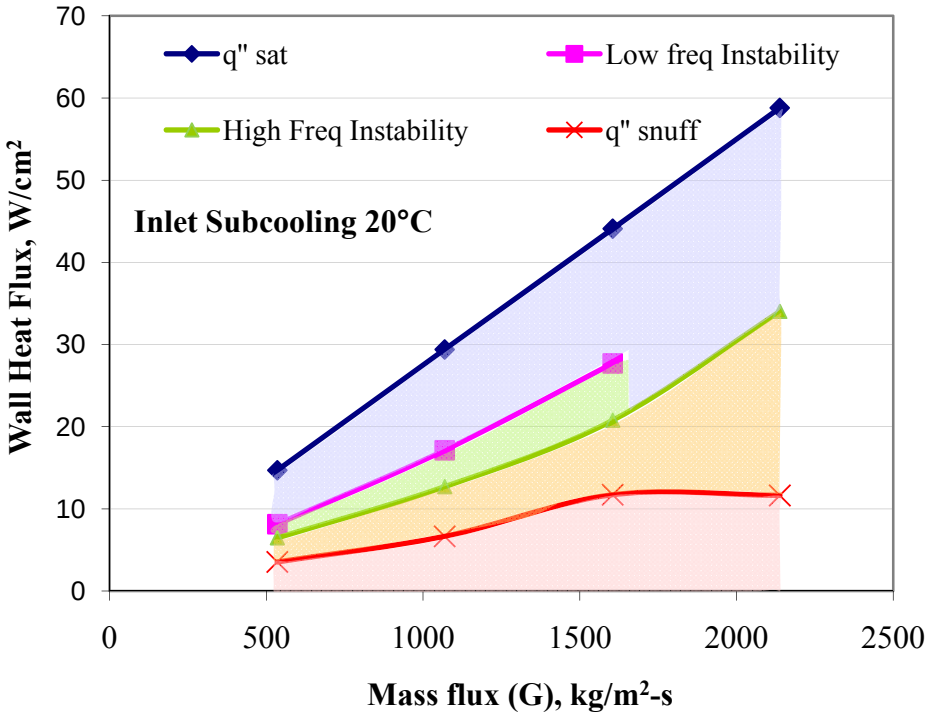

Figure 4.76 Flow pattern map at 20°C inlet subcooling

4.4.5 Single microchannel configuration

To draw a comparison with the flow behavior in a single microchannel, it was observed that the high amplitude pressure drop fluctuations were completely absent and the flow was stable for most of the tested conditions. It is to be noted that the flow behavior observed in a single channel is unlike the multichannel test device which includes possible channel-to-channel interaction.

The high speed photographs shown in Figure 4.77 were recorded during single channel experiments (SC 100-2). In all the images, the flow takes place from right to left. At low to moderate heat flux range, the flow was bubbly and stable as seen in the images in Figure 4.77 (a) to (c). The instabilities which were present under subcooled conditions in experiments conducted on the multi channel device, were completely absent in all single channel test device at all tested conditions. However with an increase in heat flux,

as the exit conditions shifted from subcooled to saturated conditions, for both two and six cavity test devices, it was observed that hints of flow reversal or small bursts of vapor bubbles existed at the inlet of the channel which can be observed in the images in Figure 4.78 (a) to (i).

This shift from completely stable flow to hints of unstable behavior under saturated conditions was marked by an appreciable jump in the pressure drop curve as shown in Figure 4.36 for the case of 15°C inlet subcooling. This may be due to a shift in flow regime i.e. from bubbly to annular flow which leads to a sudden growth in vapor production leading to an increase in pressure drop. However, this did not lead to oscillations in the pressure drop signal at all combinations of inlet subcooling, mass flux and heat flux.

These observations agree well with the results reported by Flynn et al [58] who conducted flow boiling experiments in two thermally connected and two thermally isolated microchannel test devices, to study the effect of channel-to-channel interaction on the flow instabilities. It was observed that when the channels were isolated, the instabilities reduced. Thus the results are indicative that in single microchannel flow boiling, in the absence of channel-to-channel interaction and flow maldistribution, the instabilities that are usually prevalent under subcooled conditions in the multichannel test sections have been controlled.

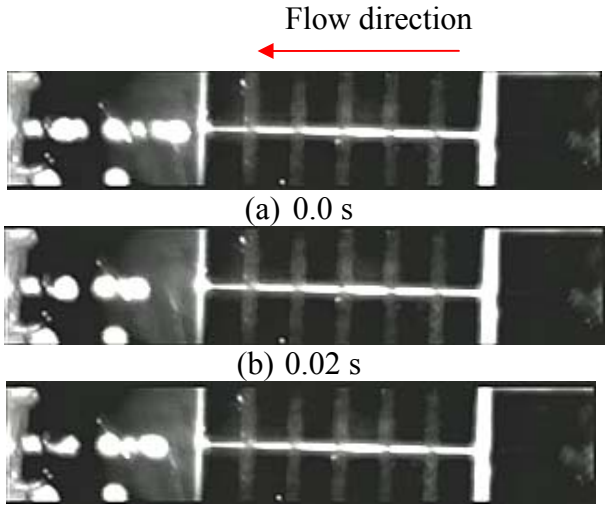

(a) 0.0 s

(b) 0.02 s

(c) 0.04 s

Figure 4.77 Stable flow in single microchannel recorded at intervals of 0.2 s at G=1605kg/m^{2}s & 15°C inlet subcooling

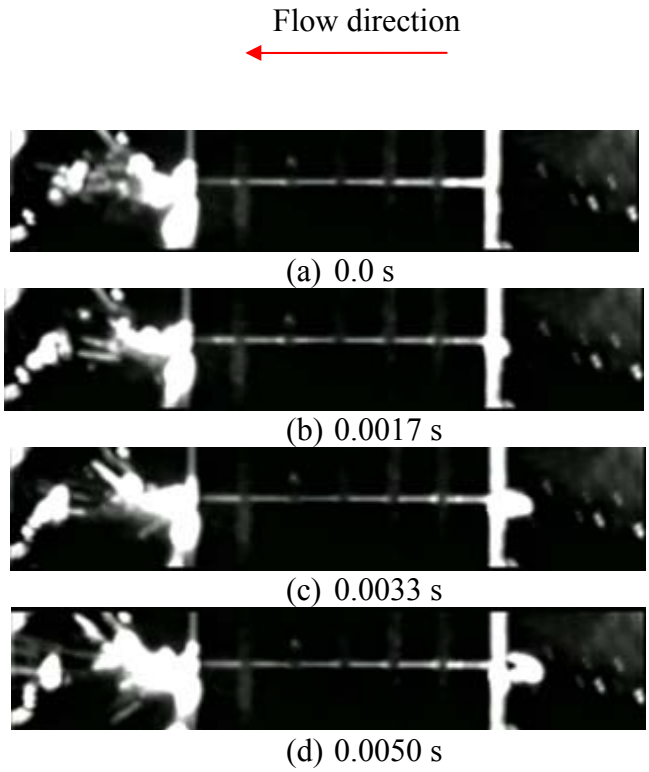

(a) 0.0 s

(b) 0.0017 s

(c) 0.0033 s

(d) 0.0050 s

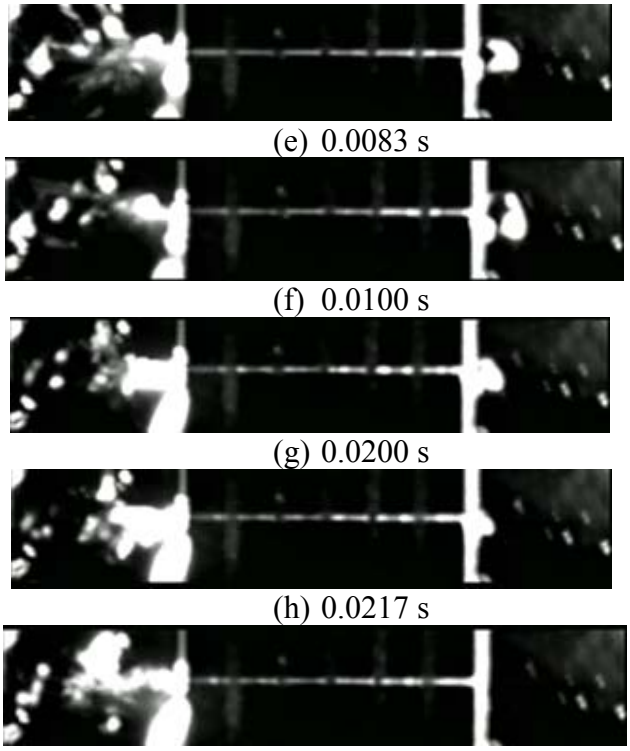

(e) 0.0083 s

(f) 0.0100 s

(g) 0.0200 s

(h) 0.0217 s

(i) 0.0233 s

Figure 4.78 Small scale oscillations in a single channel test section recorded at intervals of 0.002 s

CHAPTER 5: CONCLUSIONS

A detailed study of flow boiling of FC72 in microchannels augmented with heterogeneous nucleation sites (reentrant cavities) was performed. Experiments were conducted with multichannel test devices and with single channel test devices of varying width and number of cavities. Thermal and hydraulic characteristics of the nucleate boiling regime of the boiling curve were analyzed. Parametric effects of mass flux, inlet subcooling and heat flux on the aforementioned characteristics were also investigated.

The primary findings of the study are:

5.1 Flow friction characteristics

- The friction factor decreased with decreasing hydraulic diameter as reported by many investigators and the trends show that friction factors in single channel test devices deviate from classical theories more than the multichannel configuration.
- However, early transition to turbulence at □□ = 200- 700 as reported by Peng et al. [5] was not observed in the case of multichannel test devices up to the tested Reynolds number of 800.

5.2 Nucleation incipience and temperature overshoot and the parametric effects

- Nucleation occurred only at the re-entrant cavities and was delayed due to the highly wetting nature of FC72.

- The incipient heat flux increased with both increasing subcooling and mass flux and the trends agreed well with those reported by Pate [24] and Liu et al. [20]
- The temperature overshoot was found to decrease with increasing subcooling and the maximum overshoot of 31.5°C was observed at 5°C subcooling and a mass flux of 535kg/m^2-s. However, mass flux did not seem to affect the temperature overshoot.

5.3 Parametric effects on heat transfer co-efficient

- Heat transfer co-efficient increase with exit quality
- Mass flux and inlet subcooling had little or no effect on heat transfer in the partial nucleate boiling regime. This trend agrees well with the results reported by Harirchian and Garimella [33].
- Predictions of large channel heat transfer correlations were significantly different from the experimental data.
- A nucleate boiling correlation has been proposed which predicts the experimental data within ±20%.

5.4 Parametric effects on pressure drop

- Pressure drop remains constant in the single phase flow regime and increases sharply after the inception of nucleate boiling.
- Increase in mass flux resulted in an increase in the single and two-phase pressure drop. However at higher heat flux, the trend appears to reverse due to the suppression of boiling at higher mass flux.

- Two-phase pressure drop increased with decreasing inlet subcooling.
- The homogeneous flow model was expected to predict the pressure drop to good accuracy owing to the small bubble sizes of FC72 which would result in bubbly flow regime. However, the homogeneous models predicted the experimental data only under certain conditions. For the majority of tested conditions, the separated flow model of Chisolm [82] and Lockhart Martinelli model (Laminar liquid, turbulent vapor) [75] predicted the two-phase pressure drop with good accuracy, although the hysteresis phenomena was not captured.
- In a single channel test device, the effects of mass flux and inlet subcooling on the two phase pressure drop in the single microchannel agreed well with the results obtained for multichannel test sections.
- Increase in number of cavities was found to have no appreciable effect on the pressure drop.

5.5 Flow Instabilities

- The flow was completely stable at saturated exit conditions in all the experiments.
- Instabilities due to slug formation were eliminated due to the presence of cavities, although instabilities due to rapid condensation downstream of the channels were present. Dominant frequency of instabilities was calculated by Fast Fourier Transform analysis of the pressure drop data. Results revealed the existence of two types of instabilities-the high frequency instabilities (~15 to 20Hz) at low heat fluxes and low frequency instabilities (~6 to 10Hz) at higher heat flux values.

- At a given mass flux, the instabilities increased with increasing subcooling, and at a given subcooling, the instabilities decreased with increasing mass flux. Plotting the dominant frequency versus quality revealed that the instabilities are a stronger function of quality than heat flux since the data collapses well against each other, falling within a quality range of -0.15 to 0.
- Flow pattern maps were constructed which demarcated the various flow patterns observed at various operating conditions. These maps reveal a range of heat and mass flux allowing stable flow, at which a microchannel heat sink may be operated. It was observed that instabilities were eliminated or decreased at low subcooling and high mass flux.
- No pressure drop oscillations were observed in the case of single microchannel case and the flow was completely stable at all tested conditions. However, signs of flow reversal were observed under saturated exit conditions, even though they did not have any effect on the pressure drop.
- This is indicative of the fact that channel-to-channel interaction and the plenum-channel relationship play a significant role in promoting instabilities.

REFERENCES

[1] Ross P. , 2008, "Why CPU Frequency Stalled," IEEE Spectrum, p. 72.

[2] Tummala R. R., Rymaszewski E. J., and Klopfenstein A. G. , 1997, Microelectronics Packaging Handbook: Technology Drivers, Kluwer Academic Publishers.

[3] Shakouri A., and Zhang Y. , 2005, "On-chip solid-state cooling for integrated circuits using thin-film microrefrigerators," IEEE Transactions on Components and Packaging Technologies, **28**, pp. 65-69.

[4] Wang P., and Bar-Cohen A. , 2007, "On-chip hot spot cooling using silicon thermoelectric microcoolers," Journal of Applied Physics, **102**, p. 34503.

[5] Tuckerman D. B., and Pease R. F. , 1981, "High-performance heat sinking for VLSI," IEEE Electron Device Letters, **2**, pp. 126-129.

[6] Tuckermann D. B., and Pease R. F. , 1982, "Optimized convective cooling using micromachined structures," J. Electrochem. Soc, **129**.

[7] Colgan E. G., Furman B., Gaynes M., Graham W., LaBianca N., Magerlein, J. H. Polastre J. R., Rothwell M. B., Bezama J. R., Choudhary R., Marston K., Toy H., Wakil J., Zitz J., and Schmidt R. , 2007, "A Practical Implementation of Silicon Microchannel Coolers for High Power Chips," IEEE Transactions On Components And Packaging Technologies, **vol.30, no.2**, pp. 218-225.

[8] Philips R. J. , 1987, "Forced convection, liquid cooled microchannel heat sinks master's thesis," Massachusetts Institute of Technology, Cambridge, MA.

[9] Chowdhury I., Prasher R., Lofgreen K., Chrysler G., Narasimhan S., Mahajan R., Koester D., Alley R., and Venkatasubramanian R. , 2009, "On-chip cooling by superlattice-based thin-film thermoelectrics," Nature Nanotechnology.

[10] Revellin R., Quibén J. M., Bonjour J., and Thome J. R. , 2008, "Effect of Local Hot Spots on the Maximum Dissipation Rates During Flow Boiling in a Microchannel," IEEE Transactions on Components and Packaging Technologies, **31**, p. 407.

[11] Kandlikar S., and Grande W. , 2003, "Evolution of microchannel flow passages--thermohydraulic performance and fabrication technology."

[12] Cheng P., Wu H. Y., and Hong F. J. , 2007, "Phase-change heat transfer in microsystems," Journal of Heat Transfer, **129**, p. 101.

[13] Dhir V. K. , 1998, "Boiling heat transfer," Annual review of fluid mechanics, **30**, pp. 365-401.

[14] Bahr A. , 1966, "The Micro-convection in boiling water induced by single bubbles," Symposium on Two Phase Flow, 21-23 June 1965: proceedings, p. 287.

[15] Brown W. T. , 1967, A study of flow surface boiling.

[16] Kandlikar S. G., Shoji M., and Dhir V. K. , 1999, Handbook of phase change: boiling and condensation, CRC.

[17] Bergles A. E., and Rohsenow W. M. , 1964, "The determination of forced-convection surface-boiling heat transfer," J. Heat Transfer, **86**, pp. 365-370.

[18] Sato T., and Matsumura H. , 1964, "On the conditions of incipient subcooled-boiling with forced convection," Bulletin of JSME, **7**, pp. 392-398.

[19] Davis E. J., and Anderson G. H. , 1966, "The incipience of nucleate boiling in forced convection flow," AIChE Journal, **12**, pp. 774-780.

[20] Liu D., Lee P. S., and Garimella S. V. , 2005, "Prediction of the onset of nucleate boiling in microchannel flow," International Journal of Heat and Mass Transfer, **48**, pp. 5134-5149.

[21] Qu W., and Mudawar I. , 2002, "Prediction and measurement of incipient boiling heat flux in micro-channel heat sinks," International Journal of heat and mass transfer, **45**, pp. 3933-3945.

[22] Jones R., Pate D., and Bhavnani S. , 2006, "Phase change thermal transport in etched silicon microchannel heat sinks," 13th Int. Heat Transfer Conference.

[23] Nimkar N. D., Bhavnani S. H., and Jaeger R. C. , 2006, "Effect of nucleation site spacing on the pool boiling characteristics of a structured surface," International Journal of Heat and Mass Transfer, **49**, pp. 2829-2839.

[24] Pate D. , 2006, Experimental investigation of cavity induced two phase flow in silicon microchannels.

[25] Lie Y. M., and Lin T. F. , 2005, "Saturated flow boiling heat transfer and associated bubble characteristics of R-134a in a narrow annular duct," International journal of heat and mass transfer, **48**, pp. 5602-5615.

[26] Piasecka M., and Poniewski M. , 2004, "Hysteresis phenomena at the onset of subcooled nucleate flow boiling in microchannels," Heat Transfer Engineering, **25**, pp. 44-51.

[27] Baldwin C. S., Bhavnani S. H., and Jaeger R. C. , 2000, "Toward optimizing enhanced surfaces for passive immersion cooledheat sinks," IEEE Transactions on Components and Packaging Technologies, **23**, pp. 70-79.

[28] Nimkar N. D. , 2003, "Benchmark one dimensional heat transfer data for a structured surface: Optical study and analysis of boiling phenomena."

[29] Kosar A., Kuo C. J., and Peles Y. , 2005, "Boiling heat transfer in rectangular microchannels with reentrant cavities," International Journal of Heat and Mass Transfer, **48**, pp. 4867-4886.

[30] Kandlikar S. G., Fellow A., Kuan W. K., Willistein D. A., and Borrelli J. , 2006, "Stabilization of flow boiling in microchannels using pressure drop elements and fabricated nucleation sites," Journal of Heat Transfer, **128**, p. 389.

[31] Starke M. R. , 2005, Potential refrigerants for power electronics cooling.

[32] Mukherjee S., and Mudawar I. , 2003, "Pumpless loop for narrow channel and micro-channel boiling," Journal of Electronic Packaging, **125**, p. 431.

[33] Harirchian T., and Garimella S. V. , 2008, "Microchannel size effects on local flow boiling heat transfer to a dielectric fluid," International Journal of Heat and Mass Transfer, **51**, pp. 3724-3735.

[34] Warrier G. R., Dhir V. K., and Momoda L. A. , 2002, "Heat transfer and pressure drop in narrow rectangular channels," Experimental Thermal and Fluid Science, **26**, pp. 53-64.

[35] Bergles A. E., and Kandlikar S. G. , 2005, "On the nature of critical heat flux in microchannels," Transactions of the ASME-C-Journal of Heat Transfer, **127**, pp. 101-107.

[36] Bowers M. B., and Mudawar I. , 1994, "High flux boiling in low flow rate, low pressure drop mini-channel and micro-channel heat sinks," International Journal of Heat and Mass Transfer, **37**, pp. 321-332.

[37] Wu P., and Little W. A. , 1983, "Measurement of friction factors for the flow of gases in very fine channels used for microminiature Joule-Thomson refrigerators," Cryogenics, **23**, pp. 273-277.

[38] Choi S. B., Barron R. F., and Warrington R. O. , 1991, "Fluid flow and heat transfer in microtubes," Micromechanical sensors, actuators, and systems: presented at the Winter Annual Meeting of the American Society of Mechanical Engineers, Atlanta, Georgia, December 1-6, 1991, p. 123.

[39] Peng X. F., Peterson G. P., and Wang B. X. , 1994, "Frictional flow characteristics of water flowing through rectangular microchannels," Experimental Heat Transfer, **7**, pp. 249-264.

[40] Xie Y. Q., Yu J. Z., and Zhao Z. H. , 2005, "Experimental investigation of flow and heat transfer for the ethanol-water solution and FC-72 in rectangular microchannels," Heat and Mass Transfer, **41**, pp. 695-702.

[41] Garimella S. V., and Singhal V. , 2004, "Single-phase flow and heat transport and pumping considerations in microchannel heat sinks," Heat transfer engineering, **25**, pp. 15-25.

[42] Lee S. Y., Wereley S. T., Gui L., Qu W., and Mudawar I. , 2002, "Microchannel flow measurement using micro particle image velocimetry," Proc. ASME/IMECE.

[43] Hao P., Yao Z., He F., and Zhu K. , 2006, "Experimental investigation of water flow in smooth and rough silicon microchannels," Journal of Micromechanics and Microengineering, **16**, pp. 1397-1402.

[44] Incropera F. P., DeWitt D. P., Bergman T. L., and Lavine A. S. , 1996, Fundamentals of heat and mass transfer, John Wiley & Sons New York.

[45] Thome J. R. , 2004, "Boiling in microchannels: a review of experiment and theory," International Journal of Heat and Fluid Flow, **25**, pp. 128-139.

[46] Ledinegg M. , 1938, "Instability of flow during natural and forced circulation," Die Warme, **61**, pp. 891-898.

[47] Maulbetsch J. S., and Griffith P. , 1965, A study of system-induced instabilities in forced-convection flows with subcooled boiling., MASSACHUSETTS INST OF TECH CAMBRIDGE DEPT OF MECHANICAL ENGINEERING.

[48] Stenning A. H., and Veziroglu T. N. , 1965, instabilities in the Flow of Boiling Liquid.

[49] Kuo C. J., and Peles Y. , 2008, "Flow boiling instabilities in microchannels and means for mitigation by reentrant cavities," Journal of Heat Transfer, **130**, pp. 72401-72402.

[50] Hetsroni G., Mosyak A., and Segal Z. , 2001, "Nonuniform temperature distribution in electronic devices cooled byflow in parallel microchannels," IEEE Transactions on Components and Packaging Technologies, **24**, pp. 16-23.

[51] Hetsroni G., Mosyak A., Segal Z., and Pogrebnyak E. , 2003, "Two-phase flow patterns in parallel micro-channels," International Journal of Multiphase Flow, **29**, pp. 341-360.

[52] Kuo C. J., and Peles Y. , 2007, "Local measurement of flow boiling in structured surface microchannels," International Journal of Heat and Mass Transfer, **50**, pp. 4513-4526.

[53] Lee J., and Mudawar I. , 2005, "Two-phase flow in high-heat-flux micro-channel heat sink for refrigeration cooling applications: Part I----pressure drop characteristics," International Journal of Heat and Mass Transfer, **48**, pp. 928-940.

[54] Zhang L., Koo J. M., Jiang L., Asheghi M., Goodson K. E., Santiago J. G., and Kenny T. W. , 2002, "Measurements and modeling of two-phase flow in microchannels with nearly constant heat flux boundary conditions," Journal of Microelectromechanical Systems, **11**, pp. 12-19.

[55] Jones R. J., Pate D. T., and Bhavnani S. H. , 2005, "Control of instabilities in two-phase microchannel flow boiling using artificial nucleation sites," ASME Interpack 2005, San Francisco, CA.

[56] Kennedy J. E., Roach Jr G. M., Dowling M. F., Abdel-Khalik S. I., Ghiaasiaan S. M., Jeter S. M., and Quershi Z. H. , 2000, "The onset of flow instability in uniformly heated horizontal microchannels," Journal of Heat Transfer, **122**, p. 118.

[57] Chavan N. S., Bhattacharya A., and Iyer K. , 2005, "Modeling of two-phase flow instabilities in microchannels," 3rd international conference on microchannels and minichannels, Toronto, Canada, June 2005 : proceedings.

[58] Flynn R. D., Fogg D. W., Koo J., Cheng C., and Goodson K. E. , 2006, "IMECE2006-14696 Boiling Flow Interaction Between Two Parallel Microchannels," ASME-PUBLICATIONS-HTD, ASME; 1998, p. 317.

[59] Huh C., Kim J., and Kim M. H. , 2007, "Flow pattern transition instability during flow boiling in a single microchannel," International Journal of Heat and Mass Transfer, **50**, pp. 1049-1060.

[60] Liu J. T., and Peng X. F. , 2009, "Interface oscillation of subcooled flow boiling in locally heated microchannels," Heat and Mass Transfer, **45**, pp. 459-469.

[61] Shah R. K., and London A. L. , 1978, Laminar flow forced convection in ducts, Academic Press, New York.

[62] Carey V. P. , 1992, Liquid-vapor phase-change phenomena: an introduction to the thermophysics of vaporization and condensation processes in heat transfer equipment, Taylor & Francis London.

[63] Steiner D., and Taborek J. , 1992, "Flow boiling heat transfer in vertical tubes correlated by an asymptotic model," Name: Heat Transfer Engineering.

[64] Bao Z. Y., Fletcher D. F., and Haynes B. S. , 2000, "Flow boiling heat transfer of Freon R11 and HCFC123 in narrow passages," International Journal of Heat and Mass Transfer, **43**, pp. 3347-3358.

[65] Tran T. N., Wambsganss M. W., Chyu M. C., and France D. M. , 1997, "A correlation for nucleate flow boiling in small channels," Compact heat exchangers for the process industries conference, Snowbird, UT (United States), 22-27 Jun 1997.

[66] Shah M. M. , 1977, "A general correlation for heat transfer during subcooled boiling in pipes and annuli," ASHRAE Trans, **83**, pp. 205-215.

[67] Liu Z., and Winterton R. H. , 1991, "A general correlation for saturated and subcooled flow boiling in tubes and annuli, based on a nucleate pool boiling equation," International journal of heat and mass transfer, **34**, pp. 2759-2766.

[68] Lazarek G. M., and Black S. H. , 1982, "Evaporative heat transfer, pressure drop and critical heat flux in a small vertical tube with R-113," Int. J. Heat Mass Transfer, **25**, pp. 945-960.

[69] Kandlikar S., and Balasubramanian P. , 2004, "An extension of the flow boiling correlation to transition, laminar and deep laminar flows in minichannels and microchannels."

[70] Yu W., France D. M., Wambsganss M. W., and Hull J. R. , 2002, "Two-phase pressure drop, boiling heat transfer, and critical heat flux to water in a small-diameter horizontal tube," International Journal of Multiphase Flow, **28**, pp. 927-941.

[71] Cooper M. G. , 1984, "Heat flow rates in saturated nucleate pool boiling: a wide-ranging examination using reduced properties," Advances in heat transfer, **16**, pp. 157-239.

[72] Buchberg I. I., Romie F., Lipkis R., and Greenfield M. , 1951, "Heat transfer pressure drop, and burnout studies with or without surface boiling for de-aerated and gased water at elevated pressures in a forced flow system," Heat Transfer and Fluid Mech. Inst. Preprint of Paper, pp. 117-192.

[73] Reynolds J. B. , 1954, Local Boiling Pressure Drop.

[74] Collier J. G., and Thome J. R. , 1996, Convective boiling and condensation, Oxford University Press, USA.

[75] Lockhart R. W., and Martinelli R. C. , 1949, "Proposed correlation of data for isothermal two-phase, two-component flow in pipes," Chem. Eng. Prog, **45**, pp. 39-48.

[76] Mishima K., and Hibiki T. , 1996, "Some characteristics of air-water two-phase flow in small diameter vertical tubes," International Journal of Multiphase Flow, **22**, pp. 703-712.

[77] Lee J. H., and Lee Y. S. , 2001, "Pressure drop correlations for two-phase flow within horizontal rectangular channels with small heights," International Journal of Multiphase Flow, **27**, pp. 783-796.

[78] Chisholm D. , 1982, Two-phase flow in pipelines and heat exchangers.

[79] Tran T. N., Chyu M. C., Wambsganss M. W., and France D. M. , 2000, "Two-phase pressure drop of refrigerants during flow boiling in small channels: an experimental investigation and correlation development," International Journal of Multiphase Flow, **26**, pp. 1739-1754.

[80] Qu W., and Mudawar I. , 2003, "Measurement and prediction of pressure drop in two-phase micro-channel heat sinks," International Journal of Heat and Mass Transfer, **46**, pp. 2737-2753.

[81] Zhang M., and Webb R. L. , 2001, "Correlation of two-phase friction for refrigerants in small-diameter tubes," Experimental Thermal and Fluid Science, **25**, pp. 131-139.

[82] Chisholm D. , 1973, "Pressure gradients due to friction during the flow of evaporating two-phase mixtures in smooth tubes and channels," Int. J. Heat Mass Transfer, **16**, pp. 347-358.

[83] Wang Q., Chen X. J., Kakac S., and Ding Y. , 1996, "Boiling onset oscillation: a new type of dynamic instability in a forced-convection upflow boiling system," International Journal of Heat and Fluid Flow, **17**, pp. 418-423.

[84] Balasubramanian P., and Kandlikar S. , 2005, "Experimental study of flow patterns, pressure drop, and flow instabilities in parallel rectangular minichannels," Heat Transfer Engineering, **26**, pp. 20-27.

[85] Kline S. J., and McClintock F. A. , 1953, "Describing uncertainties in single-sample experiments," Mechanical engineering, **75**, pp. 3-8.

APPENDIX A
PROPERTIES OF COMMONLY USED FLUIDS FOR ELECTRONICS COOLING

The table below summarizes the thermo physical properties of some of the commonly used electronics cooling fluids [28,31].

Table A.1 Comparison of commonly used electronics cooling fluids

Properties	**FC72**	**Water**	**R134a**	**FC87**
Fluid description	Perfluoro carbon	De-ionized	1,1,1,2 tetra fluoroethane	Perfluoro carbon
Saturation temperature at 1atm (°C)	56.6	100	-26.6	30
Latent heat at 25°C (kJ/kg)	88	2440	178	103
Dielectric strength (kV/mil) Liquid/Vapor	3.8	1.778	7.2/6.7	4.8
Thermal conductivity (W/m-k)	0.0522	0.613	0.0819	0.056
Density 25°C (kg/m^3)	1620.88	997	1210	1650
Specific heat 25°C (kJ/kg/K)	1.1	4.13	1.4	1.1
Prandtl number	9.588	47.863	55.81	8.75
Surface Tension (N/m)	0.00833	0.0589	0.00613	0.009
Global Warming Potential (GWP)	9000	<1	1300	8900

It can be observed that while water has the highest latent heat, its boiling point and poor dielectric strength makes it a poor coolant for electronics cooling applications.R134a has superior latent heat, a very high dielectric strength and low global warming potential compared to the fluorinert fluids. However, the boiling point of R134a is very low and requires a high operating pressure.

The fluorinert liquids which have poor latent heat, offer other advantages such as high dielectric strength, a boiling point that is achievable at atmospheric pressure but has a very high global warming potential.

APPENDIX B
PRESSURE DROP CORRECTIONS IN MICROCHANNELS DUE TO LOSSES IN VARIOUS SECTIONS

The pressure drop in the microchannels can be expressed as the difference between the total pressure drop and the pressure losses due to the flow through various cross-sections.

$$\Delta p_{microchannel} = \Delta p_{total} - \Delta p_{losses} \tag{A.1}$$

The total pressure drop was obtained from the pressure transducer measurements at the inlet and exit,

$$\Delta p_{total} = p_{in} - p_{out} \tag{A.2}$$

The pressure losses include the losses in the inlet and exit tubes, 90° bends of the elbow and the plenum entry, inlet and exit plenums and sudden contraction and expansion at the inlet and exit respectively.

$$\Delta p_{losses} = \Delta p_{tube,in} + \Delta p_{tube,out} + \Delta p_{90^\circ,in} + \Delta p_{90^\circ,out} + \Delta p_{plenum,in} + \Delta p_{plenum,out} + \Delta p_{contraction} + \Delta p_{expansion} \tag{A.3}$$

The pressure loss in the tube section is,

$$\Delta p_{tube} = f_{lam}\left(\frac{L}{D_h}\right)\left(\frac{U^2}{2}\right)\rho \tag{A.4}$$

$$f_{lam} = \frac{64}{Re} \tag{A.5}$$

The pressure losses in the 90° bends into and from the plenum entry were obtained using,

$$\Delta p_{90^\circ} = \rho\left(\frac{U^2}{2}\right)k_{90^\circ} \tag{A.6}$$

Where, $k_{90^\circ} = \begin{cases} 1.53 & , Re_D < 4000 \\ 0.7\left(\frac{2\times10^5}{Re_D}\right), & Re_D \geq 4000 \end{cases}$ from [20]

The pressure losses in the plenums were calculated as,

$$\Delta p_{pl} = f_{pl}\left(\frac{L_{pl}}{D_{h,pl}}\right)\left(\frac{U^2}{2}\right)\rho \tag{A.7}$$

where □$_{□□}$ utilizes the developing flow correlation.

The pressure losses due to sudden contraction and expansion at the inlet and exit of microchannel were calculated using expressions from [21],

$$\Delta p_{contraction} = \rho\left(\frac{U^2}{2}\right)\frac{1-k_e\sigma^2C_c^{\,2}-2C_c+2C_c^{\,2}k_d}{C_c} \tag{A.8}$$

$$\Delta p_{expansion} = \rho\left(\frac{U^2}{2}\right)\frac{1-2k_d\sigma+\sigma^2\left(2k_d-1\right)}{2} \tag{A.9}$$

where, $C_c = 1-\frac{1-\sigma}{2.08(1-\sigma)+0.5371}$; k_e, k_d from Shah and London [19].

APPENDIX C
UNCERTAINTY CALCULATIONS

(i) Uncertainty in temperature

Uncertainty in temperature measurements can be estimated by using the calibration curve that was obtained by calibrating with a thermistor.

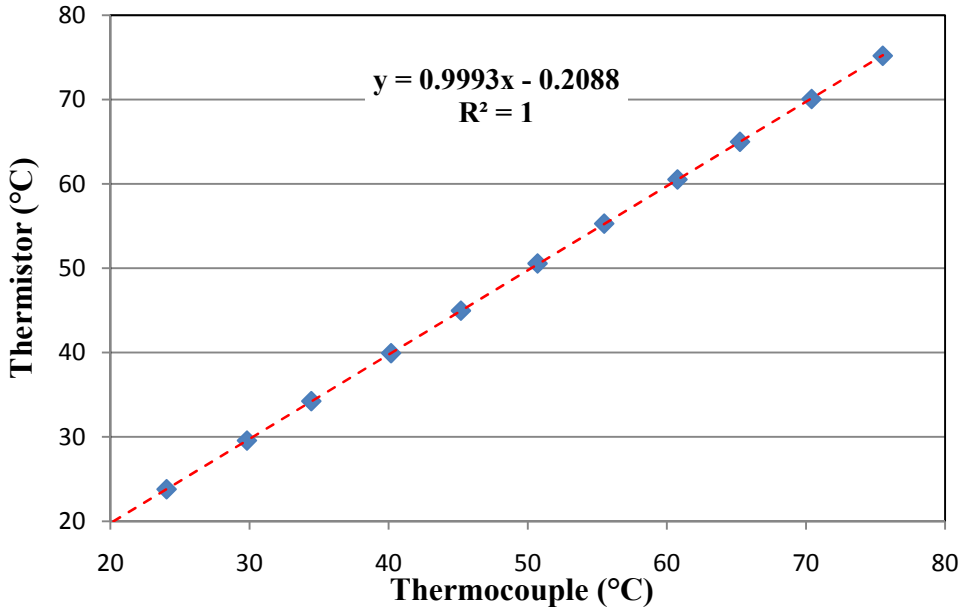

Figure A.1 Calibration curve for the thermocouple

Using the calibration curve, the uncertainty can be expressed as ,

$$U = t_{\alpha,\upsilon} S_{y/x} \tag{A.10}$$

Where, $t_{\alpha,\upsilon}$ = 2.228 (from student T- distribution)

$S_{y/x}$ = Standard deviation = $\sqrt{\frac{\sum(y_{std} - y_{cal})}{n-2}}$

Using these relations the uncertainty in temperature measurements is ±0.119°C (or) 0.213%

(ii) Uncertainty in friction factor

The friction factor for the single phase flow was calculated using the expression,

$$f = \frac{2d_h \Delta p}{\rho U^2 L} \tag{A.11}$$

The uncertainty in friction factor can be calculated using the procedure outlined in Kline and McClintock [85],

$$\frac{u_f}{f} = \sqrt{\left(\frac{u_{d_h}}{d_h}\right)^2 + \left(\frac{u_{\Delta p}}{\Delta p}\right)^2 + \left(\frac{u_\rho}{\rho}\right)^2 + \left(2\frac{u_U}{U}\right)^2 + \left(\frac{u_L}{L}\right)^2} \tag{A.12}$$

The contributions of hydraulic diameter (□□), length (L) and density (□) can be assumed negligible. Hence the expression reduces to,

$$\frac{u_f}{f} = \sqrt{\left(\frac{u_{\Delta p}}{\Delta p}\right)^2 + \left(2\frac{u_U}{U}\right)^2} \tag{A.13}$$

Uncertainty in Δp = ±0.339% of full scale in pressure measurements (or) ±2.334 kPa

Maximum Uncertainty in U = ±5% of full scale in flow rate measurements (or) ±3 ml/min

Using equation (A.12),the relative uncertainty in friction factor, u_f = 10%.

(iii) Uncertainty in heat flux ($u_{q_{wall}}$)

The wall heat flux is calculated as,

$$q_{wall} = \frac{P_{in}}{A} \tag{A.14}$$

If the uncertainty in area (A) is negligible, the relative uncertainty in wall heat flux is same as that of supplied power.

For the multichannel test devices,

$$u_{q_{wall}} = u_{P_{in}} = \pm 0.16179W = \pm 0.404\% \, of \;\; full \, scale \text{ [24]}$$

For the single channel test device,

$$u_{q_{wall}} = u_{P_{in}} = \pm 0.06115W = \pm 0.679\% \, of \;\; full \, scale$$

(iv) Uncertainty in quality (u_{x_e})

The quality at the exit of the microchannels were evaluated using the expression,

$$x_e = \frac{q_{wall} - \dot{m} C_p (T_{sat} - T_{in})}{\dot{m} h_{fg}} \tag{A.15}$$

The relative uncertainty in exit quality can be calculated as,

$$u_{x_e} = \pm \left[\left(u_{q_{wall}} \right)^2 + \left(u_{\dot{m}} \right)^2 + \left(u_T \right)^2 \right]^{1/2}$$

$$u_{x_e} = \pm \left[\left(0.00404 \right)^2 + \left(0.05 \right)^2 + \left(0.00213 \right)^2 \right]^{1/2} = \pm 0.0502 = \pm 5.02\%$$

APPENDIX D
LABVIEW VIs USED FOR DATA ACQUISITION

(i) Front panel:

The front panel of the VI is the user interface which includes controls and indicators. The front panel built for the current study by Pate [24] is shown in the Figure A.2 below. The panel indicates the inlet and exit temperature and pressure and allows the user to control data acquisition. The only input required from the user is the value of supply current as the HP power supply was not interfaced with Labview.

(ii) Block diagram:

The block diagram of the VI contains the actual code which controls the front panel objects. The required operations are controlled by functions that are inbuilt and serve a specific purpose. The various functions that constitute the code are connected by wires. The data that is entered in front panel enters the block diagram through *terminals* which then enter the functions in the order they are connected. Once processed the data exits the block diagram and re-enters the front panel to be displayed using charts or indicators. The block diagram used for the study is shown in Figure A.3.

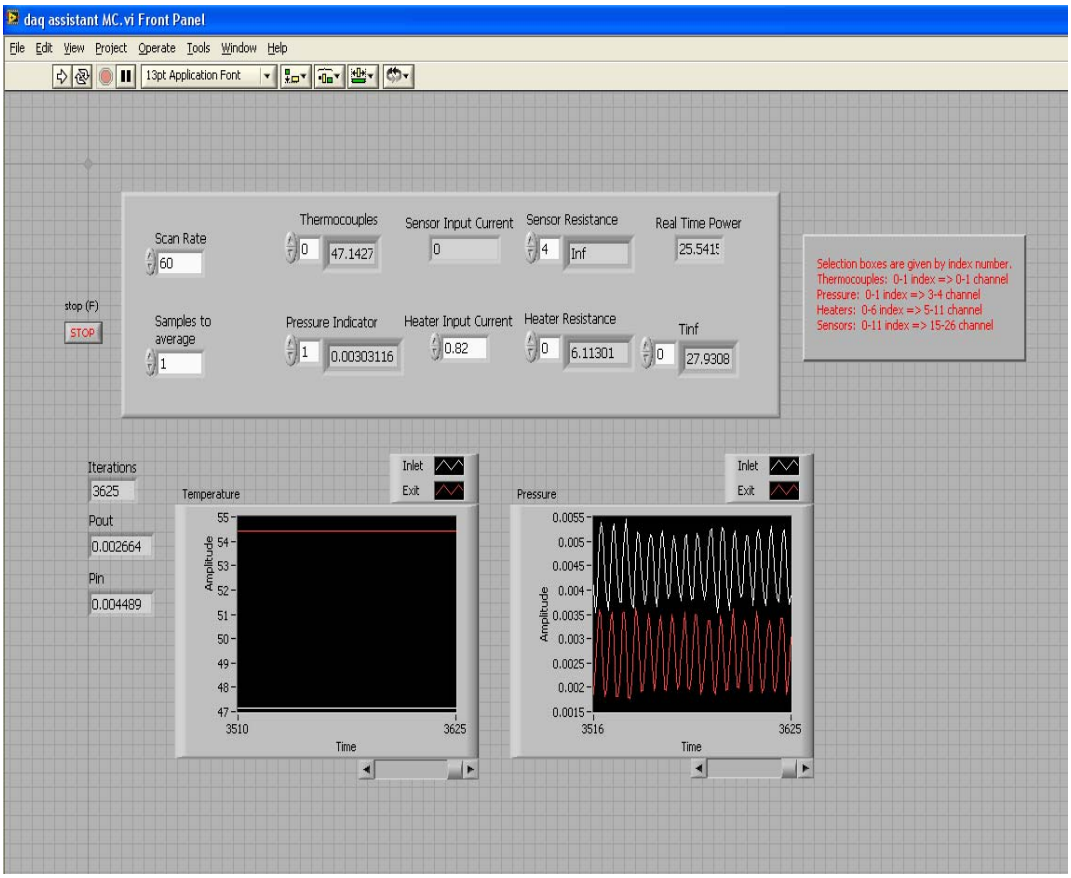

Figure A.2 Front panel used in the VI for the current study

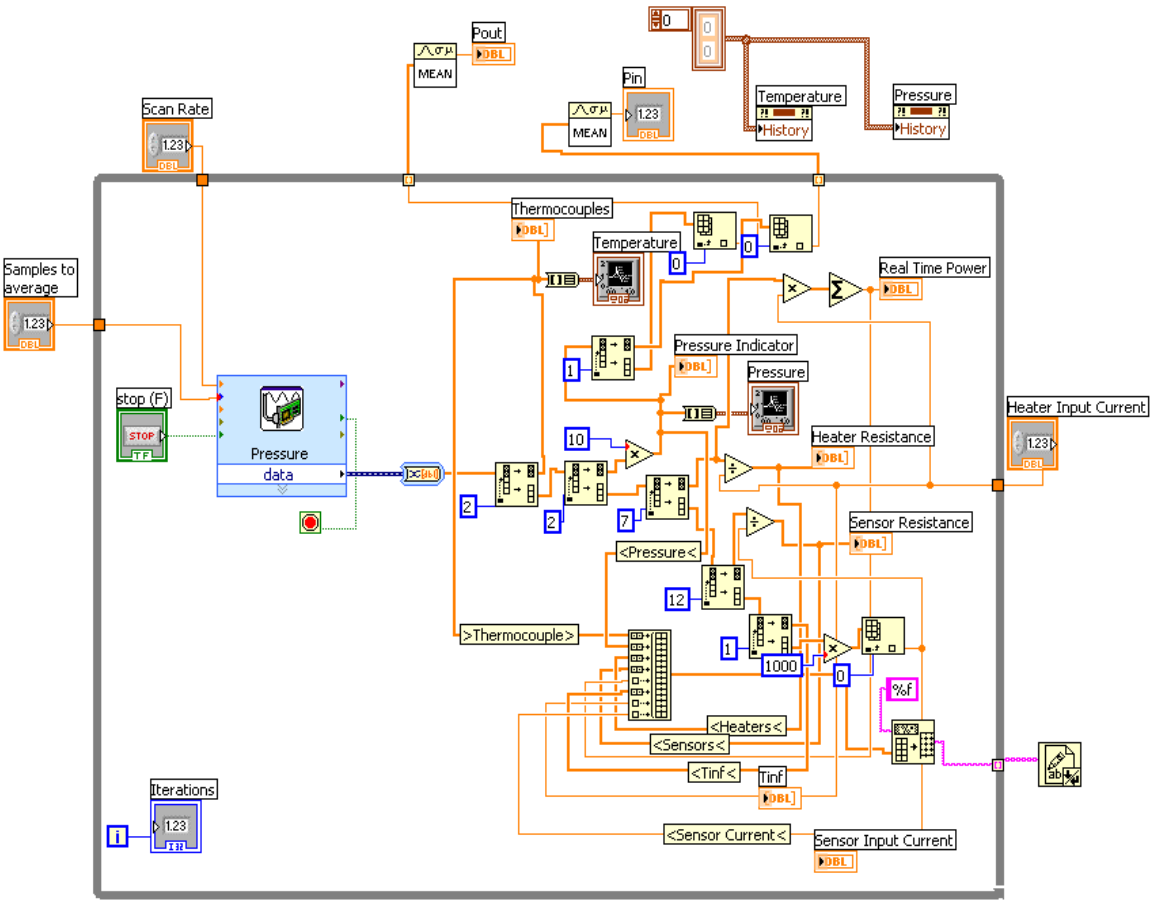

Figure A.3 Block diagram used for the study